



Task 15 Enabling Framework for the Development of BIPV

S  
T  
P  
P

## JOURNAL ARTICLES

*Energy and Buildings*

# Solar Heat Gain Coefficient of BIPV Modules for Electricity-Generating Facades

February 2025



## What is IEA PVPS TCP?

The International Energy Agency (IEA), founded in 1974, is an autonomous body within the framework of the Organization for Economic Cooperation and Development (OECD). The Technology Collaboration Programme (TCP) was created with a belief that the future of energy security and sustainability starts with global collaboration. The programme is made up of 6.000 experts across government, academia, and industry dedicated to advancing common research and the application of specific energy technologies.

The IEA Photovoltaic Power Systems Programme (IEA PVPS) is one of the TCP's within the IEA and was established in 1993. The mission of the programme is to “enhance the international collaborative efforts which facilitate the role of photovoltaic solar energy as a cornerstone in the transition to sustainable energy systems.” In order to achieve this, the Programme's participants have undertaken a variety of joint research projects in PV power systems applications. The overall programme is headed by an Executive Committee, comprised of one delegate from each country or organisation member, which designates distinct ‘Tasks,’ that may be research projects or activity areas.

The 30 IEA PVPS members are Australia, Austria, Belgium, Canada, China, Denmark, Enercity SA, European Union, Finland, France, Germany, India, Israel, Italy, Japan, Korea, Malaysia, Morocco, the Netherlands, Norway, Portugal, Solar Energy Research Institute of Singapore (SERIS), SolarPower Europe, South Africa, Spain, Sweden, Switzerland, Thailand, Turkey, United States.

Visit us at: [www.iea-pvps.org](http://www.iea-pvps.org)

## What is IEA PVPS Task 15?

The objective of Task 15 of the IEA Photovoltaic Power Systems Programme is to create an enabling framework to accelerate the penetration of BIPV products in the global market of renewables, resulting in an equal playing field for BIPV products, BAPV products and regular building envelope components, respecting mandatory issues, aesthetic issues, reliability and financial issues.

Sub-task E on “Pre-normative international research on BIPV characterisation methods” addressed aspects of BIPV characterisation and testing which were not yet completely covered by BIPV standards at the outset of Phase 2 of Task 15 in 2019. Researchers from four continents collaborated in four Activities on “Determination of Solar Heat Gain Coefficient (SHGC)”, “Fire safety of BIPV modules and installations”, “Electrical and mechanical safety and reliability of BIPV and “Standardised procedures to quantify the annual electricity yield of installed BIPV systems”. The theoretical and experimental work on SHGC of BIPV glazing resulted not only in the journal papers presented in this report but also in proposals to standards which are in the public enquiry phase at the time of this report's publication.

### Authors

- **Paper 1:** Hisashi. Ishii, Helen Rose Wilson, Shinji Hagihara, Ulrich Amann, Veronika Shabunko, Simon Boddart
- **Paper 2:** Helen Rose Wilson, Tilmann E. Kuhn, Hisashi Ishii, Daniel Valencia-Caballero, Nuria Martin Chivelet, Jinqing Peng, Rebecca Jing Yang, Yukun Zang, Hua Ge, Kai Ye, Jacob C. Jonsson, Konstantinos Kapsis

### DISCLAIMER

The IEA PVPS TCP is organised under the auspices of the International Energy Agency (IEA) but is functionally and legally autonomous. Views, findings and publications of the IEA PVPS TCP do not necessarily represent the views or policies of the IEA Secretariat or its individual member countries.

### COVER PICTURE

BIPV glazing manufactured by Onyx Solar and installed in the Kubik experimental building at Tecnia facilities in Derio, Spain, within the BIPVBoost project. Source: Eneko Setien, Tecnia in Paper 2.



INTERNATIONAL ENERGY AGENCY  
PHOTOVOLTAIC POWER SYSTEMS PROGRAMME

**IEA-PVPS Task 15**  
**Enabling framework for the acceleration of BIPV**

**International inter-laboratory comparison of  
solar heat gain coefficient of building-integrated  
photovoltaic modules - results of tests with or  
without power generation and tests with PV cell  
coverage ratios (Paper 1)**

Published under the terms of the Creative Commons CC-BY license in:

Energy and Buildings  
Volume 329, 2025, 114843  
<https://doi.org/10.1016/j.enbuild.2024.114843>

To access original publication:  
<https://www.sciencedirect.com/science/article/pii/S0378778824009599>

**Component-based SHGC determination of  
BIPV glazing for product comparison (Paper 2)**

Published under the terms of the Creative Commons CC-BY license in:

Energy and Buildings  
Volume 320, 2024, 114592  
<https://doi.org/10.1016/j.enbuild.2024.114592>

To access original publication:  
<https://www.sciencedirect.com/science/article/pii/S0378778824007084>



## ACKNOWLEDGEMENTS

---

These two papers received valuable contributions from numerous IEA-PVPS Task 15 members and other international experts. The authors would like to thank all Task 15 experts who were involved in preparing and reviewing the papers.

The work presented in the manuscript is an output from collaborations in the International Energy Agency, Photovoltaics Power Systems Technology Collaboration Programme, Task 15 Enabling Framework for the Development of BIPV and Programme.

The research presented in Paper 1 is the result of work commissioned by the New Energy and Industrial Technology Development Organization (NEDO) as part of the project entitled “Wall-Installed Solar PV System Technology Development”, grant number 20000951-0. Sincere thanks are extended to the German Federal Ministry for Economic Affairs and Climate Action (BMWK), within the Standard BIPV-System project, grant number 03EE1061A. Furthermore, thanks go to Dr. Michio Kondo (Waseda University: formerly at National Institute of Advanced Industrial Science and Technology), and Dr. Carlos Clement (Solar Energy Research Institute of Singapore, SERIS) for their support.

Sincere thanks are extended to the following sources of funding for the research reported in Paper 2:

- the German Federal Ministry for Economic Affairs and Climate Action (BMWK), within the Standard BIPV-System project, grant number 03EE1061A.
- the Japanese New Energy and Industrial Technology Development Organization (NEDO), within the Wall-Installed Solar PV System Technology Development project.
- the European Union’s Horizon 2020 research and innovation programme, within the BIPVBOOST project, under grant agreement No. 817991.
- the Spanish Ministry of Science and Innovation and the European Regional Development Fund, within the RINGS-BIPV project, grant number PID2021-124910OB-C31.
- the Assistant Secretary for Energy Efficiency and Renewable Energy, Building Technologies Program, of the U.S. Department of Energy, United States under Contract No. DE-AC02-05CH11231.



## EXECUTIVE SUMMARY

---

The solar heat gain coefficient (SHGC) is one of the important indicators to evaluate the performance of the building envelope components. In a BIPV module, secondary heat transfer to the indoors is reduced, compared to conventional glazing, due to the shielding effect of the PV cells and energy conversion by power generation. There is a difference in SHGC between power-generating (MPP) and effectively open-circuit (OC) states.

This report focuses on SHGC evaluation methodology for BIPV modules. Two approaches to assess the SHGC for BIPV module are treated, 1) calorimetric measurement of the complete BIPV glazing unit and 2) calculation based on measured component properties. This report collects two scientific publications published within the Special Issue “Photovoltaics in the Built Environment” of Energy and Building journal: the first presents the results of calorimetric measurement for BIPV from an international round robin test and the second focuses on the calculation-based approach.

In the first paper, in order to prepare a calorimetric SHGC evaluation methodology for BIPV modules, we documented the current status of the experimental calorimetric test methods and test apparatus adopted by test laboratories in four different countries and identified the differences. Differences between the test laboratories were found in the applied test methods, solar simulator types, spectral distributions, DC or AC power supplies for the solar simulator, irradiation inhomogeneity on the light-receiving surface of the test sample, temperature conditions between the test chamber and the metering box, and surface heat transfer coefficients. Especially, the round robin test results obtained in an inter-laboratory comparison clarified that the differences in the characteristics of the Calorimetric Hot Box and the Heat Flux Metering methodologies with a cooled plate, the differences in irradiation inhomogeneity on the light-receiving surface of the test sample and differences in surface heat transfer coefficients significantly affect the SHGC evaluation for BIPV modules. In addition, for the SHGC test in the MPP state, it was confirmed that an absolute SHGC reduction effect of 0.02 to 0.04 due to electricity extraction was obtained for a PV laminate with 81 % cell coverage, for all SHGC test methods and test apparatus.  $P_e$  characterises the effect of converting part of the sunlight absorbed by the PV cell into electric power and extracting it from the BIPV module, reducing the heat re-radiated indoors compared to the OC state. Due to this mechanism, the reduction effect  $P_e$  always occurs during power generation, regardless of the type of PV cell technology and whether the PV cells are opaque or transparent. In addition, the decrease in SHGC for a given glazing configuration was found to be proportional to the increase in PV cell coverage ratio. SHGC tests with four different cell coverage ratios confirmed that the relationship between PV cell coverage ratio and SHGC is linear to a high degree of accuracy when no electric power is extracted (OC state), provided that the incident radiation is spatially homogeneous. The results obtained will be useful when proposing a calorimetric SHGC evaluation methodology for international standardization, as they document the differences due to a range of test facilities and testing conditions, differences caused by power generation and extraction, and the effect of varying PV cell coverage ratios. The insights gained were valuable in identifying which aspects of test methodology and boundary conditions must be specified with particular attention to detail when calorimetric testing standards are extended to explicitly address the SHGC determination of BIPV modules. The paper was published in “Energy and Buildings”.



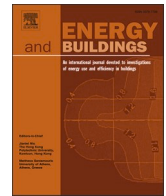
Next, in the calculation-based approach, the procedures documented in international standards for architectural glazing (e.g. ISO 9050 and EN 410) form a suitable starting point. Easily implemented modifications to these procedures are proposed to take both optical inhomogeneity (if relevant) and extraction of electricity from BIPV glazing units into account. Geometrically complex glazing and shading devices, and light-scattering glazing layers, are outside the scope of the proposed methodology; SHGC determination for obliquely incident solar radiation is also excluded. For these cases, the experimental calorimetric approach documented in the first paper, ISO 19467:2017 and ISO 19467-2:2021 is recommended. The paper also presents results and conclusions from an implementation exercise and sensitivity study carried out by participants of the IEA-PVPS Task 15 on BIPV. The cell coverage ratio in the PV laminate, the thermal resistance offered by the glazing configuration, the choice of boundary conditions and the effect of extracting electricity were all identified as parameters which significantly affect the SHGC value determined for a given type of BIPV glazing. A practicable approach to accommodate the great variety of dimensions typical for BIPV glazing is also proposed. These findings should pave the way for modifying the existing component-based standards for architectural glazing to take the specific features of BIPV glazing into account. The paper was published in “Energy and Buildings”.

The outcome of this collaborative research was published in two papers of the Special Issue “Photovoltaics in the Built Environment” of Energy and Buildings, edited by Angèle Reinders (Eindhoven University of Technology, the Netherlands) and Francesco Frontini (University of Applied Sciences and Arts of Southern Switzerland).

The results were also transferred to two standards, which are both – at the time of publication of this report – in the public enquiry phase:

CD:2024-12 - IEC 63092-3 ED1 - Photovoltaics in buildings - Part 1-1: Evaluation methodology of SHGC for Building integrated photovoltaic modules with various designs  
prEN 410: 2024 Glass in building — Determination of luminous and solar characteristics of glazing (Annex E: Modifications to the formulae to permit calculation and declaration of the luminous and solar properties of BIPV glazing)

Keywords: BIPV modules, Solar Heat Gain Coefficient (SHGC, g value, Total Solar Energy Transmittance), MPP state, Open Circuit state, PV cell coverage ratio, PV cell arrangement, Irradiance inhomogeneity, BIPV glazing, electricity extraction, optical inhomogeneity



# International inter-laboratory comparison of solar heat gain coefficient of building-integrated photovoltaic modules - results of tests with or without power generation and tests with PV cell coverage ratios

Hisashi Ishii<sup>a,\*</sup>, Helen Rose Wilson<sup>b</sup>, Shinji Hagihara<sup>c</sup>, Ulrich Amann<sup>b</sup>, Veronika Shabunko<sup>d</sup>, Simon Boddart<sup>e</sup>

<sup>a</sup> LIXIL Corporation, LIXIL Housing Technology, Technology Research Institute, 4-13-14, Higashi Shinagawa, Shinagawa City, Tokyo, Japan

<sup>b</sup> Fraunhofer Institute for Solar Energy Systems ISE, Heidenhofstr. 2, 79110 Freiburg, Germany

<sup>c</sup> Japan Testing Center of Construction Materials, Central Test Laboratory, Inari 5-21-20, Soka City, Saitama, Japan

<sup>d</sup> Formerly at Solar Energy Research Institute of Singapore, SERIS, 7 Engineering Drive 1, #06-01 Block E3A, 117574, Singapore

<sup>e</sup> CSTB, Energy Environment Department, 290 Route des Lucioles, 06904 Sophia Antipolis, France

## ARTICLE INFO

### Keywords:

BIPV modules  
SHGC  
MPP state  
Open Circuit state  
PV cell coverage ratio  
PV cell arrangement  
Irradiance inhomogeneity

## ABSTRACT

The solar heat gain coefficient is one of the important indicators to evaluate the performance of the building envelope components. In a BIPV module, secondary heat transfer to the indoors is reduced, compared to conventional glazing, due to the shielding effect of the PV cells and energy conversion by power generation. There is a difference in SHGC between power-generating (MPP) and effectively open-circuit (OC) states. In this paper, in order to prepare a calorimetric SHGC evaluation methodology for BIPV modules, we documented the current status of the experimental calorimetric test methods and test apparatus adopted by test laboratories in four different countries and identified the differences. Differences between the test laboratories were found in the applied test methods, solar simulator types, spectral distributions, irradiation inhomogeneity on the light-receiving surface of the test sample, temperature conditions between the test chamber and the metering box, and surface heat transfer coefficients. Especially, the round-robin test results obtained in an interlaboratory comparison clarified that the differences in the characteristics of the Calorimetric Hot Box and the Heat Flux Metering methodologies with a cooled plate, the differences in irradiation inhomogeneity on the light-receiving surface of the test sample and differences in surface heat transfer coefficients significantly affect the SHGC evaluation for BIPV modules. In addition, for the SHGC test in the MPP state, it was confirmed that an absolute SHGC reduction effect of 0.02 to 0.04 was obtained for a PV laminate with 81 % cell coverage, for all SHGC test methods and test apparatus.  $P_e$  characterises the effect of converting part of the sunlight absorbed by the PV cell into electric power and extracting it from the BIPV module, reducing the heat re-radiated indoors compared to the OC state. Due to this mechanism, the reduction effect  $P_e$  always occurs during power generation, regardless of the type of PV cell technology and whether the PV cells are opaque or transparent. In addition, the decrease in SHGC for a given glazing configuration was found to be proportional to the increase in PV cell coverage ratio. SHGC tests with four different cell coverage ratios confirmed that the relationship between PV cell coverage ratio and SHGC is linear to a high degree of accuracy when no electric power is extracted (OC state), provided that the incident radiation is spatially homogeneous. The results obtained will be useful when proposing a calorimetric SHGC evaluation methodology for international standardization, as they document the differences due to a range of test facilities and testing conditions, differences caused by power generation and extraction, and the effect of varying PV cell coverage ratios. The insights gained were valuable in identifying which aspects of test methodology and boundary conditions must be specified with particular attention to detail when calorimetric testing standards are extended to explicitly address the SHGC determination of BIPV modules.

\* Corresponding author.

E-mail address: [hisashi.ishii@lixil.com](mailto:hisashi.ishii@lixil.com) (H. Ishii).

<https://doi.org/10.1016/j.enbuild.2024.114843>

Received 30 March 2024; Received in revised form 31 August 2024; Accepted 25 September 2024

Available online 26 September 2024

0378-7788/© 2024 The Authors. Published by Elsevier B.V. This is an open access article under the CC BY-NC-ND license (<http://creativecommons.org/licenses/by-nc-nd/4.0/>).

Nomenclature <sup>1</sup>			
AC	alternating current	$q_i$	the secondary heat transfer factor of the glazing towards the inside
$A_{cog}$	projected area of the centre of glazing in the test sample ( $m^2$ )	$q_{in}$	the net density of heat flow rate through the test sample with irradiance ( $W/m^2$ ), also including center of glazing
$A_g$	glazing area of the test sample ( $m^2$ )	$q_{in} (I_{net} = 0)$	the net density of heat flow rate through the test sample due to thermal transmission without irradiance when the temperature difference between internal side and external side is $(\theta'_{ne} - \theta'_{ni})$ ( $W/m^2$ )
AM	air mass	$q'_{in} (I_{net} = 0)$	the net density of heat flow rate through the test sample due to thermal transmission without irradiance when the temperature difference between internal side and external side is $(\theta'_{ne} - \theta'_{ni})$ ( $W/m^2$ )
$A_{me}$	effective aperture area of measurement ( $m^2$ )	$Q_S$	rate of heat flow through the specimen (W)
$A_s$	test sample area ( $m^2$ )	$Q_{Sp}$	rate of heat flow conducted through surround panel (W)
$A_{sp}$	the projected area of the test sample ( $m^2$ )	$Q_U$	rate of heat flow through the test sample due to thermal transmission (W)
BIPV	building-integrated photovoltaics	$Q_{Wl}$	rate of heat loss through metering box wall (W)
BIPV-m	building-integrated photovoltaic module	RRT	round robin test
BM	benchmark	SC	short circuit
c	specific heat of air ( $Wh/(kg \cdot K)$ )	SERIS	Solar Energy Research Institute of Singapore
CHB	calorimetric hot box	SHGC	solar heat gain coefficient (or g value, total solar energy transmittance)
CIGS	copper indium gallium selenide	$SHGC_{FL3}$	SHGC of FL (3 mm)
CSTB	Centre Scientifique et Technique du Bâtiment	Solar-sim	solar simulator
DC	direct current	SR	spectral response (W/A)
EVA	ethylene vinyl acetate	$S_{\lambda} \Delta_{\lambda}$	component at wavelength lambda of normalized relative spectral distribution of global solar radiation
FF	fill factor	$T_{av, CHB}$	average temperature in CHB ( $^{\circ}C$ )
FL	transparent float glass	$T_{in}$	inlet temperature of metering box (K)
Fraunhofer ISE	Fraunhofer Institute for Solar Energy Systems	$T_{out}$	outlet temperature of metering box (K)
G	circulating air volume ( $m^3/h$ )	$TE_{Cd}$	corrected data of output heat exchanger (W)
g	the total solar energy transmittance (or SHGC, g value, g factor)	$TE_{Rd}$	raw data of output heat exchanger (W)
$g_{cog}$	the solar heat gain coefficient for the centre of glazing in fenestration systems	$U_N$	the thermal transmittance of the test sample without irradiance ( $W/m^2 \cdot K$ )
$g_m$	the measured solar heat gain coefficient of windows and doors	$V_{pm}$	maximum power voltage (V)
$h_e$	outdoor heat transfer coefficient ( $W/(m^2 \cdot K)$ )	$V_{oc}$	open-circuit voltage (V)
HFM-CP	method of heat flux metering using cooled plate	Xe-L	xenon long arc lamp
HFM-CB	method of heat flux metering using cooled box	Xe-S	xenon short arc lamp
$h_i$	indoor heat transfer coefficient ( $W/(m^2 \cdot K)$ )	$\alpha_1(\lambda)$	the spectral direct absorptance of the outer pane of double glazing, measured in the direction of the incident solar radiation
HTC	heat transfer coefficient	$\alpha'_1(\lambda)$	the spectral direct absorptance of the outer pane of double glazing, measured in the opposite direction to the incident solar radiation
IEC	International Electrotechnical Commission	$\alpha_2(\lambda)$	The spectral direct absorptance of the second pane of double glazing, measured in the direction of the incident solar radiation
$I_{net}$	the net radiant flux of incident radiation ( $W/m^2$ ) (N.B. this is the same quantity as $q_{solar}$ and $I_{solar}$ )	$\alpha_e$	solar direct absorptance, measured in the direction of the incident solar radiation
$I_{pm}$	maximum power current (A)	$\alpha_{e1}$	the solar direct absorptance of the outer pane within the double glazing, measured in the direction of the incident solar radiation
$I_r$	the density of heat flow rate of the incident radiation that is transmitted to the external side of the metering box after being reflected from the internal side of the metering box ( $W/m^2$ )	$\alpha_{e2}$	the solar direct absorptance of the second pane within the double glazing, measured in the direction of the incident solar radiation
$I_{sc}$	short-circuit current (A)	$\alpha_{eh}$	heat component of the total solar direct absorptance $\alpha_e = \alpha_{eh} + P_e$
$I_{solar}$	solar irradiance ( $W/m^2$ ) (N.B. this is the same quantity as $q_{solar}$ and $I_{net}$ )		
IV	current-voltage characteristic		
JTCCM	Japan Testing Center for Construction Materials		
$LE_{Fl}$	Flow of liquid exchanger ( $m^3/h$ )		
MH-S	metal halide short arc lamp		
MPP	maximum power point		
NIR	near-infrared		
OC	open circuit		
$P_e$	SHGC reduction effect coefficient in MPP state		
$P'_e$	$P_e$ for light incident from indoor side		
PERC	passivated emitter and rear cell		
$P_m$	maximum power (or peak power)		
PV	photovoltaics		
Q	amount of solar heat gain (W)		
$Q_C$	rate of heat flow removed by chilled water (W)		
$Q_E$	rate of heat flow input by electrical devices (W)		
$Q_{Fl}$	rate of heat loss through surround panel flanking (W)		
$Q_{FL3}$	amount of solar heat gain for FL (3 mm) (W)		

<sup>1</sup> Please note that nomenclature from different standards addressing the same subject has been retained to facilitate traceability. As result, different symbols have been used to refer to the same quantity, in some cases.



$\gamma$	air density (kg/m <sup>3</sup> )		
$\Delta T_{TE}$	temperature difference across output heat exchanger (°C)		
$\theta_{ne}$	the environmental external temperature with irradiance (°C)	$\phi_C$	rate of heat flow removed by the cooling device with irradiance (W)
$\theta_{ni}$	the environmental internal temperature with irradiance (°C)	$\phi'_C$	rate of heat flow removed by the cooling device without irradiance (W)
$\theta'_{ne}$	the environmental external temperature without irradiance (°C)	$\phi_{C,cog}$	rate of heat flow removed by the cooled plate for the centre of glazing with irradiance (W)
$\theta'_{ni}$	the environmental internal temperature without irradiance (°C)	$\phi'_{C,cog}$	rate of heat flow removed by the cooled plate for the centre of glazing without irradiance (W)
$q_{solar}$	the net density of heat flow rate of incident radiation (W/m <sup>2</sup> ) (N.B. This is the same quantity as $I_{net}$ and $I_{solar}$ )	$\phi_F$	rate of heat flow supplied by one or more internal fans with irradiance (optional) (W)
$\lambda$	wavelength (in the solar spectral range between 300 nm and 2500 nm)	$\phi'_F$	rate of heat flow supplied by one or more internal fans without irradiance (optional) (W)
$\Lambda$	the thermal conductance between the outdoor surface and the indoor surface of the glazing unit (W/(m <sup>2</sup> ·K))	$\phi_H$	rate of heat flow supplied by the heating device with irradiance (optional) (W)
$\rho'_1(\lambda)$	spectral reflectance of the outer (first) pane of double glazing, measured in the opposite direction to incident solar radiation	$\phi'_H$	rate of heat flow supplied by the heating device without irradiance (optional) (W)
$\rho_2(\lambda)$	spectral reflectance of the second pane of double glazing, measured in the direction of incident radiation	$\phi_{in}$	the net heat flow rate through the test sample with irradiance (W)
$\rho_e$	solar direct reflectance measured in the direction of incident solar radiation	$\phi_{in} (q_{solar} = 0)$	net heat flow rate through the test sample due to thermal transmission without irradiance when the temperature difference between the external side and internal side is $(\theta_{ne} - \theta_{ni})$ , (W)
$\Sigma A_c$	total PV cell area in BIPV-m (m <sup>2</sup> )	$\phi'_{in}(q_{solar} = 0)$	rate of net heat flow through the test sample due to thermal transmission without irradiance when the temperature difference between external side and internal side is $(\theta'_{ne} - \theta'_{ni})$ , (W)
$\tau_1(\lambda)$	the spectral transmittance of the outer pane of double glazing	$\phi_P$	rate of heat flow through the surround panel with irradiance (W)
$\tau_e$	solar direct transmittance of the double glazing unit	$\phi'_P$	rate of heat flow through the surround panel without irradiance (W)
$\phi_B$	the heat flow rate through the planes of peripheral wall of the metering box with irradiance (W)	$\phi_{solar}$	the net heat flow rate of incident radiation (W)
$\phi'_B$	the rate of heat flow through the planes of the peripheral wall of the metering box without irradiance (W)		

## 1. Introduction

Building-Integrated Photovoltaics (BIPV) is one of the approaches that can contribute to the realization of carbon neutrality in the construction sector, and is expected to become more widespread in the future. Unlike conventional rooftop-mounted photovoltaic systems, BIPV is considered as a building envelope element. (The building envelope is hereafter referred to as “façade”, although integration into the roof is also implied). BIPV glazing is expected to be fitted into the vision and spandrel areas as part of the curtain wall systems in the same way as conventional glazing products (Fig. 1). BIPV is classified into five

categories, Category A to E, as shown in Table 1, according to IEC 63092-1 [1] and EN 50583-1 [2]. By definition, BIPV is required to be integrated into the façade or roof and satisfy at least one of the basic performance requirements there. For example, the basic performance requirements of a façade include wind pressure resistance, watertightness, and airtightness, and these functions should be reliably maintained by the façade. For this reason, the BIPV modules need to meet at least those requirements in addition to energy generation.

The most important features of BIPV façades with regard to energy-economy performance are the ability to generate electric power and the ability to block solar radiation with PV cells. In other words, PV cells can play a role in reducing the heat load in summer while generating electricity on the façade. In particular, BIPV modules belonging to Categories B and D are expected to have a direct effect on the indoor comfort environment. Therefore, in this paper, we focused on Categories B and D, for which the solar heat gain coefficient (SHGC) is a significant property. It characterises the extent to which solar radiation is shielded by a façade component, and is expressed as a dimensionless number.

In previous research on the solar heat gain coefficient of BIPV, Olivieri et al. [3] reported on the construction and application of an experimental testing facility, but no comparison with another one was made. The simulation-based study by Zhou et al. [4] shows the difference in the solar heat gain coefficient between the power-generating (MPP) and effectively open-circuit (OC) states. However, it does not address measurement and verification of how much difference actually occurs. Experimental studies by Kapsis et al. [5] and Ishii [6,7] reported that SHGC decreased more (compared to equivalent glazing units without solar cells) when BIPV modules were in the MPP state than in

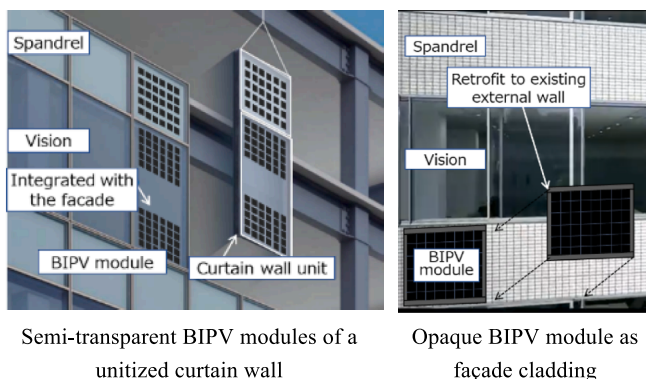


Fig. 1. BIPV systems.

**Table 1**  
Summary of BIPV Categories, as specified in IEC 63092-1 [1] and EN 50583-1 [2].

System type	Roof systems		Façade systems		External devices
Category	A	B	C	D	E
Examples					
Tilt angle of BIPV-m (deg.)	0 ~ 75	0 ~ 75	75 ~ 115	75 ~ 115	No specification
Access from indoors to BIPV-m	Impossible	Possible	Impossible	Possible	Depends on usage
Sunlight transmitted indoors	No	Yes	No	Yes	Depends on façade layer

Note: The tilt angle is 0° in the horizontal plane and 90° in the vertical plane.

the OC state. There are differences in the measurement conditions and the type of test samples that were reported in these publications, and none of these studies included round robin tests (RRT) within an international inter-laboratory comparison.

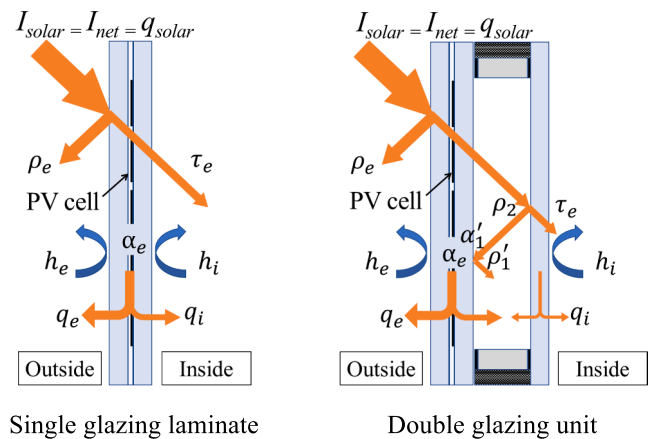
International standards addressing SHGC for windows and doors include ISO 19467-1 [8] and ISO 19467-2 [9], which are calorimetric measurement methodologies. ISO 9050 [10], ISO 15099 [11] and EN 410 [12] document approaches to calculate SHGC on the basis of the optical spectra and thermal properties of the glazing unit components. At the time of writing, none of the standards specify how to determine the SHGC of BIPV modules when power is generated and extracted (MPP state). However, it is expected that the next releases of EN 410 and ISO 9050 will contain annexes addressing this topic. In addition, IEC 63092-3 NP has currently been proposed as a calorimetric method, adapted from work presented in a paper by Ishii [13].

Therefore, in this study, we started by researching and documenting the SHGC evaluation standards, measurement methodologies, and test apparatus adopted by main laboratories of the four countries represented in this paper. Then, in an international RRT, SHGC tests were conducted of BIPV modules with and without extraction of PV power (called “Test Series 1”) and with different PV cell coverage ratios (called “Test Series 2), applying the methods usually adopted by each research and testing laboratory. Based on these results, we confirmed the previously reported phenomena and behavior, determined some requirements, and identified the problems which must be solved in order to adapt the existing calorimetric evaluation methodology for SHGC to be suitable for testing BIPV glazing units.

## 2. Characteristics of SHGC in BIPV modules

### 2.1. SHGC of BIPV modules in the OC state

It is to be expected that normal windows and BIPV-m behave differently after receiving solar energy. Here, we briefly discuss the general single glazing laminate of Fig. 2 as an example. First, the behavior of sunlight when it reaches the glass surface differs depending on the type and thickness of the glass, and depends on the reflectance, transmittance, and absorptance components as optical properties.



**Fig. 2.** Glazing configurations of single-glazed and double-glazed BIPV modules in the open-circuit (OC) state.

Among them, the solar direct transmittance  $\tau_e$  and the solar direct absorptance  $\alpha_e$  are directly related to the SHGC, and are defined in more detail in standards such as ISO 9050 [10] and EN 410 [12]. The solar direct transmittance  $\tau_e$  characterises the proportion of incident solar radiation that passes through the glass and reaches the indoors directly, and the solar direct absorptance  $\alpha_e$  characterises the proportion of incident solar radiation that is absorbed by the glass. This absorbed energy in turn is usually transferred as heat to the indoor and outdoor surroundings, primarily by radiation and convection. The ratio of indoor to outdoor heat transfer depends on their respective heat transfer coefficients (HTC). In ISO 9050 [10], the SHGC for any glazing configuration is evaluated by summing the solar direct transmittance  $\tau_e$  and the secondary heat transfer factor of the glazing towards the indoors  $q_b$ , as expressed in Equation (1). In Equation (2), which is valid for single glazing, it can be seen that the secondary radiation component  $q_i$  depends on the absorptance component  $\alpha_e$  in the glass shown, the HTC towards the inside  $h_i$ , and the HTC towards the outside  $h_e$ .

$$g = \tau_e + q_i \tag{1}$$

$$q_i = \alpha_e \cdot \frac{h_i}{h_e + h_i} \quad (2)$$

Similarly, Equations (3)–(5) indicate the equivalent calculation formulas for  $q_i$  for double glazing. Double glazing differs from single glazing, not only because the transmission and absorption properties of the two panes must be taken into account, but also because multiple reflections occur between the two panes of the glazing unit. Thus, the expressions for  $\alpha_{e1}$  and  $\alpha_{e2}$  include the transmittance component  $\tau_1(\lambda)$  for the outdoor glass layer, the reflectance component  $\rho'_1(\lambda)$  for radiation incident on the cavity-facing surface of the outdoor glass layer, the reflectance component  $\rho_2(\lambda)$  for radiation incident on the cavity-facing surface of the indoor glass layer, and the absorptance component  $\alpha'_1$  for radiation incident on the cavity-facing surface of the outdoor glass layer and absorbed in that glass layer. The quantity  $\Lambda$ , the thermal conductance between the outdoor surface and the indoor surface of the glazing unit ( $W/(m^2 \cdot K)$ ), is also introduced to allow partitioning of the heat flow to the outdoors and the indoors, based on simplifying assumptions about the indoor and outdoor surface temperatures, as documented in ISO 10292 [16] and EN 673 [17].

$$q_i = \frac{\left(\frac{\alpha_{e1} + \alpha_{e2} + \frac{\alpha_{e2}}{\Lambda}}{h_e} + \frac{1}{h_i} + \frac{1}{h_e + \Lambda}\right)}{\left(\frac{1}{h_i} + \frac{1}{h_e + \Lambda}\right)} \quad (3)$$

$$\alpha_{e1} = \frac{\int_{\lambda=300nm}^{2500nm} \left\{ \alpha_1(\lambda) + \frac{\alpha'_1(\lambda)\tau_1(\lambda)\rho_2(\lambda)}{1 - \rho'_1(\lambda)\rho_2(\lambda)} \right\} S_\lambda \Delta\lambda}{\int_{\lambda=300nm}^{2500nm} S_\lambda \Delta\lambda} \quad (4)$$

$$\alpha_{e2} = \frac{\int_{\lambda=300nm}^{2500nm} \left\{ \frac{\alpha_2(\lambda)\tau_1(\lambda)}{1 - \rho'_1(\lambda)\rho_2(\lambda)} \right\} S_\lambda \Delta\lambda}{\int_{\lambda=300nm}^{2500nm} S_\lambda \Delta\lambda} \quad (5)$$

The basic principle for triple glazing is the same, with a further cavity and glass layer added to the configuration; the corresponding equations are documented in ISO 9050 [10] and EN 410 [12].

## 2.2. SHGC of BIPV modules in the power-generating (MPP) state

Most conventional glazing has homogeneous optical properties over its main area. (Glazing with patterns applied by digital or screen printing represent an exception, which is addressed in Annex C of EN 410 [12].) By contrast, BIPV-m almost always contains areas with differing optical properties due to the presence of transparent regions, like glass and the encapsulant, and the PV cells. The transmissive part can be treated in the same way as conventional glass, but the PV cell part must be treated differently, at least when the power it generates is extracted to an external load. Fig. 3 shows the AM1.5 global solar spectrum and the

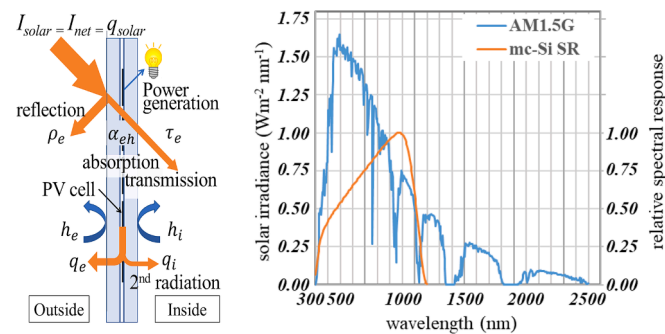


Fig. 3. (Left) Mechanism of SHGC for a single-glazed BIPV-m during power generation and extraction (MPP state). (Right) The AM 1.5 global (or hemispherical) solar spectrum and the relative spectral response (SR) of a monocrystalline silicon PV cell (mc-Si).

spectral response (SR) of a monocrystalline silicon PV cell (mc-Si). The SR of the PV cell is non-zero in the visible to near-infrared (NIR) range of the solar spectrum, indicating that some of the solar energy in this range is converted photovoltaically into electric power.

In other words, in BIPV-m, some of the incident solar energy is converted into electric power by the photovoltaic effect due to the large absorption in the PV cell part, and is removed from the glazing system to an external electric circuit. The absorbed component  $\alpha_{eh}$  that is not converted to electric power is transferred indoors and outdoors as thermal energy, and the secondary inward-flowing radiation component  $q_i$  is reduced. Therefore, the rate of re-radiation of BIPV-m decreases during power generation compared to the open-circuit state. This phenomenon has been experimentally documented by past studies, and when mc-Si is used, the decrease is 2.3 % to 10.3 %, depending on the coverage ratio of cells in the module and whether single or double glazing was studied [6,7]. Therefore, we believe that it is necessary to consider the effects of power generation and extraction when the SHGC of BIPV-m is evaluated.

Eq. (6) is a simple expression for  $q_i$  in single glazing considering the effect of power generation. Here,  $P_e$  is the proportion of incident solar energy converted into electric power by the photovoltaic effect. It is responsible for the reduced value of SHGC for the area of the BIPV-m covered by solar cells. Also,  $P_e$  can be calculated from the SR of the encapsulated PV cell, the open-circuit voltage  $V_{OC}$ , the fill factor  $FF$  and the solar spectrum, resulting in a quantity corresponding to the power conversion efficiency of a PV cell encapsulated in a module. As shown in Fig. 3, crystalline silicon PV cells are sensitive in the wavelength range from 300 nm to 1200 nm. The spectral sensitivity characteristics differ depending on the PV cell technology.

In the case of double glazing with the PV cells in the outer pane, subtracting the component  $P_e$  from the corresponding absorptance spectrum  $\alpha_{e1}(\lambda)$  results in Eq. (8) [13]. For the sake of simplicity, the spectral dependence of  $P_e$  from Eq. (7) has not been included explicitly in Eq. (8) but this could be done if spectral effects are to be analysed in detail. Please see references [4,39] for more detailed discussions of this point. Eq. (8) replaces Eq. (4) for the area of the BIPV-m covered by solar cells in the MPP state, and this expression for  $\alpha_{e1}$  is inserted into Eq. (3) to obtain  $q_i$  for double glazing with the PV module in the MPP state. Needless to say, in order to absorb more solar energy, it is common to position PV modules as the outer pane of double glazing (see Fig. 2). If the BIPV module contains bifacial PV cells, the solar absorptance in the outer pane can be expressed as in Eq. (9). Eq. (9) then replaces Eq. (4) for the area of the BIPV-m covered by solar cells in the MPP state, and this expression for  $\alpha_{e1}$  is inserted into Eq. (3) to obtain  $q_i$  for double glazing with the bifacial PV module in the MPP state.

$$q_i = (\alpha_e - P_e) \cdot \frac{h_i}{h_e + h_i} \quad (6)$$

$$P_e = \frac{\int_{\lambda=300nm}^{2500nm} SR(\lambda) V_{OC} FF S_\lambda d\lambda}{\int_{\lambda=300nm}^{2500nm} S_\lambda \Delta\lambda} \quad (7)$$

$$\alpha_{e1} = \frac{\int_{\lambda=300nm}^{2500nm} \left\{ \alpha_1(\lambda) - P_e + \frac{\alpha'_1(\lambda)\tau_1(\lambda)\rho_2(\lambda)}{1 - \rho'_1(\lambda)\rho_2(\lambda)} \right\} S_\lambda \Delta\lambda}{\int_{\lambda=300nm}^{2500nm} S_\lambda \Delta\lambda} \quad (8)$$

$$\alpha_{e1} = \frac{\int_{\lambda=300nm}^{2500nm} \left\{ \alpha_1(\lambda) - P_e + \frac{(\alpha'_1(\lambda) - P'_e)\tau_1(\lambda)\rho_2(\lambda)}{1 - \rho'_1(\lambda)\rho_2(\lambda)} \right\} S_\lambda \Delta\lambda}{\int_{\lambda=300nm}^{2500nm} S_\lambda \Delta\lambda} \quad (9)$$



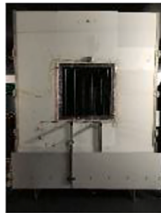






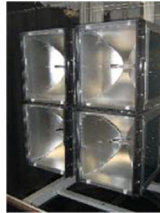


## 3. Purpose of this study

In this study, we aim to adapt calorimetric SHGC evaluation methodology for BIPV-m. In order to realize this, we first confirmed three items that should be understood and clarified as our research objectives.

- The first is to document the differences between SHGC measurement methodologies and test apparatus, and the factors that influence SHGC evaluation during measurement.
- The second is to clearly prove that SHGC is stably lower during power generation than during the open-circuit state as a phenomenon which is independent of the choice of test standards or test apparatus.
- The third is to clarify the effect of differences in the ratio of PV cell area to the module area on SHGC.

In order to achieve these objectives, we conducted SHGC tests with and without power generation using similar test samples at testing laboratories in Japan (JTCCM), Germany (Fraunhofer ISE), and Singapore (SERIS), which apply different testing methods and equipment. This test is named Series 1. In addition, SHGC tests with different PV cell coverage ratios were conducted using similar test samples in the OC state at testing laboratories in Japan (JTCCM) and France (CSTB), and the trends were objectively confirmed. This test is named Series 2. The purpose of these tests is to identify the features of the different existing test processes which should be taken into account when

**Table 2**  
Comparison list regarding general characteristics of SHGC measurement equipment owned by each testing laboratory [8,9,12,18,19,20,24,29,34,35,36].

Country Location	Japan Soka	Germany Freiburg	Singapore	France Grenoble
Testing laboratory	Japan Testing Center for Construction Material JTCCM	Fraunhofer Institute for Solar Energy Systems Fraunhofer ISE	Solar Energy Research Institute of Singapore SERIS	Centre Scientifique et Technique du Bâtiment CSTB
Appearance of test apparatus				
				
Start of operation (y)	1993	1998	2012	2021
Implemented standards (including those defining boundary conditions)	JSTM K6101 [18]	ISO 19467-2 [9], ISO 52022-3 [29] and EN 410 [12]	ASTM C1363 [34], C1199 [35], and NFRC 201 [36]	ISO 19467 [8]
Measurement method	CHB	HFM-CP	CHB	CHB
Effective aperture dimensions (m)	1.00 × 1.00	0.95 × 0.95	0.95 × 0.95	0.95 × 0.95
Environmental conditions	N/A	configurable	N/A	configurable
Climatic chamber temp. (°C)	20	25	32	20
Metering box temp. (°C)	20	25	24	20
Outdoor HTC (W/(m <sup>2</sup> ·K))	18 ± 2	25 ± 3	18.0 ± 10 %	23 or 24
Indoor HTC (W/(m <sup>2</sup> ·K))	12	7.7 ± 1	7.7 ± 5 %	8
Outdoor wind velocity (m/s)	–	determined by outdoor HTC	2	–
Indoor wind velocity (m/s)	–	controlled by cavity size	0.3	–
Solar simulator type	Xe-L lamp	MH-S lamp	MH-S lamp	MH-S lamp
Set up of solar simulator				
Number of lamps	2	4	1	5
Total lamp power (W)	6000	16000	18000	5000
Characterised spectral range (nm)	350-2100	300-2500	300-1678	300-2500
Dist.from solar-sim (m)	1.5	app. 2 – 3.5	10	–
Type of lamp power supply	AC	AC	AC	AC
Environmental conditions	N/A	N/A	N/A	Summer Winter
Irradiance (W/m <sup>2</sup> )	800	500	500	500 300
Linit of error range	±0.1	For SHGC values < 0.20, the error is typically ± 0.02. It is higher for higher SHGC values. See [21] for error analysis.	±0.02*2, ±0.05*3	±0.05

\*1 Distance from integration lens \*2 in case of uniform samples \*3 in case of non-uniform samples.

developing an SHGC evaluation methodology for BIPV-m, and subsequently to make use of this knowledge during the formulation of international standards.

#### 4. Documentation of experimental facilities and methodologies

##### 4.1. Comparison of the testing facilities

In this section, we briefly describe the experimental SHGC testing facilities of each testing laboratory to identify their common points and differences, before presenting and analysing the international RRT. Table 2 summarizes the characteristics of SHGC measurement test apparatus owned by each test laboratory, allowing quick comparison.

##### 4.2. Test apparatus of JTCCM

JTCCM's test apparatus (see Fig. 4) complies with JSTM K 6101 [18] and consists of a solar simulator (Solar-sim), a calorimetric hot box (CHB), a temperature control chiller, a heater, and a test sample mounting frame, applying the CHB method. The test sample is installed directly on the test sample mounting frame over an opening in the metering box. The effective aperture of the test sample is 1 m × 1 m. The SHGC test apparatus is installed in an air-conditioned room with a controlled constant temperature of 20 °C, and there is no climatic chamber Fig. 4. The average temperature in the metering box was controlled to 20 °C so that it would be the same as the temperature in the air-conditioned room, to prevent thermal transmission between the air-conditioned room and the metering box via the test sample.

The solar simulator uses two xenon long arc (Xe-L) lamps connected to a 50 Hz AC power supply, so the radiation fluctuates. Fig. 5 shows the results of measuring the spectral characteristics of the Xe-L lamp. The spectral distribution obtained from the discharge in high-pressure xenon gas matches that of solar radiation to a certain extent in the ultraviolet to visible light range, but there is fairly strong intensity also in the NIR from 800 nm to 1000 nm. Therefore, one of the two lamps is equipped with a KF-1 filter supplied by DAIPLA WINTES and HOYA to block the line spectrum in this range. The irradiance is 800-1000 W/m<sup>2</sup> which is similar to the intensity of sunlight at AM 1.5, and is different from 500 W/m<sup>2</sup> that is recommended (but not prescribed) in ISO 19467 [8].

In ISO 19467-2 [9], a procedure is included for determining the average irradiance from measured values of the irradiance at different positions over the test area of interest. ISO 19467 [8] contains the following specification on spatial homogeneity of the irradiance: "The non-uniformity of the irradiance on the test plane shall be measured in accordance with IEC 60904-9 [21] and shall be within 5 %." For evaluation of photovoltaic glazing units, the irradiation inhomogeneity is also significant. A map of the inhomogeneity for the JTCCM facility is presented in Table 5.

The measurement principle applied to determine the solar heat gain Q is as shown in Equation 10. The amount of solar heat gain Q that enters the metering box through the test sample during irradiation by the solar

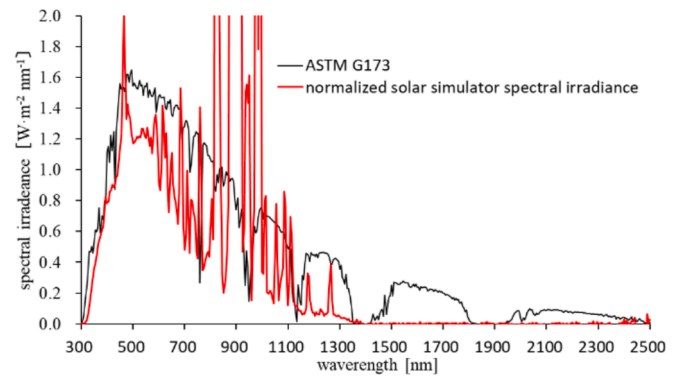


Fig. 5. Hemispherical spectral distribution of the solar simulator in JTCCM (Xe-L lamp) [19] and the hemispherical AM 1.5 solar spectrum according to ASTM G 173 [30].

simulator is replaced by cooling air, and it is derived from the amount of replaced air during that time and the temperature difference  $T_{out}-T_{in}$  before and after replacement. According to the standard [18], the outdoor surface HTC is 18 W/(m<sup>2</sup>K) ± 2, and the indoor surface HTC is 12 W/(m<sup>2</sup>K). The SHGC is determined according to Eq. 11, using the solar heat gain  $Q_{FL3}$ (W) for 3 mm thick, transparent float glass (FL3) with the same effective area as the test sample and the SHGC value for FL3 ( $SHGC_{FL3}$ ) of 0.88.

$$Q = c \gamma \cdot (T_{out} - T_{in}) \cdot G \tag{10}$$

$$SHGC = \frac{Q}{Q_{FL3}} \cdot SHGC_{FL3} \tag{11}$$

where Q is amount of the solar heat gain (W), c is the specific heat of air,  $\gamma$  is the air density,  $T_{out}$  and  $T_{in}$  are the external and internal air temperatures, respectively, and G is the circulating air volume.

##### 4.3. Test apparatus of Fraunhofer ISE

The Fraunhofer ISE test apparatus applies a methodology called Center-of-Glazing g-value determination which eliminates the effects of the four edges around the irradiated surface of the test sample. A paper by Kuhn presents two test methodologies, both of which are based on the use of heat flux metering (HFM): the cooled-plate method (HFM-CP) and the cooled-box method (HFM-CB) [20]. The applied HFM-CP method is almost identical to the HFM-CP method specified in [9], and is the method which is most commonly applied at Fraunhofer ISE and which is relevant to BIPV-m characterization. The HFM-CB methodology is applied only for very specific geometric configurations of a test sample. As shown in Fig. 6, the test apparatus consists of a solar simulator, climatic chamber, metering box, cooled absorber plate connected to an external thermostat, air conditioner, etc. Usually, a test sample with an area of 1 m × 1 m (height × width) is installed over the aperture to the metering box within the climatic chamber, and the effective aperture

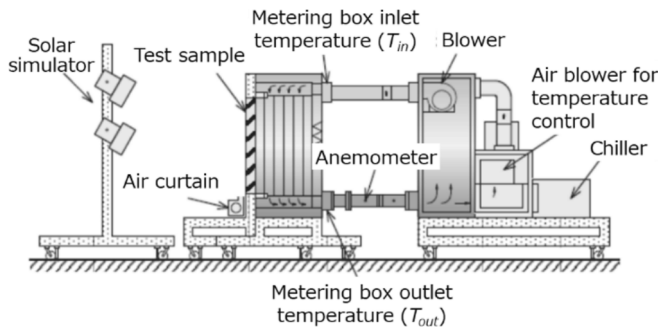


Fig. 4. Schematic cross-section of test apparatus at JTCCM[18].

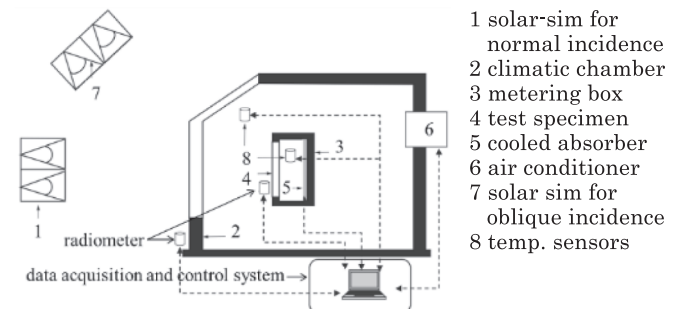


Fig. 6. Schematic cross-section of test apparatus at Fraunhofer ISE [9].

area of the test sample after perimeter masking is usually  $0.95 \text{ m} \times 0.95 \text{ m}$ . However, for the inter-laboratory comparison, the exposed area was  $0.866 \text{ m} \times 0.866 \text{ m}$ , as agreed with the client, to reduce the effect of heat flow through the edge area of the glazing.

The climatic chamber and the cooled absorber plate of the metering box can be independently temperature-controlled. The temperatures are selected to reduce the experimental error for a specific sample. If the SHGC is required for the boundary conditions that are specified by a standard, this value can be calculated by applying conversion functions to the originally determined value. Behind the test sample, there is a cavity of 10 mm thickness which separates it from the cooled absorber plate. An additional metal plate with an area of  $1000 \text{ mm} \times 1000 \text{ mm}$  and a thermally separated zone in the middle of the plate (width  $\times$  height:  $200 \text{ mm} \times 970 \text{ mm}$ ) was inserted in front of the cooled absorber plate to homogenise the heat flux behind the inhomogeneous BIPV-m sample (see Fig. 23). The cooled absorber plate absorbed the heat flux that passed through the test sample and additional metal plate, and was responsible for removing that heat. Heat flux sensors are embedded within the cooled absorber plate as shown in Fig. 7 to measure the heat flux. The signal from the central heat-flux sensor No. 5 is the one that is primarily evaluated to determine the SHGC, but for this test, the signals from heat-flux sensors 4 and 6 were also evaluated. For the SHGC determination reported here, the solar simulator was equipped with four 4 kW metal halide short arc (MH-S) lamps which are operated from an AC power supply. The climatic chamber is designed to allow irradiation at normal and oblique incidence, as indicated by the two different positions of the solar simulator in Fig. 6. The spectrum of the solar simulator (Fig. 8) is similar to the standard spectrum specified in EN 410:2011 [12]. With reference to the global AM 1.5 spectrum specified in IEC 60904-3:2008 [21] (Fig. 8), this corresponds to a Class A spectral match according to the specifications of IEC 60904-9:2007 [22].

In HFM-CP, the convective-radiative HTC between the indoor surface of the test sample and the surface of the absorber is set by choosing the cavity width shown in Fig. 7. The measurement evaluation is based on the local energy balance at the center of the test sample, directly resulting in the SHGC of the center of the glazing. The SHGC according to the HFM-CP methodology is determined from the measurement results by Equations 12 to 16, corresponding to Eq. (1), Eqs. (9)-(11) and Eq. (13) of ISO 19467-2 [9]. The net density of the heat flux through the test sample with irradiance, using the HFM-CP methodology,  $q_{in}$  is calculated using Eq. (13). The net density of the heat flux through the test sample without irradiance  $q_{in}(I_{net} = 0)$  should be calculated using Eq. (14). The edge effect can be analyzed using the heat flux sensors No. 1, 3, 7, 10 and 11 in Fig. 7.

$$g_{cog} = \frac{q_{in} - q_{in}(I_{net} = 0)}{I_{net}} \quad (12)$$

$$q_{in} = \frac{\phi_{C,cog}}{A_{cog}} \quad (13)$$

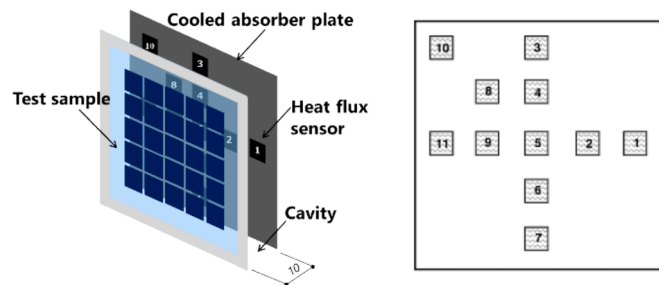


Fig. 7. Schematic configurations of metering box, including test sample, (left) and heat-flux sensors embedded within the absorber plate (right) for the HFM-CP measurement at Fraunhofer ISE. Dimensions are in mm [9,20].

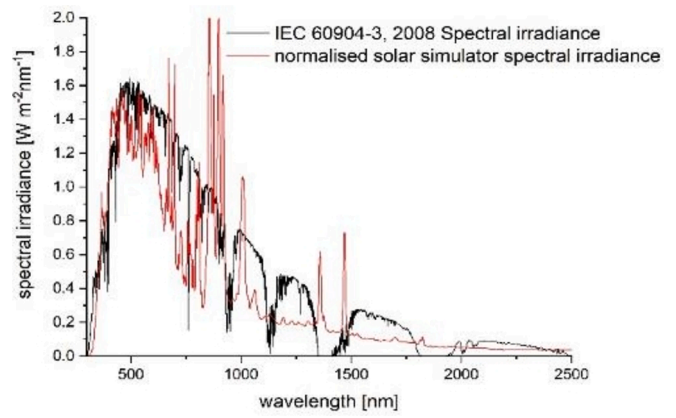


Fig. 8. Spectrum of the solar simulator at Fraunhofer ISE (MH-S lamps) and the solar spectrum specified as a reference for measurement of PV module power in IEC 60904-3 [21].

$$q_{in}(I_{net} = 0) = U_N \cdot (\theta_{ne} - \theta_{ni}) \quad (14)$$

$$U_N = \frac{q'_{in}(I_{net} = 0)}{(\theta'_{ne} - \theta'_{ni})} \quad (15)$$

$$q'_{in}(I_{net} = 0) = \frac{\phi'_{C,cog}}{A_{cog}} \quad (16)$$

where  $I_{net}$  is the net radiant flux (power) of incident radiation ( $\text{W}/\text{m}^2$ ),  $q_{in}$  is the net density of heat flow rate through the test specimen in the centre of glazing with irradiance ( $\text{W}/\text{m}^2$ ),  $q_{in}(I_{net} = 0)$  is the net density of heat flow rate through the test specimen in the centre of glazing due to thermal transmission without irradiance when the temperature difference between internal side and external side is  $(\theta_{ne} - \theta_{ni})$  ( $\text{W}/\text{m}^2$ ),  $\phi_{C,cog}$  is the heat flow rate removed by the cooled plate for the centre of glazing with irradiance (W),  $U_N$  is the thermal transmittance of the test specimen without irradiance ( $\text{W}/(\text{m}^2 \cdot \text{K})$ ),  $\theta_{ne}$  is the environmental external temperature with irradiance ( $^\circ\text{C}$ ),  $\theta_{ni}$  is the environmental internal temperature with irradiance ( $^\circ\text{C}$ ).  $q'_{in}(I_{net} = 0)$  is the net density of heat flow rate through the test specimen in the centre of glazing due to thermal transmission without irradiance when the temperature difference between internal side and external side is  $(\theta'_{ne} - \theta'_{ni})$  ( $\text{W}/\text{m}^2$ ),  $\theta'_{ne}$  is the environmental external temperature without irradiance ( $^\circ\text{C}$ ),  $\theta'_{ni}$  is the environmental internal temperature without irradiance ( $^\circ\text{C}$ ) and  $\phi'_{C,cog}$  is the flow rate of heat removed by the cooled plate for the centre of glazing without irradiance (W).

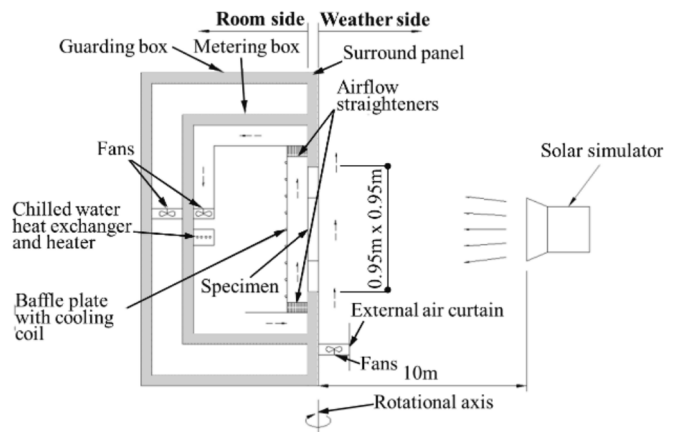


Fig. 9. Schematic cross-section of test apparatus at SERIS [23].

#### 4.4. Test apparatus of SERIS

The SERIS test apparatus combines a CHB system [23] with an SHGC measurement system [24]. Fig. 9 shows a schematic cross-section of the SERIS test apparatus. The test apparatus consists of a thermal guard, a metering box, a chiller, a surround panel, a solar simulator, and an external air curtain. In this test apparatus, on the outdoor side the climate box was replaced by a solar simulator and an external air curtain, because the test room itself, in which the test apparatus is placed, plays the role of a climate-controlled room in this system. The baffle plate has a solar absorptance of 0.952, and the absorbed heat is removed by cold water supplied from the chiller to the copper coil on the back of the baffle plate. The copper coils and the back of the baffle plate are covered by a 20 mm thick insulation sheet in order to limit direct heat exchange. The other chilled water loop and DC powered electric heater are mainly for air cooling and heating. The air temperature can be precisely controlled with a high temporal stability of better than ± 0.01 °C after reaching a steady state. Heat extraction by the baffle plate cooling water loop is determined by the volumetric flow rate and the differential temperature. The size of the test sample that can be installed is 1 m × 1 m, but the 25 mm perimeter is masked with extruded polystyrene (XPS) foam, so the nominal test sample width and height dimensions exposed to solar radiation are 0.95 m × 0.95 m.

The solar simulator has one metal halide-short arc (MH-S) lamp operated with an AC power supply, and is positioned 10 m away from the test sample surface. Fig. 10 shows the spectrum of the solar simulator. Since SERIS is unable to measure the spectral characteristics in the 300 nm – 2500 nm range of the solar spectrum, the measurement results for 300 nm – 1700 nm [23,24] are shown in Fig. 10 together with the AM1.5 direct normal and hemispherical irradiance spectra [25]. However, it is believed that the measured range is sufficiently representative, as it contains approximately 93.5 % of the total solar energy in the 300 nm – 2500 nm range of the direct normal AM1.5 spectrum prescribed in NFRC 300 [26,27]. In the subsequent calculations, the solar spectrum in the range of 1678 nm – 2500 nm is assumed to be identical to the standard AM1.5 spectrum [24].

The mean irradiance of the solar simulator is 616 W/m<sup>2</sup>, and the non-uniformity is 10 % according to the definition of IEC 60904-9 [22,28]. In order to adjust the outdoor convective HTC, an air curtain was installed on the outdoor side of the test sample to provide forced convection. The air curtain was created by five AC-powered axial fans arranged in a row. An upward air flow rate of up to 6 m/s was achieved.

The SHGC can be derived by adding up all the input heat amounts and dividing the input heat total by the irradiance from the solar simulator and the irradiated sample area. Equations 17 and 18 show the calculation formulas. However, SHGC results determined using this test apparatus for conventional glazing deviate from the SHGC calculated according to ISO 9050 [10], EN 410 [12], or NFRC 300 [27] procedures,

which apply three different reference solar spectra for their evaluations. The deviation is mainly caused by the mismatch with the spectrum of the solar simulator. In general, the test results are close to the ISO 9050 [10] calculation results, where an AM 1.5 global (or hemispherical) solar spectrum is used, but are not very close to the NFRC calculation results obtained with an AM 1.5 direct normal solar spectrum. The spectral selectivity of the glazing makes a difference, but compared to ISO 9050 [10] the deviation is generally 0.02 for low spectral selectivity and 0.05 for high spectral selectivity.

$$Q_S = - (Q_C + Q_E + Q_{WI} + Q_{FI} + Q_{Sp} + Q_U) \tag{17}$$

$$SHGC = \frac{Q_S}{I_{Solar} \times A_S} \tag{18}$$

where  $Q_S$  is rate of heat flow through specimen (W),  $Q_C$  is rate of heat flow removed by chilled water (W),  $Q_E$  is rate of heat flow input by electrical devices (W),  $Q_{WI}$  is rate of heat loss through metering box wall (W),  $Q_{FI}$  is rate of heat loss through surround panel flanking (W),  $Q_{Sp}$  is rate of heat flow conducted through surround panel (W),  $Q_U$  is rate of heat flow through the test sample due to thermal transmission (W),  $I_{Solar}$  is mean solar irradiance (W/m<sup>2</sup>) and  $A_S$  is test sample area (m<sup>2</sup>).

#### 4.5. Test apparatus of CSTB

CSTB has the only CHB test apparatus that was designed to comply completely with ISO 19467 [8] among all the tests conducted this time. Fig. 11 shows the test apparatus “Gmètre” developed at CSTB. “Gmètre” consists of one CHB unit with dimensions (width × height × depth) of 4 m × 4 m × 4 m and consisting of three chambers. The first is a climatic chamber for the outdoor environment, the second is a metering box for the indoor environment, and the third is a thermal guard to stabilize the environment inside the metering box. Temperature control of the climatic chamber and the metering box is possible, and the solar simulator and a cooling device are positioned outside the climatic chamber. The test sample is placed between the climatic chamber and the metering box, and the effective measurement aperture of the test sample is 0.95 m × 0.95 m.

The temperature of all chambers is controlled to minimize the amount of thermal transmission through each wall. The energy balance of the box measurement (solar simulator on or off) is determined by measuring the heat exchange at the exchanger level. The solar simulator has five AC-powered MH-S lamps placed outside the climatic chamber. The SHGC is determined at CSTB according to Eqs. (19)–(24) from the measured data, corresponding to Eq. (1) and (2), Eqs. (4)–(7) of ISO 19467 [8]. ISO 19467 also specifies the temperature difference between the climatic chamber and the metering box depending on the conditions

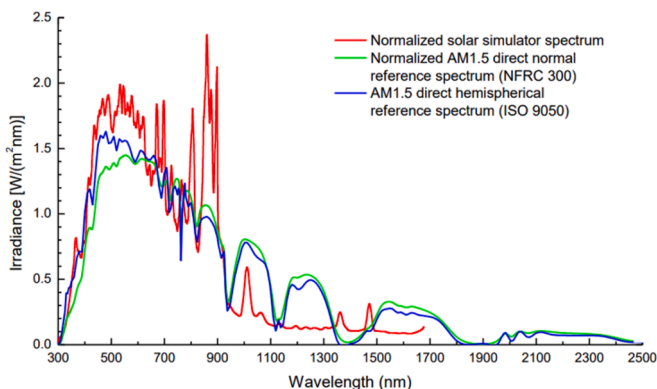


Fig. 10. Spectrum of the solar simulator at SERIS (MH-S lamp) [24] and the normalised solar spectra from the NFRC 300 [27] and ISO 9050 [10] standards.

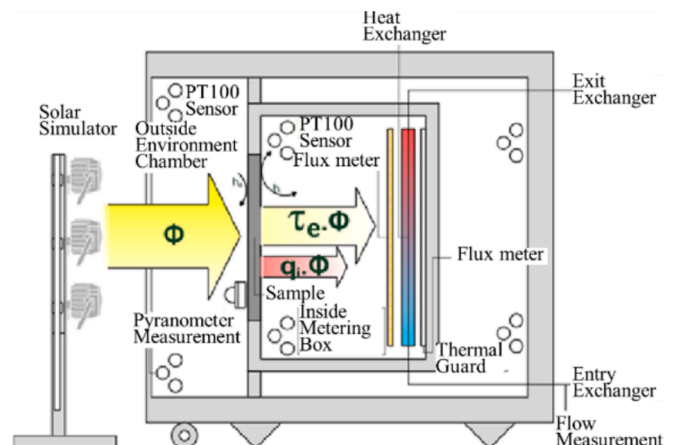


Fig. 11. Schematic cross-cction of test apparatus at CSTB.

in summer and winter, and the thermal transmittance without irradiation by the solar simulator is determined by Eqs. (22)–(24).

$$g_m = \frac{q_{in} - q_{in}(q_{solar} = 0)}{q_{solar}} \quad (19)$$

$$q_{solar} = \frac{\phi_{solar}}{A_{sp}} = \frac{I_{solar} \times A_{sp} - I_r \times A_g}{A_{sp}} \quad (20)$$

$$q_{in} = \frac{\phi_{in}}{A_{sp}} = \frac{\phi_C - \phi_B - \phi_F - \phi_H - \phi_P}{A_{sp}} \quad (21)$$

$$q_{in}(q_{solar} = 0) = \frac{\phi_{in}(q_{solar} = 0)}{A_{sp}} = U_N \cdot (\theta_{ne} - \theta_{ni}) \quad (22)$$

$$U_N = \frac{q'_{in}(q_{solar} = 0)}{(\theta'_{ne} - \theta'_{ni})} \quad (23)$$

$$q'_{in}(q_{solar} = 0) = \frac{\phi'_{in}(q_{solar} = 0)}{A_{sp}} = \frac{\phi'_C - \phi'_B - \phi'_F - \phi'_H - \phi'_P}{A_{sp}} \quad (24)$$

where  $g_m$  is the measured solar heat gain coefficient of test sample,  $q_{in}$  is the net density of heat flow rate through the test sample with irradiance ( $W/m^2$ ),  $q_{solar}$  is the net density of heat flow rate of incident radiation ( $W/m^2$ ),  $\phi_{solar}$  is the net heat flow rate of incident radiation (W),  $A_{sp}$  is the projected area of the test sample ( $m^2$ ),  $I_{solar}$  is the density of heat flow rate of the incident radiation ( $W/m^2$ ),  $I_r$  is the density of heat flow rate of the incident radiation that is transmitted to the external side of the metering box after being reflected from the internal side of the metering box ( $W/m^2$ ),  $A_g$  is the glazing area of the test sample ( $m^2$ ),  $\phi_{in}$  is the net heat flow rate through the test specimen with irradiance (W),  $\phi_C$  is the heat flow rate removed by the cooling device with irradiance (W),  $\phi_B$  is the heat flow rate through the planes of peripheral wall of the metering box with irradiance (W),  $\phi_F$  is the heat flow rate supplied by the one or more internal fans with irradiance (optional) (W),  $\phi_H$  is the heat flow rate supplied by the heating device with irradiance (optional) (W) and  $\phi_P$  is the heat flow rate through the surround panel with irradiance (W).  $U_N$ ,  $\theta_{ne}$  and  $\theta_{ni}$  are the same as specified in Eq. (14). The quantities with the prime symbol,  $q'_{in}$ ,  $\theta'_{ne}$ ,  $\theta'_{ni}$ ,  $\phi'_C$ ,  $\phi'_B$ ,  $\phi'_F$ ,  $\phi'_H$  and  $\phi'_P$  represent the same quantities as the corresponding unprimed symbols, but without irradiance.

#### 4.6. Difference in test conditions

##### 4.6.1. Outline

In this section, we will compare the differences in the test conditions that are generally adopted by each research and test institute for the SHGC evaluation of BIPV-m, concentrating on the requirements that have a large impact. Specific comments applying to the conditions used during the round robin tests are presented in Section 5.6.

##### 4.6.2. Differences due to environmental conditions

The configuration of the test apparatus for SHGC evaluation in each country is basically similar, consisting of a solar simulator, climatic chamber, metering box and cooling device, but there are differences in the conditions during the SHGC measurement, as documented in Table 2. SERIS and CSTB take into consideration the thermal transmission caused by the temperature difference between the climatic chamber and the metering box via the test sample when “summer” or “winter” boundary conditions are imposed. At Fraunhofer ISE, the temperature difference between indoors and outdoors is kept as small as possible to minimize the effect of thermal transmission through the test sample on the SHGC. The effect of the small remaining temperature difference is corrected when calculating the final SHGC value. At JTCCM, an SHGC evaluation is applied which does not cause a temperature difference between indoors and outdoors and is not affected by

thermal transmission via the test sample.

Since a higher HTC has the effect of accelerating the transfer of absorbed heat, it is directly related to the secondary radiation component  $q_i$  shown in Equations (2) and (3), and has a large impact on the evaluation of the SHGC. The indoor and outdoor HTC values are divided into two cases: “summer” and “winter”, and no seasonal variation. CSTB takes seasonal factors into account, and recommends the conditions of ISO 15099 [11] and ISO 52022-3 [29] listed in ISO 19467 [8]. Seasonal factors are not taken into account in the test facilities of JTCCM and SERIS, where there is no temperature difference between the climatic chamber and the metering box. Fraunhofer ISE currently uses the HTC values that are specified as reference conditions in EN 410, as documented in Table 2. The outdoor surface HTC is the same for JTCCM and SERIS. The indoor surface HTC is the same for Fraunhofer ISE, SERIS and CSTB, and JTCCM has a slightly higher setting.

##### 4.6.3. Differences due to solar simulator and spectral distribution

Each testing laboratory has a different type of solar simulator, with different spectral distributions (see Table 3 and Figs. 5, 8, and 10). The main differences are the types of lamps such as Xe-S, Xe-L and MH-S lamps, the number of lamps, the spatial distribution of the lamps and the distance from the solar simulator to the test sample surface. The Xe-S lamp has a spectral distribution and color that are closest to those of natural sunlight, but it has a high near-infrared radiant intensity, so durability is a problem. JTCCM uses two AC-powered Xe-L lamps. In addition, there is a strong spectral increase in the NIR range from 800 nm to 1000 nm, so the line spectrum in this spectral range is intentionally blocked with a filter. Since the intensity of Xe-L lamps is greater than Xe-S lamps, and the temperature is higher, the temperature of the Xe-L lamp is controlled by water cooling. As a result, the long-wavelength components in the NIR tend to decrease Fig. 5. The MH-S lamp has a spectral distribution close to that of daylight, good color rendering and high efficiency, and has characteristics close to that of a point light source, so that in combination with parabolic reflectors, a quite parallel beam of light with a large cross-section can be provided. It has been adopted by many research and testing laboratories such as Fraunhofer ISE Fig. 8, SERIS Fig. 10 and CSTB. However, these light sources are all AC-powered, such that the light intensity oscillates at 100 Hz.

ISO 19467 [8] specifies that the spectral match rating of the solar simulator is determined according to the method described in IEC 60904-9 [22] and must be within the range of 0.55 to 1.45. Table 3 shows the results for the investigated facilities, applying the criteria of IEC 60904-9:2007 [22] for spectral matching over the spectral range of 400 nm – 1100 nm, as not all participants were able to supply data for the solar spectral range (300 nm – 2500 nm) which is specified in ISO 19467 [8]. However, it is emphasized that radiation at all wavelengths within the solar spectral range is relevant when the SHGC value is determined. The spectral match rating over the complete solar spectrum will be determined in a future inter-laboratory comparison. In Table 3, the bold printed values are the ones where the degree of spectral matching over the limited spectral range is not satisfied according to the

**Table 3**  
Comparison of spectral match rating for each solar simulator [8].

Wavelength range [nm]	range specified by [8]	JTCCM	Fraunhofer ISE	SERIS	CSTB
300–400	from				compliant
400–500	0.55 to	0.66	1.20	1.33	with
500–600	1.45	0.62	1.04	1.18	ISO 19467
600–700		0.55	0.90	0.94	
700–800		<b>0.45</b>	0.61	0.76	
800–900		<b>2.32</b>	1.22	0.88	
900–1100		<b>1.88</b>	1.04	0.78	
1100–1700					
1700–2500					



criteria of IEC 60904-9:2007 [22]. The solar simulators of Fraunhofer ISE and SERIS each have a high spectral match rating (see Table 3, Fig. 8 and Fig. 10). Since the solar simulator of JTCCM did not aim to conform to ISO 19467, it does not satisfy the spectral match rate requirement [4,10]. However, a revised version of the standard specifying mismatch requirements, IEC 60904-9:2020 [28] has been published since ISO 19467 appeared in 2017 [8]. It specifies spectral matching over an extended spectral range (300 nm – 1200 nm), which would be more relevant for the evaluation of solar simulators that are intended for determining the SHGC of BIPV glazing. It will still be necessary also to specify mismatch criteria in the NIR range between 1200 nm and 2500 nm.

4.6.4. Differences due to DC light and AC light

ISO 19467 [8] does not specify the type of solar simulator, and there is a possibility that there is a difference due to the difference between DC-powered or AC-powered light, or between xenon and metal halide lamps. In the PV industry, the continuous-wave solar simulator is widely adopted for IV measurement. The reason for adopting the DC light is that the continuity of the IV characteristics can be guaranteed. If AC light is used as the light source for IV measurement, there may be oscillations in the IV characteristic due to the AC oscillations, and there may be a problem that accurate evaluation cannot be performed. For example, Fig. 12 shows the results of measuring the power generation of a BIPV module under MPP state using a Nippon Kernel PV analyzer under irradiation with an AC lamp at JTCCM.

It is clear that the output oscillates, which is assumed to be due to the AC light source. Thus, although the total amount of energy acquired is the same, there is variation in the amount of electricity generated at given any measurement point. Whether this is a problem or not, depends on the reaction time constant of the instrument measuring the IV characteristic.

For the construction industry, the building components that are being tested for their SHGC values usually have a large thermal mass and the measurement equipment has a slow response, such that the rapid oscillations of an AC-powered light are simply averaged out when the SHGC of a non-photovoltaic glazing unit is determined. However, since one SHGC evaluation of BIPV-m is performed in the power-generating state, it is better to use DC-powered light if possible, as the problem of oscillations in the measured current is avoided. Fig. 13 as a reference shows the result of an IV measurement made by CSTB with AC light. It can be seen that there is an amplitude in the oscillating current value. By contrast, at Fraunhofer ISE, the IV curves measured with an electronic ballast and using the AC-powered solar simulator of the calorimeter do not fluctuate in the same way, presumably because the response time of the instrument was long enough to average out the 50 Hz variation – see Fig. 13.

A difference in power generation between DC-powered light and AC-

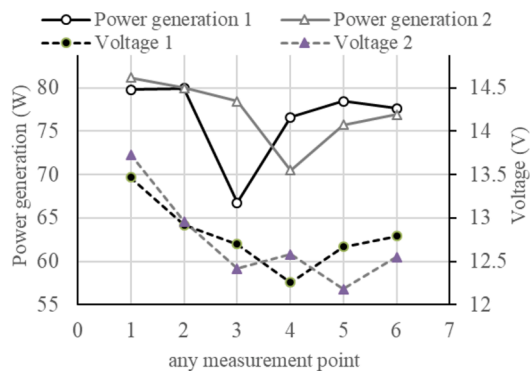


Fig. 12. Power generation and voltage derived from arbitrary measurement points in an IV characteristic measured at JTCCM using an AC lamp.

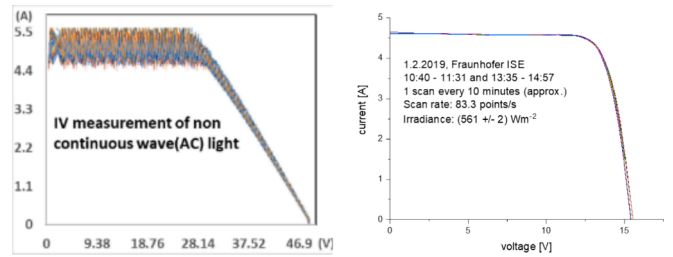


Fig. 13. IV characteristics determined for PV modules illuminated by AC light at CSTB (left) [19] and Fraunhofer ISE (right).

powered light can be observed, but it is not clear at this stage how much this will affect the amount of decrease in the secondary radiation  $q_i$ .

4.6.5. Differences due to irradiance distribution

The spatial distribution of the irradiance plays an important role in SHGC measurements during BIPV-m power generation. If the irradiance distribution is inhomogeneous, there is a concern that the output value of the BIPV-m will differ from that for homogeneous irradiance with the same average value, as the output current of a cell string will be limited by the cell receiving the lowest irradiance. The difference in output electric power then ultimately affects the SHGC evaluation. At the testing laboratories shown in Table 5, the non-uniformity of the irradiance, as defined in IEC 60904-9 [22,28], on the light-receiving surface at Fraunhofer ISE and SERIS is as small as 8 to 10 %, and it can be seen that the spatial distribution is quite smooth. On the other hand, JTCCM has large irradiance non-uniformity. This is not a problem for performing the SHGC measurement of a relatively uniform material like transparent laminated glass if the solar direct absorbance is low. However, it may affect the evaluation of SHGC if the test object itself has areas with different optical properties, as in a semi-transparent BIPV-m, or when power is generated by PV cell strings.

5. Test

5.1. Round robin test (RRT)

In an international RRT, the SHGC of BIPV-m was evaluated at each of the testing laboratories described in the previous chapter as preparation for formulating an international standard. In Test Series 1, the SHGC test was conducted with the BIPV-m in the OC state or MPP state. The SHGC values of single glazing test samples with different PV cell coverage ratios were also investigated in Test Series 2. The reason for using single glazing is that the structure is simple, comparison of results is easier, as the absolute effect of power extraction on the SHGC is larger than in better insulating double or triple glazing, and the influencing factors are easy to identify.

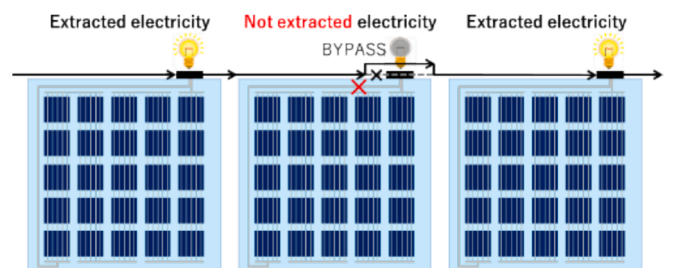


Fig. 14. Example of operation when an error occurs in a string of a BIPV system.

### 5.2. Test Series 1 – SHGC tests in the OC and MPP states

A BIPV-m is in the power-generating state if it is connected to a load in an environment exposed to solar radiation. This will change the SHGC value if the generated electricity is actually extracted. On the other hand, a BIPV-m is not always in the power-generating state, as it may have an electrical fault, or it may be an intentionally designed dummy module. A BIPV-m that does not generate power due to an error will be bypassed within the string and no power will be extracted from that part of the module (see Fig. 14). Dummy modules are often installed in buildings to achieve a uniform appearance, even at positions like a north-facing surface where power generation would be low, or at positions where the voltage is not uniform due to complicated geometrical shapes (see Fig. 15). In addition, some BIPV-m include dummy cells in the parts where frequent shading can be predicted, e.g. close to the window frame (see Fig. 15). Dummy modules, etc. have the same geometrical configuration as the active BIPV module, with no difference in appearance. Furthermore, even if BIPV-m are electrically connected and are irradiated, no electricity will be extracted if the output voltage of the BIPV installation at the inverter input is lower than the pre-programmed inverter threshold voltage. Therefore, SHGC evaluation of BIPV-m requires evaluation both with and without power generation and extraction.

Three main factors affecting the SHGC evaluation of BIPV-m were investigated here: the presence of various components such as PV cells, the uneven spatial distribution of materials up to the edges, and the effect of power generation by PV cells. Therefore, in this test, in order to cover these influencing factors, the test objects we used were a transparent glass laminate and a BIPV-m (25 PV cells) in the OC and MPP states. In addition, the RRT was conducted in order to confirm that, independent of test standards or test apparatus, SHGC during power generation and extraction is always smaller than that without power generation, in agreement with the law of conservation of energy as a phenomenon. Measurement and evaluation of BIPV-m in the OC and MPP states were conducted at three locations: JTCCM in Japan, Fraunhofer ISE in Germany, a major European laboratory, and SERIS in Singapore, which is located right on the equator.

### 5.3. Test Series 2 – SHGC tests with variation of PV cell coverage ratio

The SHGC test for varying PV cell coverage ratios investigated the effect on the SHGC of the ratio ( $\Sigma A_c / A_m$ ) of the total PV cell coverage ( $\Sigma A_c$ ) to the BIPV-m area ( $A_m$ ), for BIPV-m in the OC state only. As a hypothesis, it was predicted that SHGC would increase as the PV cell coverage ratio decreased, and that the slope would be constant. As shown in Fig. 16, a BIPV-m contains multiple materials with different optical characteristics, such as glass, encapsulant, PV cells, and bus bars, and PV cells in particular may have a significant impact on the SHGC evaluation. Therefore, the area ratio of PV cells in a BIPV-m is defined as the PV cell coverage ratio ( $\Sigma A_c / A_m$ ). In this test, four different BIPV-m with 0, 25, 16, and 9 PV cells were used as test objects, as specified in Table 4. In order to clarify the relationship between PV cell coverage ratios in test samples containing a mixture of multiple materials, it is

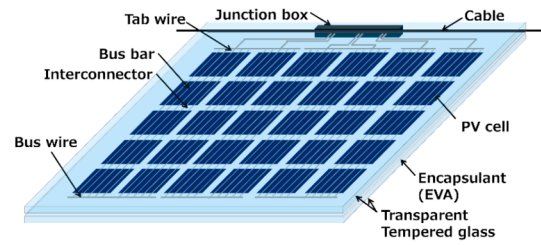


Fig. 16. Example of diverse materials composing a BIPV-m.

simpler to exclude the effect of power generation. Thus, the SHGC without power generation (OC state) was evaluated here. The measurement and evaluation of SHGC were conducted at two locations: JTCCM in Japan and CSTB in France.

### 5.4. General test methods for SHGC of BIPV modules

As mentioned above, there are some differences in the SHGC evaluation methods, depending on international standards, national standards, and standards of testing laboratories. Basically, the test sample is placed between the climatic chamber and the metering box. The solar simulator emits radiation with a spectrum close to that of natural AM 1.5 sunlight from the outside of the climatic chamber. This is transmitted, directly and as secondary heat, to the metering box, and the total amount of inward heat flux is measured. A cooled plate is installed in the metering box to keep the internal temperature constant, and the energy input for the cooling is used to identify the total amount of heat flux acquired in a “hot-box” method (CHB), or the heat flux is measured directly by heat flux meters in the “cooled-plate” method (HFM-CP). The thermal transmission through the walls and ceiling of the metering box must be well characterised and matches the heat balance including the input from the solar simulator. There are two fundamental types of measurement methodology. One is to set the temperature difference between the climatic chamber and the metering box by the test apparatus and to take the thermal transmission through the sample explicitly into account. The other measurement method avoids thermal transmission through the sample, as far as practicable, by setting the ambient “outdoor” and “indoor” temperatures to be almost equal.

As an example, Fig. 17 shows a schematic diagram of the ISO 19467 [8] measurement equipment with the additional electronic ballast instrument necessary for measuring BIPV power generation. This consists of an electronic load that matches the output characteristics of the BIPV-m in order to evaluate the MPP condition. The electronic load device is designed and programmed such that the BIPV-m can track the MPP during power generation. During the SHGC measurement, it is necessary to confirm that the test sample was generating electricity reliably. One approach is to attach a 100 mΩ shunt resistor to the terminal block and to check the IV (current voltage) periodically with a PV analyzer. In another approach, it is possible to program the commercially available electronic ballast to briefly interrupt the MPP tracking by an IV measurement, e.g. once every five minutes.

The IV curve is used to document the status with and without power generation, and to identify whether BIPV-m electrical errors occur during testing. Fig. 18 shows an example of IV curve measurement results. The IV curve shows the relationship between the operating current and operating voltage in a PV module for a specified incident irradiance level. In the figure, the vertical axis indicates current and the horizontal axis indicates voltage. When no power is generated, the PV module voltage is equal to the open-circuit voltage  $V_{oc}$  and no current flows; when power is generated, the output value is determined according to the IV curve. Equation 25 is the formula for calculating the maximum output at the MPP, and Equation 26 shows the fill factor (FF). The fill

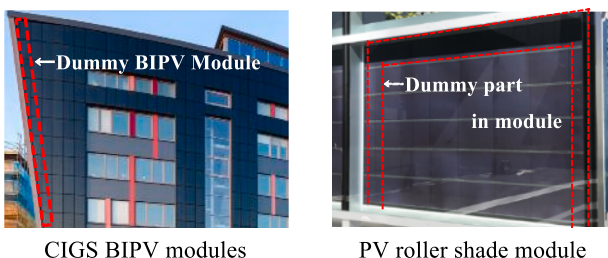
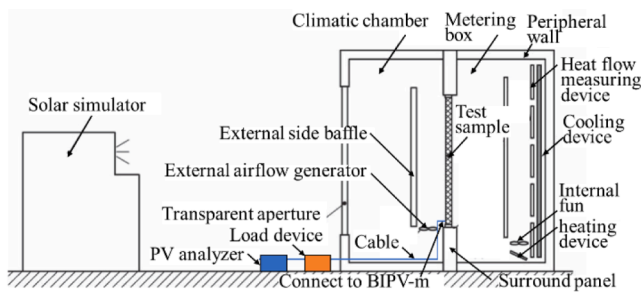


Fig. 15. Dummy BIPV-m [14] and dummy PV cells [31].

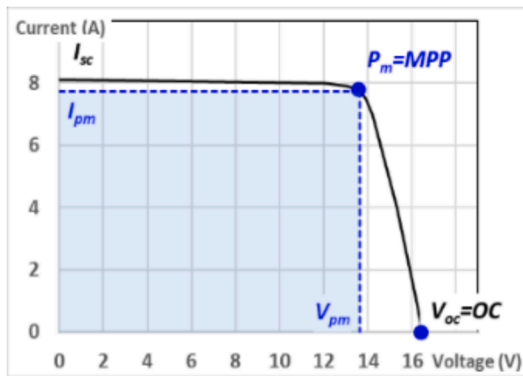
**Table 4**  
List of BIPV-m test samples with different PV cell coverage ratios [37,38].

Test sample	A0		A1		A2		A3	
Test sample No.	A0		A1		A2		A3	
Number of PV cell	0 PV cell		25 PV cells		16 PV cells		9 PV cells	
PV cell configuration	0 × 0		5 × 5		4 × 4		3 × 3	
Gap between PV cells (mm)	-		Each direction 3.5		Each direction 3.5		Each direction 3.5	
Cell-to-edge distance (mm)	-		101		181.15		261.3	
PV cell coverage ratio	0		0.61		0.39		0.22	
Peak power for 1.0 sun and 0.5 sun (W)	-		1 sun	0.5 sun	1 sun	0.5 sun	1 sun	0.5 sun
	0		Av.105	Av.52	Av.67	Av.33	Av.38	Av.19

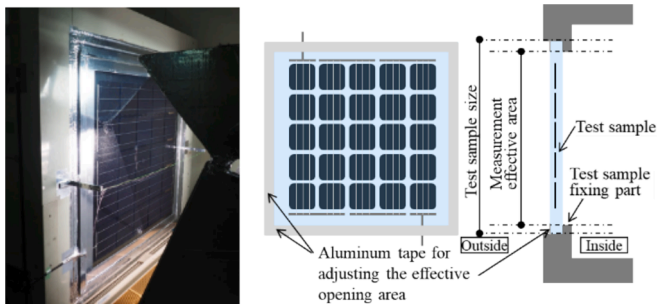


**Fig. 17.** Schematic SHGC evaluation for BIPV-m test apparatus with electronic ballast connection.

Adapted from Fig. 3 of [8]



**Fig. 18.** IV characteristic of BIPV-m.



**Fig. 19.** Adjustable mounting conditions to accommodate the difference in size between the test sample and the measurement aperture.

factor is one of the parameters that express the power generation characteristics of PV modules, and is mainly affected by the internal series resistance, parallel resistance, and diode factor. Therefore, the higher this value, the lower are the internal losses within the PV module and the higher is the power conversion efficiency of the PV module.

$$P_m = I_{pm} \times V_{pm} \tag{25}$$

$$FF = P_m / (I_{sc} \times V_{oc}) \tag{26}$$

At each testing laboratory, there is a dimensional difference between the test sample size and the effective aperture of the test apparatus, due to the test sample mounting (see Fig. 19).

Therefore, the edges of the test sample were masked with aluminum tape with a high reflectance in order to eliminate the influence of the edge region in the test samples so that the test conditions would be similar in all test facilities (see Fig. 19).

Although the effective aperture ( $A_{me}$ ) of the test sample for the measurement at all testing laboratories is slightly reduced compared to the width × height dimensions of the sample, the influence of the transparent perimeter can be effectively reduced. Both test samples were treated in the same way to achieve comparable test conditions in the tests with and without power generation and for the comparison of different PV cell coverage ratios. However, the width of the aluminum tape was 67 mm for the tests with and without power generation (test series 1), and 50 mm for the tests with different PV cell coverage ratios (test series 2). Thus, they were slightly different for the two types of tests, but the effects of the edges of the test samples were minimized in both cases.

### 5.5. Test samples

#### 5.5.1. Test samples for testing in the OC and MPP states

Considering the test facilities of each testing laboratory, the SHGC test samples for testing with or without power generation (Test Series 1) had width by height dimensions of 1 m × 1 m. The laminated glass test sample consisted of one pane of 5 mm low-iron, fully tempered glass and another pane of 5 mm fully tempered glass, and the PV cells and bus wires were encapsulated using two sheets of 600 μm ethylene vinyl acetate (EVA) film. These test samples were distributed to each testing laboratory by the Japanese PV module manufacturer. The total thickness of the test sample is 11.5 mm. However, it is evident from the spectra shown in Fig. 20 that the composition varied from sample to sample. The sample supplied to JTCCM and SERIS for this optical measurement are presumed to contain two panes of low-iron glass. By contrast, the samples supplied to Fraunhofer ISE were described as consisting of one low-iron glass pane and one iron-oxide-containing glass pane, which is consistent with the spectra shown. The absorption bands caused by the encapsulant in the samples supplied to Fraunhofer ISE also indicate that

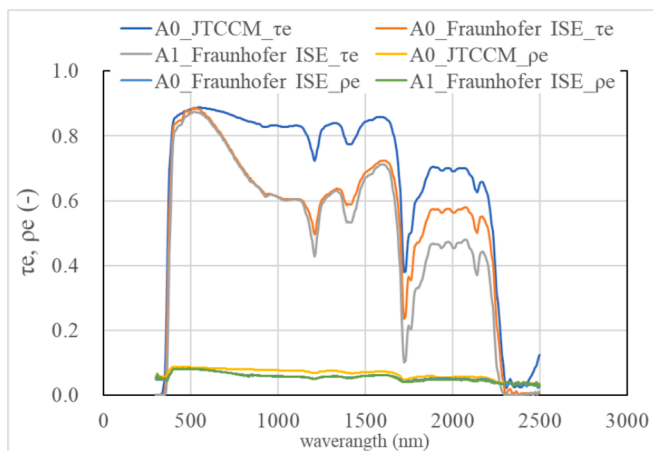


Fig. 20. Optical properties of the transparent areas of each test sample.

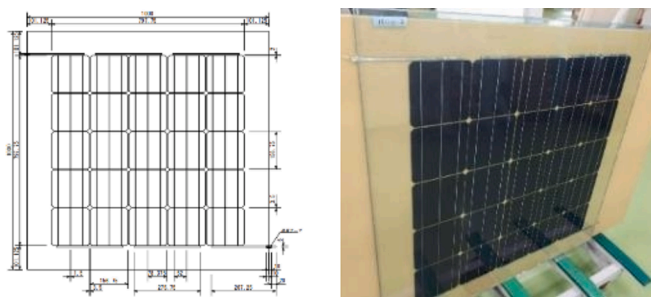


Fig. 21. Test sample (25 PV cells connected in series) [37].

the encapsulant layer was thicker for the A1 sample than the A0 sample. This discrepancy is probably explained by insufficient production time and a lack of awareness by the PV module manufacturer that the samples were intended to be used for a comparison of SHGC evaluation. Within the PV industry, it is of course widely known that a variation in the back glass pane composition or the encapsulant thickness has very little effect on the IV characteristic or the power conversion efficiency of a mono-facial module. The effect of the solar direct absorptance on the SHGC is less widely known.

As shown in Fig. 21, 25 single 6" PV cells were distributed to form a square matrix. The distance between adjacent PV cells in the test sample was set to 3.5 mm in the horizontal and vertical directions for ease of fabrication, and the distance from the PV cell edge to the glass edge was approx. 101 mm along all four sides of the BIPV-m. The PV cell used in this test sample is a mono-crystalline silicon PV cell (mc-Si) of the Passivated Emitter and Rear Cell type (PERC). The output was measured by irradiating the test sample three times under two irradiation conditions of 1 sun ( $1000 \text{ W/m}^2$ ) and 0.5 sun ( $500 \text{ W/m}^2$ ) using a Class AAA solar simulator in an environment with a room temperature of  $25 \text{ }^\circ\text{C}$  (STC: standard test conditions) according to IEC (International Electrotechnical Commission) 61215-2 [32]. The average output was about  $105 \text{ W/m}^2$  at 1 sun and about  $52 \text{ W/m}^2$  at 0.5 sun at the time of shipment.

### 5.5.2. Test samples with different PV cell coverage ratios

The test samples with different PV cell coverage ratios for Test Series 2 also have width  $\times$  height dimensions of  $1 \text{ m} \times 1 \text{ m}$ , again taking the requirements of the test apparatus in both countries into consideration. The A1 test sample was specified to be the same as the A1 test sample used for Test Series 1. Table 4 shows the test parameters such as the PV cell coverage ratio of the test samples. Different BIPV-m were prepared as single glazing laminates, with a PV cell coverage ratio of 0.00 when

the number of PV cells is 0, 0.61 with 25 PV cells, 0.39 with 16 PV cells, and 0.22 with 9 PV cells. Regardless of the number of PV cells, the same type and thickness of encapsulant was used for all test samples. The configuration and dimensions are all the same except for the direction in which the electrodes are taken out (e.g. A1, A3 vs A2). The output of each PV module was measured by irradiating the test sample three times under two irradiation conditions of 1 sun ( $1000 \text{ W/m}^2$ ) and 0.5 sun ( $500 \text{ W/m}^2$ ) according to IEC 61215-2 [32], similar to the SHGC test sample with and without power generation. Table 4 shows the average output values at the time of shipment. The BIPV module test samples with different PV cell coverage ratios were manufactured by the same manufacturer and with the same specifications as the test samples for the SHGC tests with and without power generation. However, it appears probable that different glass types were used for the two series of samples.

## 5.6. Test conditions at each testing laboratory

### 5.6.1. Overview of test conditions

Section 5.6 describes the test conditions applicable to each testing laboratory for the two different test series of the inter-laboratory comparison. Table 5 summarises the test conditions for all test laboratories. Tables 6 and 7 show the specific sample parameters and the effective PV cell coverage ratios for the two different test series. The effective sample aperture dimensions are the sample area values excluding the perimeter area that was covered by aluminum tape. The measurement was made with normally incident radiation (angle of incidence:  $0^\circ$ ) at all testing laboratories.

### 5.6.2. JTCCM

JTCCM conducted both test series, Test Series 1 in the OC and MPP states, and Test Series 2 with different PV cell coverage ratios. The basic test procedure was according to JSTM K 6101 [18], similar to the content explained in Chapter 4. However, the cross-flow ventilator was adjusted such that the outdoor surface HTC was  $20.3 \pm 2 \text{ W/(m}^2\text{K)}$ , and the indoor HTC was  $8.1 \text{ W/(m}^2\text{K)}$  in this test. The indoor and outdoor surface HTCs are close to those of other standards due to this change. The gap between the test sample and the installation frame of the test sample was filled with thermally insulating material and covered with aluminum tape in both tests.


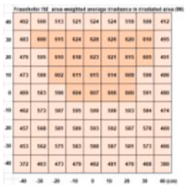
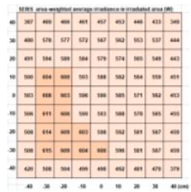
An electronic load as illustrated in Fig. 22 is connected for SHGC evaluation during BIPV-m power generation. The permissible values of this electronic load are 0 to 200 V, 0 to 20 A, and 185 W or less at DC, such that the BIPV-m power generation, open-circuit voltage  $V_{OC}$ , and short-circuit current  $I_{SC}$  all lie within its measurement range.

### 5.6.3. Fraunhofer ISE

The HFM-CP method was used to measure both the BIPV-m and the benchmark transparent glass laminate samples at Fraunhofer ISE. The measurement method conforms to Reference [20]. The samples were each mounted with air-tight sealing material in front of the cooled absorber plate of the calorimeter. Lateral heat losses were minimised with an insulating frame of polystyrene. For measurement of the BIPV-m test sample, an additional black painted metal plate with an area of  $1000 \text{ mm} \times 1000 \text{ mm}$  and a thermally separated zone in the middle of the plate (width: 200 mm) was mounted behind the sample in front of the measurement absorber, covering this completely. This was done to average the measurement for the cell areas and the transparent gaps between the cells by homogenising the heat flux behind the sample, especially in the separated zone of the plate. The averaged heat flux of an area of about  $200 \text{ mm} \times 520 \text{ mm}$  behind the centre of the sample was measured (see Fig. 23). The three heat flux meters 4, 5 and 6 were evaluated to determine the SHGC value. 520 mm is the height between the upper edge of heat flux meter 4 and the lower edge of heat flux meter 6. The test for the reference glass laminate was carried out without the additional metal plate (see Fig. 23).

**Table 5**

Test conditions applied by the different testing laboratories during the two SHGC test series of the inter-laboratory comparison.

Country Testing laboratory	Japan Japan Testing Center for Construction Materials JTCCM	Germany Fraunhofer Institute for Solar Energy Systems Fraunhofer ISE	Singapore Solar Energy Research Institute of Singapore SERIS	France Centre Scientifique et Technique du Bâtiment CSTB
OC or MPP state test period (Test Series 1)	Jan. 2019	Feb. 2019	Feb. 2019	-
PV cell coverage ratio test period (Test Series 2)	Jan. 2020	-	-	Mar. 2020
Implemented standards	JSTM K6101 [18]	ISO 19467-2 [9]	ASTM C1363[34], C1199[35], and NFRC 201[36]	ISO 19467[8]
Incidence angle of solar-sim radiation (°)	0	0	0	
Sample type	A0 A1, A1(MPP) A1, A2, A3	A0 A1, A1(MPP)	A0 A1, A1(MPP)	A0 A1, A2, A3
Average irradiance over evaluated sample area (W/m <sup>2</sup> )	803 828, 881, 934	303* <sup>3</sup> 606* <sup>3</sup>	539 539, 542* <sup>2</sup>	
Test Series	1 2	1	1	2
Maximum irradiance in irradiated sample area (W/m <sup>2</sup> )	1091 1091	322 632	615 615	N/A
Minimum irradiance in irradiated sample area (W/m <sup>2</sup> )	364 364	269 541	505 506	N/A
Mean irradiance over irradiated sample area (W/m <sup>2</sup> )	803 802	298 594	580 582	N/A
Irradiance spatial distribution of effective measurement area* <sup>4</sup> (W/m <sup>2</sup> )				not available
inhomogeneity	0.50	0.08	0.10	N/A
“Outdoor” temperature (°C)	20	25 – 26	23.2~21.2	20
Metering box temperature (°C)	20	25 - 26* <sup>1</sup>	24.1~24.3	20
Outdoor HTC (W/(m <sup>2</sup> ·K))	20.3	25 ±3	-	12.7~ 13.2
Indoor HTC (W/(m <sup>2</sup> ·K))	8.1	7.7 ±1	-	12.3~12.5
Outdoor wind velocity (m/s)	-	-	1.9	-
Indoor wind velocity (m/s)	-	controlled by cavity size	0.2	-

\*<sup>1</sup> The “metering box temperature” for Fraunhofer ISE refers to the surface temperature of the cooled absorber plate during measurement.

\*<sup>2</sup> The average irradiance of SERIS is 539 W/m<sup>2</sup> for the OC measurement and 542 W/m<sup>2</sup> for the MPP measurement.

\*<sup>3</sup> This is the irradiance value for the centre of the glazing that is used for the SHGC evaluation.

\*<sup>4</sup> It should be noted that the values given for all the regions along the four edges in all institutions are low because they included the areas behind the opaque masking where the irradiance is 0 W/m<sup>2</sup>.

**Table 6**

Sample parameters and measured effective cell coverage ratio for test series 1 in the OC and MPP states.

Test parameter	Effective areas during measurement			PV cell coverage ratio in irradiated area	Japan JTCCM	Germany Fraunhofer ISE	Singapore SERIS	France CSTB
	Irradiated width × height (m)	Irradiated area (m <sup>2</sup> )	PV cell area (m <sup>2</sup> )					
0 PV cell	0.866 × 0.866	0.7499	0.0000	0.0000	A0	A0	A0	-
25 PV cells (OC)	0.866 × 0.866	0.7499	0.6084	0.8113	A1	A1	A1	-
25 PV cells (MPP)	0.866 × 0.866	0.7499	0.6084	0.8113	A1(MPP)	A1(MPP)	A1(MPP)	-

**Table 7**

Sample parameters and measured effective cell coverage ratios for test series 2 with different PV cell coverage ratio in the OC state.

Test parameter	Effective areas during measurement			PV cell coverage ratio in irradiated area	Japan JTCCM	Germany Fraunhofer ISE	Singapore SERIS	France CSTB
	Irradiated width × height(m)	Irradiated area (m <sup>2</sup> )	PV cell area (m <sup>2</sup> )					
0 PV cell	0.900 × 0.900	0.8100	0.0000	0.0000	A0	-	-	A0
25 PV cells	0.900 × 0.900	0.8100	0.6084	0.7511	A1	-	-	A1
16 PV cells	0.900 × 0.900	0.8100	0.3894	0.4807	A2	-	-	A2
9 PV cells	0.900 × 0.900	0.8100	0.2190	0.2704	A3	-	-	A3

With a cross-flow ventilator, wind conditions were established on the outdoor surface of the sample with a wind speed of 3 m/s - 4 m/s. This corresponds to an outdoor heat transfer coefficient HTC of 25 ± 3 W/(m<sup>2</sup>K), corresponding to the standard conditions of EN 410:2011 [12]. The distance between the inner surface of the sample and the absorber was chosen such that the indoor HTC was 7.7 ± 1 W/(m<sup>2</sup>K), again corresponding to the standard conditions according to EN 410:2011 [12]. The absorber surface temperature (internal temperature for the

measurement) and the air temperature in the measurement chamber (external temperature) were each about 25 - 26 °C. Depending on the position of the lamps, the light from the solar simulator has a divergence of 3° - 12°; the effect of divergence on the measured SHGC is thoroughly analysed in [33]. The four lamps were set up in a 2 × 2 configuration (as illustrated in Table 2), such that the resulting divergence was as small as possible in the plane in which the tested sample in question would react sensitively to divergent radiation. The spectrum of the incident radiation

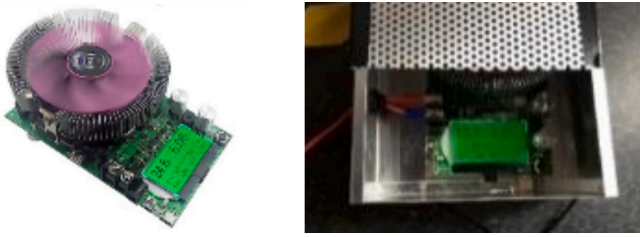


Fig. 22. Electronic load device as used by JTCCM and SERIS [37].

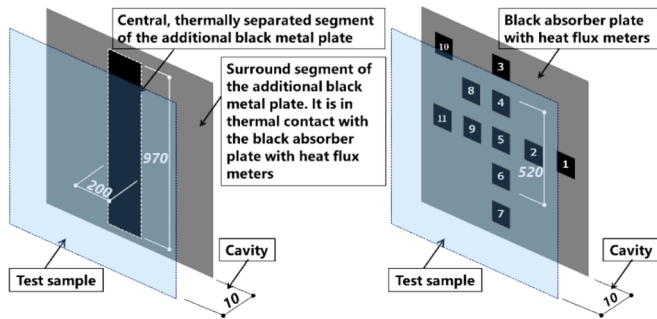


Fig. 23. Schematic image of the usual HFM-CP configuration at Fraunhofer ISE (right) and the additional black metal plate (left) that was positioned in direct thermal contact with the cooled absorber plate for the BIPV-m sample measurement.

from MH-S lamps is practically identical to the standard spectrum specified in EN 410:2011 [12]. For this reason, the measurement results were not corrected spectrally. For the test of the transparent glass laminate, the incident irradiance on the centre of the sample was set to  $306 \text{ W/m}^2$ , and was  $606 \text{ W/m}^2$  during the test of the BIPV-m (see Table 4). An electronic ballast (type: ESL solar) which adjusts the resistance automatically was used by Fraunhofer ISE for the MPP tracking.

#### 5.6.4. SERIS

SERIS conducted its measurements using a CHB and a solar simulator (see Fig. 8). Both devices are installed in a large air-conditioned room, which also serves as a temperature-controlled room. The test sample was placed in the  $0.95 \text{ m} \times 0.95 \text{ m}$  portion of the effective aperture area of the metering box (see Fig. 9). A gap of less than 5 mm between the edge of the test sample and the surrounding panel was filled with cotton wool to achieve thermal insulation, and all joints were sealed with packaging tape to ensure airtightness. The outdoor surface of the test sample was ventilated with a wind speed of  $2.0 \text{ m/s}$  by an external air curtain so that the outdoor surface HTC was kept within the range of  $18 \text{ W/(m}^2\text{K)} \pm 10 \%$ . In addition, by setting the wind speed on the back of the test sample in the metering box to  $0.2 \text{ m/s}$ , the indoor surface HTC was kept within  $7.7 \text{ W/(m}^2\text{K)} \pm 5 \%$  as specified. The temperature in the air-conditioned room during the test was  $21.1 \text{ }^\circ\text{C}$  to  $23.2 \text{ }^\circ\text{C}$ , and the temperature inside the metering box and guard box was set to  $24 \text{ }^\circ\text{C}$ , but the actual temperature was  $24.1 \text{ }^\circ\text{C}$  to  $24.3 \text{ }^\circ\text{C}$ . Fig. 10 shows the spectrum of incident light generated by the solar simulator with one 18 kW MH-S lamp. Here, the average irradiance was  $539 \text{ W/m}^2$  when the transparent glass and the BIPV-m in the OC state were measured and  $542 \text{ W/m}^2$  when the BIPV-m was measured in the MPP state. The steady-state heat flux through the test sample was measured to determine the SHGC. The electronic load device used in SERIS was the same as JTCCM (see Fig. 22).

#### 5.6.5. CSTB

CSTB's "Gmètre" is based on the CHB methodology, and consists of three chambers, the solar simulator, a cooling device, and peripheral

devices. The test sample is installed between the climatic chamber and the metering box. The effective aperture of the measuring device was  $0.95 \text{ m} \times 0.95 \text{ m} (\pm 0.05 \text{ m})$ , and the gap between the aperture and the test sample was filled with thermal insulating material. The temperature in each chamber was maintained at  $20 \text{ }^\circ\text{C}$ . The surface HTC values of the test sample differ slightly from the test parameters before and after irradiation, such that the outdoor HTC was  $12.7$  to  $13.2 \text{ W/(m}^2\text{K)}$  and the indoor surface HTC was maintained within the range of  $12.3$  to  $12.5 \text{ W/(m}^2\text{K)}$ . At the time of measurement, it took at least 3 h to reach a steady state. The estimated uncertainty of the g-value measurement is  $\pm 0.05$ .

## 6. Test results and discussion

### 6.1. Test Series 1 – SHGC tests by OC state and MPP state

#### 6.1.1. Test results

Table 8 shows the results of SHGC measurements conducted at each testing laboratory, and Table 9 shows the measurement results of each element necessary in the SHGC evaluation process. The SHGC of the A0 test sample (transparent glass laminate) was close to 0.77 for JTCCM and 0.76 for Fraunhofer ISE, but SERIS was 0.82 which was 6 - 7.5 % higher. As discussed in Section 6.1.2, this is assumed to be due to the fact that the tested samples had different compositions.

The SHGC of the A1 test sample (BIPV-m under OC state) was close to 0.40 for JTCCM and 0.40 for SERIS, but Fraunhofer ISE was 0.27, which was approx. 30 % lower than JTCCM and SERIS using CHB. In addition, the SHGC of the A1(MPP) test sample (BIPV-m under MPP state) was close to 0.38 for JTCCM and 0.37 for SERIS, but Fraunhofer ISE was 0.23 which was approx. 40 % lower than JTCCM and SERIS using CHB. Reasons for these differences are discussed in Section 6.1.2. The relation of the A1(MPP) test result to the A1 test result was similar for each individual laboratory. Although there were some differences in the test results among the testing laboratories, when comparing the SHGC measurement results for the OC and MPP states, the SHGC value for the MPP state is always lower than for the OC state. The difference between the SHGC value without and with power generation was 0.02 (5 %) for JTCCM, 0.04 (14.8 %) for Fraunhofer ISE and 0.03 (6.8 %) for SERIS. This reduction  $P_e$  is caused by the conversion of some of the light energy absorbed by the PV cell into electricity and its extraction from the BIPV-m, reducing the amount of heat transferred indoors. Due to this mechanism, the reduction  $P_e$  always occurs during power generation, regardless of the type of PV cell technology and whether the PV cells are opaque or transparent. From the above, it was reconfirmed by the international RRT that the SHGC is lowered when power is generated and extracted (MPP) compared to the OC state, regardless of the test methodology or test apparatus.

#### 6.1.2. Discussion of glass laminate results (A0)

Fig. 20 shows the result of the spectral measurements made by Fraunhofer ISE of the provided A0 test sample and the transparent area of the provided A1 test sample, and those made by JTCCM of a small laminate sample which the PV manufacturer described as being identical to the distributed test samples. It is evident that the three spectra differ more than the usual experimental error of 0.01 for these straightforward optical measurements of non-scattering, transparent samples. The spectral distribution for the samples provided to Fraunhofer ISE show strong absorption in the range that is typical for iron oxides in glass ( $\alpha_e = 0.22$  and  $0.24$ ), whereas the sample measured by JTCCM shows much weaker absorption in this range ( $\alpha_e = 0.11$ ), indicating that the laminate probably contained only low-iron glass panes. Applying the method of ISO:9050 [10] to calculate the SHGC value from the transmittance and reflectance spectra, values of 0.77 and 0.76 were calculated for the A0 and A1 (transparent region) samples provided to Fraunhofer ISE, which agrees well with the calorimetrically determined value at Fraunhofer ISE of 0.76 reported in Table 9. By

**Table 8**  
Comparison of SHGC test results and reduction  $P_e$  due to power generation [37].

Test parameter	JTCCM			Fraunhofer ISE			SERIS			
		SHGC	Reduction ratio relative to A0	SHGC	Reduction ratio relative to A0		SHGC	Reduction ratio relative to A0		
PV cell 0	A0	<b>0.77</b>	1.000	A0/A0	<b>0.76</b>	1.000	A0/A0	<b>0.82</b>	1.000	A0/A0
PV cell 25 OC	A1	<b>0.40</b>	0.526	A1/A0	<b>0.27</b>	0.351	A1/A0	<b>0.40</b>	0.485	A1/A0
PV cell 25 MPP	A1(MPP)	<b>0.38</b>	0.500	A1(MPP)/A0	<b>0.23</b>	0.299	A1(MPP)/A0	<b>0.37</b>	0.452	A1(MPP)/A0
Absolute difference	A1-A1(MPP)	<b>0.02</b>			<b>0.04</b>			<b>0.03</b>		
Reduction effect	$P_e^{*1}$	<b>5.0</b>			<b>14.8</b>			<b>6.8</b>		

\*1  $P_e$  (%):(A1-A1(MPP))/A1.

**Table 9**  
Measurement results for each element required for evaluation of SHGC with and without power generation [37].

JTCCM	Fraunhofer ISE				SERIS							
	BM 3mm (= FL3)	A0	A1	A1(MPP)	A0	A1	A1(MPP)					
	0 cell	0 cell	25 cell	25 cell	0 cell	25 cell	25 cell					
	–	–	OC	MPP	–	OC	MPP	–	OC	MPP		
$I_{solar}$ (W/m <sup>2</sup> )	882	888	802	801	$I_{solar}$ (W/m <sup>2</sup> )	306	606	606	$I_{solar}$ (W/m <sup>2</sup> )	539	539	542
$A_s$ (m <sup>2</sup> )	0.7499	0.7499	0.7499	0.7499	$A_s$ (m <sup>2</sup> )	0.7499	0.7499	0.7499	$A_s$ (m <sup>2</sup> )	0.7499	0.7499	0.7499
Q (W)	582.4	512.7	264.7	251.0	$Q_c$ (W)				$Q_c$ (W)	–372.4	–188	–173.6
c (J/(kg K))	1008	1008	1008	1008	$Q_e$ (W)				$Q_e$ (W)	12.9	12.9	12.9
$\gamma$ (kg/m <sup>3</sup> )	1.191	1.183	1.190	1.187	$Q_{wi}$ (W)				$Q_{wi}$ (W)	5.3	3.3	4.2
$T_{out}$ (°C)	25.04	26.94	24.48	25.05	$Q_{fi}$ (W)				$Q_{fi}$ (W)	10.5	10.5	10.5
$T_{in}$ (°C)	21.57	23.87	22.92	23.56	$\theta_{ne}$ (°C)	25.4	25.4	25.6	$Q_{sp}$ (W)	7.5	2.83	–2.77
$T_{av, CHB}$ (°C)	23.305	25.405	23.7	24.305	$\theta_{ni}$ (°C)	24.7	26.4	25.8	$Q_u$ (W)	5.4	–1.66	–1.47
G (m <sup>3</sup> /h)	503.24	504.29	509.42	506.77	$Q_s$ (W)				$Q_s$ (W)	330	160	150
shading coefficient		0.88	0.45	0.43								
$Q_{FL3}$	582.4	–	582.4	582.4								
SHGC <sub>FL3</sub>	0.88	–	–	–								
SHGC	–	<b>0.77</b>	<b>0.40</b>	<b>0.38</b>	SHGC	<b>0.76</b>	<b>0.27</b>	<b>0.23</b>	SHGC	<b>0.82</b>	<b>0.40</b>	<b>0.37</b>

**Table 10**  
Measurement results for each quantity required for evaluation of the SHGC for varying PV cell coverage ratios [38].

JTCCM	CSTB													
	BM 3mm (= FL3)	A0	A1	A2	A3									
	0 cell	0 cell	25 cell	16 cell	9 cell									
$I_{solar}$ (W/m <sup>2</sup> )	832	835	827	834	828	$I_{solar}$ (W/m <sup>2</sup> )	306	606	606	606				
$A_s$ (m <sup>2</sup> )	0.81	0.81	0.81	0.81	0.81	$A_s$ (m <sup>2</sup> )	0.81	0.81	0.81	0.81				
Q (W)	593.0	568.1	321.4	459.1	496.5	Solar sim	off	on	off	on	off	on		
c (J/(kgK))	1008	1008	1008	1008	1008	$\Delta T_{TE}$ (°C)	0.59	2.03	0.59	1.60	0.59	1.69	0.57	1.79
$\gamma$ (kg/m <sup>3</sup> )	1.185	1.184	1.193	1.193	1.191	$LE_{fl}$ (m <sup>3</sup> /h)	0.51	0.50	0.49	0.47	0.48	0.47	0.51	0.49
$T_{out}$ (°C)	26.48	26.62	23.72	24.1	24.81	$TE_{rd}$ (W)	285	959	276	709	276	751	276	838
$T_{in}$ (°C)	23.13	23.38	21.89	21.5	22	$TE_{cd}$ (W)	146	826	137	577	135	618	138	706
$T_{av, CHB}$ (°C)	533.41	528.75	525.69	528.5	529.99	$hi$ (W/(m <sup>2</sup> K))	12.2	12.5	12.2	12.3	12.2	12.3	12.2	12.3
G (m <sup>3</sup> /h)	24.805	25	22.805	22.8	23.405	$he$ (W/(m <sup>2</sup> K))	13.0	13.2	12.8	13.2	12.8	13.1	12.4	12.7
shading coefficient		0.96	0.54	0.77	0.84	Balance	680	440	482	482	568			
$Q_{FL3}$	582.4	–	–	–	–	on / off								
SHGC <sub>FL3</sub>	0.88	–	–	–	–									
SHGC	–	<b>0.84</b>	<b>0.48</b>	<b>0.68</b>	<b>0.74</b>	SHGC	<b>0.82</b>	<b>0.44</b>	<b>0.56</b>	<b>0.66</b>				

contrast, the SHGC value resulting from the small sample provided to JTCCM is 0.84, which agrees with the value determined calorimetrically by JTCCM and reported in Table 10. Comparing these SHGC values with those reported in Table 9 and Table 10 for the A0 samples provided to the different test institutes, it seems probable that the A0 results apply to clear laminates of at least two different compositions. The SHGC values determined calorimetrically for A0 in the first measurement series by JTCCM and Fraunhofer ISE almost certainly refer to laminates that contain at least one pane of iron-containing glass, whereas the values determined for A0 samples by SERIS in Test Series 1 and by JTCCM and CSTB in Test Series 2 probably refer to laminates containing only panes of low-iron glass. Assuming that this hypothesis of two different sample compositions is correct, the agreement in calorimetrically determined SHGC values between the different institutes is good. Unfortunately, it was not possible to measure the relevant spectra for all distributed

samples four years after the round robin had taken place. This observation underlines the importance of initial sample screening to ensure that “identical” samples are indeed very similar, before they are distributed for measurement in an inter-laboratory comparison.

6.1.3. Discussion of BIPV-m results (A1)

At present, our hypothesis is that one of the reasons for the different results obtained by the testing laboratories for the BIPV-m sample is the difference due to the characteristics of the CHB methodology, evaluating the entire irradiated aperture area of the sample, and the HFM-CP methodology in the “centre-of-glass” version as described by [9].

JTCCM and SERIS each used a CHB. The CHB methodology determines the SHGC by summing the amount of heat input into the metering box through the test sample, the amount of heat entering and exiting from the surrounding area, and the amount of heat input to keep

the temperature constant within the metering box. A BIPV-m consists of diverse materials with different optical properties, and the PV cells are not evenly distributed over the entire area of the BIPV-m, as there is a transparent region around the edges, adding a further degree of spatial complexity. However, in the case of a CHB, it is possible to collect all the heat flows input into the metering box even for a test sample in which different materials are combined, as in BIPV-m. On the other hand, in the centre-of-glass version of HFM-CP, the test methodology applied by Fraunhofer ISE, the average heat flux into the black cooled absorber plate behind the test sample is measured with one or more heat flux sensors (see Fig. 23 (right)). An additional intermediate black metal plate was used for the A1 measurements to spatially average the heat flux through the BIPV-m over an area of 200 mm × 970 mm as illustrated in Fig. 23 (left). The heat fluxes determined by the heat flux meters 4, 5 and 6 were used to determine the SHGC values of the BIPV-m. Therefore, this evaluation methodology intentionally does not evaluate the complicated heat flux contribution at the edge of the test sample; the equipment is designed to implement the procedures of ISO 19467-2 [9] to determine the centre-of-glazing g value. It is presumed that one cause of the large difference in the measurement results from the three laboratories for the A1 samples (BIPV-m with 25 PV cells) in the OC and MPP states was related to the heat flow input through the transparent glass part along the perimeter of the BIPV-m. This hypothesis is consistent with the fact that the SHGC values determined for the BIPV-m by JTCCM and SERIS, where a larger transparent share of the BIPV-m is evaluated, are significantly higher than those determined by Fraunhofer ISE, both in the OC and MPP. The measured SHGC values from JTCCM and SERIS are also very similar to each other, both in the OC state and during power generation in the test results of the A1 and A1 (MPP) test sample (25 PV cells). The lower SHGC results determined by Fraunhofer ISE are considered to be partly due to the selection of the sample area which is evaluated by the center-of-glass measurement method. One of the reasons for this is that the SHGC ratio of the A1 test sample to the A0 test sample Table 8 is 0.351 for Fraunhofer ISE and 0.526 for JTCCM. This indicates that the shielding effect by the PV cells was weighted more strongly in test results of Fraunhofer ISE. This is because the effective measurement area for the centre-of-glass version of the HFM-CP methodology is 200 mm × 520 mm in the center of the test sample, and the proportion of transparent glass in that area is as low as 6.4 % (see Fig. 24 (left)). In the JTCCM and SERIS test samples, the area of the transparent glass part in the effective measurement area of 0.7499 m<sup>2</sup> is 0.1416 m<sup>2</sup>, which accounts for 18.9 % (see Fig. 24 (right)). We consider that this is the main explanation for the difference between the two sets of results.

A further reason for the lower SHGC value determined for the A1 sample by Fraunhofer ISE is given by the values for the HTC documented in Table 5. Compared to JTCCM, the values at Fraunhofer ISE are significantly higher for the outdoor HTC and slightly lower for the

indoor HTC. In combination with the low thermal resistance offered by the tested BIPV-m sample (effectively single glazing), the proportion of absorbed radiation transferred indoors as heat should be noticeably lower at Fraunhofer ISE than at JTCCM, also contributing to the lower SHGC value. The dependence of the SHGC on the relative values of outdoor HTC, indoor HTC and thermal resistance of the BIPV-m is presented by Wilson et al. [39].

The difference between JTCCM and SERIS for the A1 sample was zero, and the difference between the A1(MPP) samples was also 2.6 %, so they are in good agreement, within experimental tolerances. Initially, it was predicted that there would be differences due to the spectral characteristics and irradiation inhomogeneity of each solar simulator, but in fact no significant difference was observed. In addition, the sensitivity of the spectral response in the mc-Si PV cells of the A1(MPP) test sample increases in the NIR (Fig. 3), but in the spectral distribution of the solar simulator, the intensity in the NIR is higher in JTCCM than in SERIS. For this reason, it was predicted that the SHGC of JTCCM would be lower than for SERIS, as the JTCCM energy conversion by the photovoltaic effect would be higher than at SERIS. However, the SHGC value determined at SERIS during power generation was actually slightly lower than at JTCCM.

The transparent and the opaque parts of the BIPV-m sample are not uniformly arranged from the center to the edge (see Fig. 17), such that the effect of irradiation non-uniformity is large. For these specific samples, it is not known whether the A1 samples provided to JTCCM and SERIS include glass with a non-negligible iron oxide content, further adding to the uncertainty of the comparison. Thus, the explanations for the difference in results must remain qualitative, but it will be necessary to make quantitative comparisons again in the future, ensuring that the sample compositions are identical and taking the spectral match rating of the solar simulator radiation, the SR of PV cells, and irradiation inhomogeneity into account.

6.2. Test Series 2 –SHGC tests for different PV cell coverage ratios

6.2.1. Test results

In contrast to the first test series discussed in Section 6.1, the BIPV-m samples presented here were all in the OC state during the SHGC measurements. Fig. 25 and Table 11 present the SHGC results as a function of the cell coverage ratio, and Table 10 shows the measurement results for each quantity needed for the SHGC evaluation process.

Firstly, as the PV cell coverage ratio increases from 0 % to 27 %, 48 %, and 75 %, the PV cell shielding effect increases, and SHGC shows a clear downward trend for both JTCCM and CSTB. The JTCCM test results show some fluctuations, but the least squares method shows that linearity is

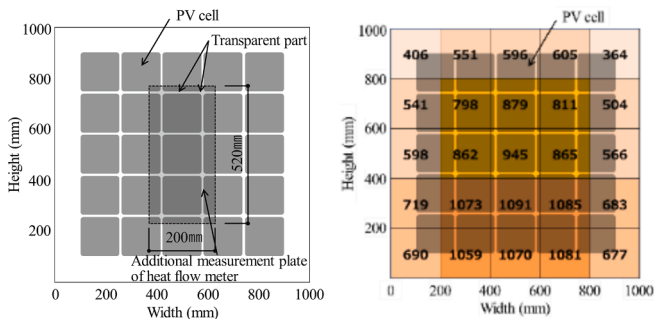


Fig. 24. Evaluated heat flux meter area for determining the centre-of-glazing SHGC of the BIPV-m sample with the HFM-CP methodology at Fraunhofer ISE (left) and PV cell positions and the spatial irradiance distribution at JTCCM (right).

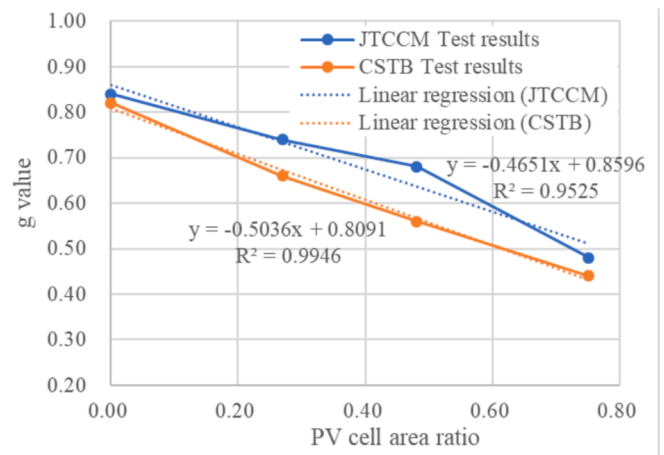
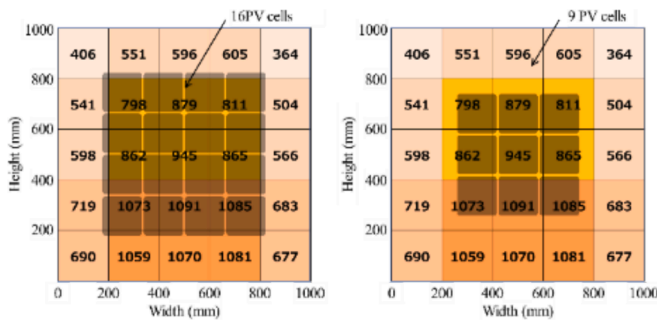


Fig. 25. SHGC [g value] measurement results versus PV cell coverage ratio [38].



**Table 11**  
SHGC test results by PV cell coverage ratio.

Test parameter	Test result of SHGC		Difference from results of CSTB	
	CSTB	JTCCM	(%)	Limit of error
A0 PV 0 cell	0.82	0.84	+2.4	OK
A3 PV 9 cells OC	0.66	0.74	+12.1	NG
A2 PV 16 cells OC	0.56	0.68	+21.4	NG
A1 PV 25 cells OC	0.44	0.48	+9.1	OK



**Fig. 26.** Relation of PV cell positions in the A2 and A3 samples and spatial distribution of the irradiance at JTCCM.

generally obtained, with  $R = 0.9525$ . On the other hand, the linear fit to the test results of CSTB is characterized by  $R = 0.9946$ , which indicates much higher linearity than at JTCCM. CSTB applies the CHB methodology according to ISO 19467 [8], and ensures that the specified measurement conditions such as spectral match and high spatial homogeneity of the irradiation are met; we thus believe that highly accurate results were obtained.

**6.2.2. Discussion of glass laminate results (A0)**

In order to clarify the differences due to test methodologies and test apparatus, it is effective to start with the transparent glass laminate, which has a simple structure. Table 11 shows the difference between the SHGC measurement results from JTCCM and CSTB. The result of JTCCM differs only by +2.4 % with that from CSTB, which is a good level of agreement. This indicates that the determined SHGC result is not sensitive to the measurement method, spectral match rating, irradiation homogeneity, etc., if the test sample is spatially homogeneous and has low absorptance and low spectral selectivity, as is the case for transparent glass laminate made of low-iron glass. Here, the limit of error (allowable error) for JTCCM is approx. 10 %. OK or NG indicates whether or not it is within the allowable difference, again assuming that results for samples with similar compositions are being compared.

**6.2.3. Discussion of BIPV-m results for different PV cell coverage ratios (A1, A2, A3)**

The difference between the test results of CSTB and JTCCM was significant when the PV cell coverage ratios were 27 % (9 PV cells) and 48 % (16 PV cells). These differences are not within the allowable range, even considering the JTCCM tolerance of  $\pm 10$  %.

This difference is assumed to be caused by the spectral match rating and the inhomogeneous spatial distribution of irradiance characterising the solar simulator of JTCCM Table 2. As a basis for analysing the effect of spatial inhomogeneity, Fig. 24 (right) shows the relationship between the irradiance distribution of the solar simulator at JTCCM and the arrangement of PV cells in the A1 test sample.

The secondary radiation  $q_i$  to the indoor side increases linearly with the absorbed incident radiation. Diverse materials with different optical properties are often combined in BIPV-m samples, and the spatial distribution of the PV cells may also differ between the central part and the perimeter, as in the A1, A2 and A3 test samples (see Fig. 24 and Fig. 26).

For this reason, measurement errors may occur, even when power is

not being generated, if the irradiance distribution for the solar simulator is very inhomogeneous and several materials with different optical properties are combined. Spatial inhomogeneity of the irradiance distribution was generally within 8–10 % for Fraunhofer ISE and SERIS in Test Series 1 but not for JTCCM. (CSTB did not provide detailed data on irradiance.) An additional error is introduced by inhomogeneous radiation in the power-generating state if the PV cells are connected in series in one or more strings within a PV module. The generated and extracted module power will be determined by the cell located at the position of lowest irradiance, rather than by the average irradiance over the evaluated irradiated aperture area.

**7. Conclusion**

In this study, in order to prepare a calorimetric SHGC evaluation methodology for BIPV modules as an international standard, we compared the SHGC measurement methods and test apparatus of four different testing laboratories. In addition, round-robin tests were conducted within an interlaboratory comparison to determine the SHGC of BIPV modules with and without power generation and differing cell coverage ratios. As a result, the following findings are noted:

- An international round-robin test confirmed that the SHGC is always lower when power is generated and extracted from the BIPV-m (MPP state) than when the BIPV-m is in the OC state, regardless of test standards, test methods, and test apparatus. This is because some of the solar energy absorbed by the PV cells is converted by the photovoltaic effect into electricity and is removed from the glazing, rather than being radiated indoors as heat. It was also confirmed in Test Series 1 that the SHGC value was reduced by 0.02 to 0.04 (5 to 14.8 %) in the case of the investigated samples, consisting only of the BIPV-m, i.e. single glazing. Absorbed solar radiation which has been converted to electricity and extracted from the PV module is no longer available to contribute to the secondary heat transfer towards the inside. Thus, the SHGC value for a BIPV-m is always lower in the MPP state than in the OC state due to power generation and extraction, regardless of the PV cell technology and regardless of whether the PV cell is opaque or semi-transparent.
- The SHGC decreased proportionally with the increase in the PV cell coverage ratio. A linear relationship, with the  $R^2$  value for each laboratory exceeding 0.95, was strongly supported by the results of Test Series 2 on BIPV-m with different coverage ratios in the OC state. However, this linear relationship applies only if the irradiance from the solar simulator used is spatially homogeneous over the BIPV-m. Thus, if this condition is met, it is possible to predict the SHGC of a BIPV-m in the OC state from the cell coverage ratio and the SHGC values of two BIPV-m samples with the same glazing configuration but significantly different coverage ratios.
- For the transparent glass laminate, which was optically homogeneous over the test sample area, very similar SHGC results were obtained by JTCCM and Fraunhofer ISE for the samples provided for Test Series 1, and between the samples provided to JTCCM and CSTB for Test Series 2 and to SERIS for Test Series 1. As the SHGC values for the two different groups also agree with the two different SHGC values calculated from the spectra presented in Fig. 20, it is assumed that the different values are caused by different sample compositions between the two groups of samples.
- Optically diverse materials are combined in the investigated BIPV modules, such that they are spatially inhomogeneous. JTCCM, SERIS, and CSTB all apply the CHB methodology, which evaluates the whole irradiated aperture area of the BIPV-m. They obtained similar results for the A1 samples in the OC state, within the allowable error margins, and assuming that the sample compositions were similar. The center-of-glass SHGC evaluation for the BIPV module by the HFM-CP methodology at Fraunhofer ISE obtains a different value primarily due to the different cell coverage ratio in the evaluated

area. Careful specification of this evaluated area is thus essential when values are determined by applying the centre-of-glazing methodology of ISO 19467-2 [9].

- Although the solar simulators differed in the type and number of xenon and metal halide lamps and the spectral match rating, this did not cause a significant difference in the SHGC test results, which were within the allowable error. This may be different when BIPV-m multi-pane glazing units contain strongly spectrally selective layers such as low-e coatings, or when the spectral response of the PV component covers a narrower portion of the solar spectrum (e.g. InGaAs solar cells).
- The complete solar spectral range (300 nm to 2500 nm) should be used when the spectral match of solar simulators for SHGC determination of BIPV-m is characterized.
- For SHGC evaluation of BIPV-m, it is recommended to reduce the irradiation inhomogeneity as much as possible; a value of 10 % or less is proposed.
- Solar simulators with DC power sources are common for module efficiency measurements in the PV industry, whereas AC-powered solar simulators are usual for calorimetric SHGC determination of construction products. It is not yet clear whether the type of power source for the solar simulator needs to be explicitly taken into account in developing a calorimetric SHGC evaluation methodology for BIPV.
- Particularly for single-glazed BIPV-m offering low thermal resistance, it is important to specify the HTC values that are used for calorimetric SHGC determination.

To summarise, the information and insights gained during the reported international round robin on calorimetric measurement of BIPV glazing provide a good basis for further refinement and development of an international standard on this topic.

#### CRediT authorship contribution statement

**Hisashi Ishii:** Writing – review & editing, Writing – original draft, Visualization, Validation, Supervision, Resources, Project administration, Methodology, Investigation, Formal analysis, Data curation, Conceptualization. **Helen Rose Wilson:** Writing – review & editing, Validation, Resources, Methodology, Investigation, Formal analysis, Data curation. **Shinji Hagihara:** Validation, Data curation. **Ulrich Amann:** Validation, Formal analysis, Data curation. **Veronika Shabunko:** Validation, Data curation. **Simon Boddaert:** Validation, Data curation.

#### Declaration of competing interest

The authors declare that they have no known competing financial interests or personal relationships that could have appeared to influence the work reported in this paper.

#### Data availability

The authors do not have permission to share data.

#### Acknowledgements

This research is the result of work commissioned by the New Energy and Industrial Technology Development Organization (NEDO) as part of the project entitled “Wall-Installed Solar PV System Technology Development”, grant number 20000951-0. Sincere thanks are extended to the German Federal Ministry for Economic Affairs and Climate Action (BMWK), within the Standard BIPV-System project, grant number 03EE1061A. Furthermore, thanks go to Dr. Michio Kondo (Waseda University: formerly at National Institute of Advanced Industrial Science and Technology), and Dr. Carlos Clement (Solar Energy Research

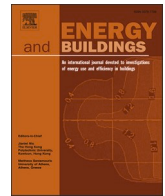
Institute of Singapore : SERIS) for their support, and to everyone involved for their cooperation.

This article is partly based on detailed analysis carried out by the authors within the framework of the IEA-PVPS Task 15, “Enabling framework for the development of BIPV”.

#### References

- [1] IEC 63092-1, Photovoltaics in buildings - Part 1: Requirements for building-integrated photovoltaic modules, International Electrotechnical Commission (2020).
- [2] EN 50583-1, Photovoltaics in buildings - Part 1, BIPV Modules (2016).
- [3] L. Olivieri, E. Caamaño-Martin, F. Olivieri, J. Neila, Integral energy performance characterization of semi-transparent photovoltaic elements for building integration under real operation conditions, Energy Build. 68 (2014), <https://doi.org/10.1016/j.enbuild.2013.09.035>.
- [4] H. Zhou, J. Peng, H.R. Wilson, M. Wang, J. Jonsson, T. Ma, B. Wu, B. Wu, G. Fu, Investigation of decoupling of thermal and electrical performance of semi-transparent photovoltaic windows based on the external quantum efficiency, Energy & Build. (2022), <https://doi.org/10.1016/j.enbuild.2022.112539>.
- [5] K. Kapsis, A. Athienitis, S. Harrison, Determination of solar heat gain coefficients for semitransparent photovoltaic windows: An experimental study, ASHRAE Conf. 123 (2017) 82–94.
- [6] H.Ishii, Thermal Performance (G-value and U-value) Evaluation of BIPV Applied to Glass Façade, EU PVSEC, 2017 ISBN 3-936338-47-7, 6BV.3.48.
- [7] H.Ishii, Evaluation of Thermal Properties for BIPV in Façade Part 2 Experimental Results of G value for Crystal Silicon BIPV Module according to ISO 19467, EU PVSEC, 2018 ISBN 3-936338-50-7, 6BV.1.31.
- [8] ISO 19467-1, Thermal performance of windows and doors - Determination of solar heat gain coefficient using solar simulator, 2017.
- [9] ISO 19467-2, Thermal Performance of windows and doors - Determination of solar heat gain coefficient using solar simulator - Part 2: Centre of glazing, 2021.
- [10] ISO 9050, Glass in building - Determination of light transmittance, solar direct transmittance, total solar energy transmittance, ultraviolet transmittance and related glazing factors, 2003.
- [11] ISO 15099, Thermal performance of windows, doors and shading devices - Detailed calculations, 2003.
- [12] EN 410, Glass in building - Determination of luminous and solar characteristics of glazing, 2011.
- [13] H.Ishii, M.Kondo and S.Hagihara, Evaluation of Thermal Properties for BIPV in Façade Proposal of SHGC evaluation method for BIPV using ISO 19467, EU PVSEC, 2019 ISBN 3-936338-60-4, 6BV.4.17.
- [14] IEA PVPS Task15, Successful Building Integration of Photovoltaics - A Collection of International Projects, 2021 <https://iea-pvps.org/key-topics/successful-building-integration-of-photovoltaics-a-collection-of-international-projects/>.
- [15] [https://www.lixil.co.jp/lineup/solar\\_roof\\_outerwall/solarack/](https://www.lixil.co.jp/lineup/solar_roof_outerwall/solarack/).
- [16] ISO 10292, Glass in building - Calculation of steady-state U values (thermal transmittance) of multiple glazing, 1994 This standard was last reviewed and confirmed in 2017.
- [17] EN 673, Glass in building - Determination of thermal transmittance (U value) - Calculation method, 2011.
- [18] Japan Testing Center for Construction and Materials, JSTM K6101, Test method for the determination of solar heat gain coefficient and shading coefficient of window's solar shading device using solar simulator 2013 (in Japanese).
- [19] Ministry of Economy, Trade and Industry commissioned project report, PVTEC, FY2018 international standard development for energy saving, etc. [Ministry 32] International standardization result report on building-integrated photovoltaic (BIPV) modules and systems, March 2019 (in Japanese).
- [20] T. Kuhn, Calorimetric determination of the solar heat gain coefficient g with steady-state laboratory measurements, Energy Build. (2014), <https://doi.org/10.1016/j.enbuild.2014.08.021>.
- [21] IEC 60904-3, Photovoltaic devices - Part 3: Measurement principles for terrestrial photovoltaic (PV), Solar Devices with Reference Spectral Irradiance Data, 2008.
- [22] IEC 60904-9:2007, Photovoltaic devices - Part 9: Solar simulator performance requirements.
- [23] C. Fangzhi, K. Stephen Wittkopf, Summer condition thermal transmittance measurement of fenestration systems using calorimetric hot box, Energy Build. (2013), <https://doi.org/10.1016/j.enbuild.2012.07.005>.
- [24] C. Fangzhi, K. Stephen Wittkopf, Ng. Poh Khai, D. Hui, Solar heat gain coefficient measurement of semi-transparent photovoltaic modules with indoor calorimetric hot box and solar simulator, Energy Build. (2013), <https://doi.org/10.1016/j.enbuild.2012.06.005>.
- [25] International Organization for Standardization, ISO 9845-1:1992, Solar energy - reference solar spectral irradiance at the ground at different receiving conditions - Part 1: Direct normal and hemispherical solar irradiance for air mass 1.5, 1992.
- [26] National Fenestration Rating Council, NFRC 200-2010, Procedure for determining fenestration product solar heat gain coefficient and visible transmittance at normal incidence, 2010.
- [27] National Fenestration Rating Council, NFRC 300 - 2010, Test method for determining the solar optical properties of glazing materials and systems, 2010.
- [28] IEC 60904-9:2020, Photovoltaic devices - Part 9: Solar simulator performance requirements.
- [29] ISO 52022-3, Energy performance of buildings - Thermal, solar and daylight properties of building components and elements - Part 3: Detailed calculation

- method of the solar and daylight characteristics for solar protection devices combined with glazing.
- [30] ASTM G173, Standard Tables for Reference Solar Spectral Irradiances: Direct Normal and Hemispherical on 37° Tilted Surface.
- [31] H. Ishii, Research and Development of Indoor Installation Type BIPV Screen (PV Roller Shade) EU PVSEC, 2021, ISBN 3-936338-78-7, 6CV.4.13.
- [32] IEC 61215-2, Terrestrial photovoltaic (PV) modules - Design qualification and type approval - Part 2: Test procedures, Int. Electrotechnical. Commission (2021).
- [33] B. Bueno, R. Schregle, H.R. Wilson, U. Amann, T.E. Kuhn, Angular divergence of solar simulators and its impact on the measured Solar Heat Gain Coefficient of fenestration systems, *Solar Energy* 236 (2022) 644–653, <https://doi.org/10.1016/j.solener.2022.02.029>.
- [34] ASTM C1363, Standard Test Method for Thermal Performance of Building Materials and Envelope Assemblies by Means of a Hot Box Apparatus,.
- [35] ASTM C1199, Standard Test Method for Measuring the Steady-State Thermal Transmittance of Fenestration Systems Using Hot Box Methods, 2010.
- [36] NFRC 201, Standard Test Method for Measuring the Solar Heat Gain Coefficient of Fenestration Systems, 2010.
- [37] Ministry of Economy, Trade and Industry commissioned project report, PVTEC, 2018 international standard development for energy saving, etc. [Ministry 32] International standardization result report on building-integrated photovoltaic (BIPV) modules and systems, March 2019 (in Japanese).
- [38] Ministry of Economy, Trade and Industry commissioned project report, PVTEC, 2019 international standard development for energy saving, etc. [Ministry 26] International standardization result report on building-integrated photovoltaic (BIPV) modules and systems, March 2020 (in Japanese).
- [39] H.R. Wilson, T.E. Kuhn, H. Ishii, D. Valencia- Caballero, N. Martin Chivelet, J. Peng, R.J. Yang, Y. Zang, H. Ge, K- Ye, J- C. Jonsson, C. Kapsis, Component-based SHGC determination of BIPV modules for glazing product comparison, *Energy and Buildings* 320 (2024) 114592, <https://doi.org/10.1016/j.enbuild.2024.114592>.



## Component-based SHGC determination of BIPV glazing for product comparison

Helen Rose Wilson<sup>a,\*</sup>, Tilmann E. Kuhn<sup>a</sup>, Hisashi Ishii<sup>b</sup>, Daniel Valencia-Caballero<sup>c</sup>,  
Nuria Martin Chivelet<sup>d</sup>, Jinqing Peng<sup>e</sup>, Rebecca Jing Yang<sup>f</sup>, Yukun Zang<sup>f</sup>, Hua Ge<sup>g</sup>, Kai Ye<sup>g</sup>,  
Jacob C. Jonsson<sup>h</sup>, Konstantinos Kapsis<sup>i</sup>

<sup>a</sup> Fraunhofer Institute for Solar Energy Systems ISE, Heidenhofstr. 2, 79110 Freiburg, Germany

<sup>b</sup> LIXIL Corporation, LIXIL Housing Technology, Technology Research Institute, Nakasato 3000, Noda City, Chiba, Japan

<sup>c</sup> TECNALIA, Basque Research and Technology Alliance (BRTA), Paseo Mikeletegi 2, San Sebastián 20009, Spain

<sup>d</sup> CIEMAT, Photovoltaic Solar Energy Unit, Avda. Complutense 40, 28040 Madrid, Spain

<sup>e</sup> College of Civil Engineering, Hunan University, Changsha 410082, Hunan, China

<sup>f</sup> RMIT University, Melbourne, VIC 3000, Australia

<sup>g</sup> Concordia University, 1455 de Maisonneuve Blvd. W., Montreal H3G 1M8, Canada

<sup>h</sup> Windows and Daylighting Group, LBNL, 1 Cyclotron Road, Mail Stop 90R3111, Berkeley, CA 94720-8134, USA

<sup>i</sup> University of Waterloo, 200 University Avenue West, CPH 3666, Waterloo, Ontario N2L 3G1, Canada

### ARTICLE INFO

#### Keywords:

BIPV glazing  
SHGC  
Solar Heat Gain Coefficient  
g value  
Total Solar Energy Transmittance  
MPP state  
OC state  
PV cell coverage ratio  
Electricity extraction  
Optical inhomogeneity

### ABSTRACT

Building-integrated photovoltaic (BIPV) systems are intrinsically designed to generate electricity and to provide at least one building-related function. When BIPV modules act as glazing products in windows, skylights or curtain walls, their ability to control the transmission of solar energy into the building must be characterised by a Solar Heat Gain Coefficient (SHGC) or g value (also known as Total Solar Energy Transmittance – TSET – or “solar factor”). For the comparison of BIPV glazing products consisting of one PV laminate and possibly further, conventional glazing layers separated by gas-filled cavities, the procedures documented in international standards for architectural glazing (e.g. ISO 9050 and EN 410) form a suitable starting point. Easily implemented modifications to these procedures are proposed to take both optical inhomogeneity (if relevant) and extraction of electricity from BIPV glazing units into account. Geometrically complex glazing and shading devices, and light-scattering glazing layers, are outside the scope of the proposed methodology; SHGC determination for obliquely incident solar radiation is also excluded. For these cases, the experimental calorimetric approach documented in [ISO 19467:2017; ISO 19467-2:2021] is recommended.

The paper also presents results and conclusions from an implementation exercise and sensitivity study carried out by participants of the IEA-PVPS Task 15 on BIPV. The cell coverage ratio in the PV laminate, the thermal resistance offered by the glazing configuration, the choice of boundary conditions and the effect of extracting electricity were all identified as parameters which significantly affect the SHGC value determined for a given type of BIPV glazing. A practicable approach to accommodate the great variety of dimensions typical for BIPV glazing is also proposed. These findings should pave the way for modifying the existing component-based standards for architectural glazing to take the specific features of BIPV glazing into account.

### 1. Introduction

Since the 1970's, architectural glazing has evolved from single

glazing to multiple-pane glazing units containing coated glass panes and gas-filled cavities that provide effective thermal insulation. With thermal transmittance values of  $1.2 \text{ Wm}^{-2}\text{K}^{-1}$  and less being achieved by commercially available glazing units, they provide adequate thermal

\* Corresponding author.

E-mail addresses: [helen.rose.wilson@ise.fraunhofer.de](mailto:helen.rose.wilson@ise.fraunhofer.de), [testlab-solarfacades@ise.fraunhofer.de](mailto:testlab-solarfacades@ise.fraunhofer.de) (H.R. Wilson), [tilmann.kuhn@ise.fraunhofer.de](mailto:tilmann.kuhn@ise.fraunhofer.de) (T.E. Kuhn), [hisashi.ishii@lixil.com](mailto:hisashi.ishii@lixil.com) (H. Ishii), [daniel.valencia@tecnalia.com](mailto:daniel.valencia@tecnalia.com) (D. Valencia-Caballero), [nuria.martin@ciemat.es](mailto:nuria.martin@ciemat.es) (N. Martin Chivelet), [jallen.peng@gmail.com](mailto:jallen.peng@gmail.com) (J. Peng), [rebecca.yang@rmit.edu.au](mailto:rebecca.yang@rmit.edu.au) (R.J. Yang), [s3679970@student.rmit.edu.au](mailto:s3679970@student.rmit.edu.au) (Y. Zang), [hua.ge@concordia.ca](mailto:hua.ge@concordia.ca) (H. Ge), [kai.ye@mail.concordia.ca](mailto:kai.ye@mail.concordia.ca) (K. Ye), [jcjonsson@lbl.gov](mailto:jcjonsson@lbl.gov) (J.C. Jonsson), [costa.kapsis@uwaterloo.ca](mailto:costa.kapsis@uwaterloo.ca) (K. Kapsis).

<https://doi.org/10.1016/j.enbuild.2024.114592>

Received 31 March 2024; Received in revised form 19 June 2024; Accepted 22 July 2024

Available online 25 July 2024

0378-7788/© 2024 The Author(s). Published by Elsevier B.V. This is an open access article under the CC BY-NC license (<http://creativecommons.org/licenses/by-nc/4.0/>).

Nomenclature	
AM	Air mass
BIPV	Building-integrated photovoltaics
CR	Coverage ratio
DGU	Double glazing unit
MPP	Maximum power point
OC	Open circuit
PV	Photovoltaic
RRT	Round robin test
SHGC	Solar heat gain coefficient (or g value)
TSET	Total solar energy transmittance (or g value)
$A_{cell}$	surface area covered by PV cells within the total PV module area
$A_{inact}$	surface area covered by electrically inactive material (e.g. transparent encapsulant) between PV cells within the total PV module area
$A_{intercon}$	surface area covered by interconnectors between PV cells within the total PV module area
$A_{jb}$	surface area covered by the junction box within the total PV module area
$A_{mod}$	total PV module area
$g$	Total Solar Energy Transmittance (or SHGC or solar factor)
$h_{in}$	heat transfer coefficient towards the inside ( $Wm^{-2} K^{-1}$ )
$h_{out}$	heat transfer coefficient towards the outside ( $Wm^{-2} K^{-1}$ )
$q_i$	secondary heat transfer factor of the glazing towards the inside
$r_{cell}$	ratio of surface area covered by PV cells to total PV module area (= cell coverage ratio CR)
$r_{inact}$	ratio of area covered by electrically inactive material (e.g. transparent encapsulant) between PV cells to total PV module area
$r_{intercon}$	ratio of total interconnector area to total PV module area
$r_{jb}$	ratio of junction box area to total PV module area
$T_{in}$	indoor glazing surface temperature ( $^{\circ}C$ )
$T_{out}$	outdoor glazing surface temperature ( $^{\circ}C$ )
$U$	thermal transmittance without irradiance ( $Wm^{-2} K^{-1}$ )
$\alpha_e$	solar direct absorptance
$\alpha_{e1}$	solar direct absorptance of the outer pane within a double glazing unit
$\alpha_{e2}$	solar direct absorptance of the second pane within a double glazing unit
$\alpha_i(\lambda)$	absorptance spectrum of the isolated $i$ th glazing layer for radiation incident on the outdoor-facing surface
$\alpha'_i(\lambda)$	absorptance spectrum of the isolated $i$ th glazing layer for radiation incident on the indoor-facing surface
$\varepsilon_{in}$	emissivity of an indoor-facing surface of a glazing layer
$\varepsilon_{out}$	emissivity of an outdoor-facing surface of a glazing layer
$\Lambda$	total thermal conductance of a glazing unit (single or multiple-pane glazing)
$\eta$	power conversion efficiency of a PV device (irradiation of outdoor-facing surface)
$\eta'$	power conversion efficiency of a PV device (irradiation of indoor-facing surface)
$\rho_e$	solar direct reflectance
$\rho_i(\lambda)$	reflectance spectrum of the isolated $i$ th glazing layer for radiation incident on the outdoor-facing surface
$\rho'_i(\lambda)$	reflectance spectrum of the isolated $i$ th glazing layer for radiation incident on the indoor-facing surface
$\tau_e$	solar direct transmittance
$\tau_i(\lambda)$	transmittance spectrum of the isolated $i$ th glazing layer

insulation and are installed over large areas of building facades. Solar radiation that enters the building provides welcome natural lighting and reduces the demand for space heating in winter, but may cause overheating in summer. Already in the 1990's, a new metric was introduced to quantify the total amount of solar radiation transmitted by glazing into the building [1–3]. This metric, variously designated as Total Solar Energy Transmittance (TSET), solar factor, Solar Heat Gain Coefficient (SHGC) or g value, takes account of both directly transmitted solar radiation and absorbed solar radiation that is transferred indoors as heat [4].

Semi-transparent building-integrated (BIPV) glazing represents a further development of architectural glazing which combines the classic optical and energy-transmitting functions of transparent areas and the shading functions of opaque areas with the electricity generation of PV cells. As has been documented in a number of experimental studies [5–9], the extraction of photovoltaically generated electricity from the BIPV glazing unit acts to lower the SHGC value of the window. In this paper, a component-based calculation method is proposed for BIPV glazing that can be readily integrated into SHGC determination methods that are already documented in standards for characterising and comparing glazing products under standardised boundary conditions. Like the underlying standards, application of the proposed method is limited to normally incident solar radiation and glazing products that consist of one PV laminate and conventional, planar glazing layers separated by gas-filled cavities. Fig. 3 shows an example of such a glazing configuration. If the PV laminate or the glazing layers contain air-permeable “holes” [10], they cannot be treated by the presented approach. The treatment of a BIPV glazing unit containing strongly light-scattering layers is also excluded from this approach. Development of a more sophisticated calculation-based dynamic approach that is based implicitly on [11] and is commensurate with the needs of building

energy simulation has been introduced by Zhou et al. [12] but is not the topic addressed here. Geometrically complex glazing (including that containing strongly light-scattering layers) and shading devices, and SHGC determination for obliquely incident radiation, are outside the scope of the proposed methodology; for these cases, the experimental calorimetric approach documented in ISO 19467-1:2017 and ISO 19467-2:2017 [13,14] is recommended.

What is explicitly addressed in the proposed methodology are features commonly encountered in BIPV glazing units, namely optical inhomogeneity of the PV “glazing layer”, analogously to Annex C of EN 410, and extraction of the photovoltaically generated electricity.

## 2. Principles of component-based SHGC determination for glazing product characterisation

The basic definition for SHGC, the fraction of incident solar radiation which is transmitted directly or by re-radiation through architectural glazing into the indoor space of a building, is expressed mathematically in Eq. (1) as

$$g = \tau_e + q_i \quad (1)$$

where  $g$  is the SHGC,  $\tau_e$  is the solar direct transmittance of the glazing unit and  $q_i$  is the secondary heat transfer factor towards the inside. As documented in ISO 9050:2003 [15], EN 410:2011 [16] or NFRC 300-2023 [17], the transmittance spectrum for a glazing unit  $\tau(\lambda)$  is calculated by multi-layer optical calculations from the transmittance and reflectance spectra of the component panes. All spectra are determined for radiation that is (near-)normally incident on the characterised sample. The solar direct transmittance for the glazing unit  $\tau_e$  is calculated by weighting the transmittance spectrum by a specified solar spectrum, which is based on the spectral distributions for AM1.0 global

in EN 410:2011 [16], AM1.5 global in ISO 9050:2003 [15] or AM1.5 direct in NFRC 300-2023 [17], respectively. Similarly, the solar direct absorptance for radiation incident on the outdoor-facing surface of the  $i$ th glazing layer within the glazing unit,  $\alpha_{ei}$ , is also calculated by multi-layer optical calculations from the transmittance and reflectance spectra of the component panes (the “glazing layers”) and weighting by the specified solar spectrum.

Each of the component glazing layers is characterised by its transmittance spectrum  $\tau(\lambda)$  and reflectance spectra  $\rho(\lambda)$  and  $\rho'(\lambda)$  for radiation normally incident on the outdoor-facing and indoor-facing surfaces, respectively. The transmittance and reflectance spectra are measured for each glazing layer separately and serve as input data for the multi-layer calculations. For each individual glazing layer  $i$  in isolation (i.e. not within the glazing unit), the absorptance spectrum  $\alpha_i(\lambda)$  for the outdoor-facing surface is calculated according to Eq. (2) as

$$\alpha_i(\lambda) = 1 - \tau_i(\lambda) - \rho_i(\lambda) \quad (2)$$

where  $\tau_i(\lambda)$  is the transmittance spectrum of the  $i$ th glazing layer and  $\rho_i(\lambda)$  is the reflectance spectrum for radiation incident on the outdoor-facing surface of the  $i$ th glazing layer. The analogous equation for the absorptance spectrum  $\alpha'_i(\lambda)$  for the indoor-facing surface is given by Eq. (3) as

$$\alpha'_i(\lambda) = 1 - \tau_i(\lambda) - \rho'_i(\lambda) \quad (3)$$

where  $\tau_i(\lambda)$  is the transmittance spectrum of the  $i$ th glazing layer and  $\rho'_i(\lambda)$  is the reflectance spectrum for radiation incident on the indoor-facing surface of the  $i$ th glazing layer.

It is emphasised that Equations (2) and (3) refer to the absorptance spectra for the individual, isolated glazing layers. The absorptance spectra for the  $i$ th glazing layer within a multiple-pane glazing unit containing two or more layers are modified by the presence of the other panes and must be calculated using the multi-layer approach documented in e.g. [15,16] or [17].

As the spectra are determined for normally incident radiation, the multi-layer calculations are not valid for strongly scattering layers and the results obtained for slightly scattering layers will have a larger error than for the originally foreseen “glass-clear” transparent layers.

In the original versions of the standards EN 410 and ISO 9050 for conventional architectural glazing, it is assumed that all of the absorbed solar radiation is converted to heat and is transported by conduction, convection or radiation either to the outdoor or the indoor environment. The cited standards follow the conventions, methods and sets of boundary conditions set out in the parallel standards for calculating the steady-state thermal transmittance  $U$  for the centre of glass of architectural glazing, [18,19], for product comparison. One-dimensional heat transport through the glazing unit is assumed, neglecting any lateral flows or edge effects. The thermal resistance  $1/U$  caused by the glazing unit between the outdoor and the indoor environment is modelled as the sum of resistances corresponding to external and internal surface heat transport, conduction through the solid glazing layers, and conduction, convection and radiation within the gas-filled cavities between panes. Thermal properties for glass, low-e coatings and the commonly used gases for inter-pane cavities are specified in these standards. For product comparison purposes, standardised values for the external and internal heat transfer coefficients are also provided. Based on the thermal properties of the component materials, the thicknesses of the component layers and the specified boundary conditions, the  $U$  value of a complete glazing unit can be calculated by applying a one-dimensional series resistance model. The same approach can be applied to calculate the partial resistances between the different glazing component surfaces.

Once the solar direct absorptance  $\alpha_{ei}$  for each glazing layer within the glazing unit and the partition of thermal resistances, as defined above, are known, the proportion of incident solar radiation that is absorbed within the glazing unit and is transported indoors,  $q_i$ , can be calculated by the equations specified in EN 410 or ISO 9050.

Corresponding to the  $U$ -value calculations, the form of the equations for  $q_i$  varies with the number of panes in the glazing unit. Specifically, for single glazing consisting only of a PV laminate, the equation specified in EN 410 or ISO 9050 for  $q_i$  is

$$q_i = \alpha_e h_{in} / (h_{out} + h_{in}) \quad (4)$$

where  $\alpha_e$  is the solar direct absorptance of the PV laminate as described above and  $h_{out}$  and  $h_{in}$  are the heat transfer coefficients towards the outside and inside, respectively, as specified in EN 673:2011 [18] or ISO 10292:1994 [19].

Making use of the definition of the thermal transmittance  $U$  from EN 673:2011 [18] or ISO 10292:1994 [19] as

$$1/U = 1/h_{out} + 1/\Lambda + 1/h_{in} \quad (5)$$

where  $h_{out}$  and  $h_{in}$  are defined as above and  $\Lambda$  is the total thermal conductance of the glazing, Eq. (4) for single glazing can be reformulated as

$$q_i = \alpha_e U / (h_{out}(1 - U/\Lambda)) \quad (6)$$

Taking into account that the thermal conductance  $\Lambda$  of a PV laminate is about 20 times larger than the corresponding  $U$  value, Eq. (6) for a PV laminate can be approximated as

$$q_i \cong \alpha_e U / h_{out} \quad (7)$$

indicating a nearly linear dependence of  $q_i$  on  $\alpha_e$  and  $U/h_{out}$ .

An analogous reformulation of the expression for  $q_i$  of double glazing from EN 410 or ISO 9050 results in the equation

$$q_i = \alpha_{e1} U / h_{out} + \alpha_{e2} (U / h_{out} + U / \Lambda) \quad (8)$$

where  $\alpha_{e1}$  and  $\alpha_{e2}$  are the solar direct absorptance values of the outer and inner panes within a double glazing unit, respectively, and the remaining terms are as defined above. Again, there is a linear dependence of  $q_i$  on  $\alpha_{e1}$ , the absorptance in the outer pane (the most common position for the PV pane in double glazing), and on  $U/h_{out}$ .

### 3. Features of semi-transparent BIPV glazing

There are two main features of semi-transparent BIPV glazing which distinguish it from most conventional architectural glazing and which demand modifications in the approach to determine the SHGC value.

The defining property of BIPV glazing is its ability to convert incident solar radiation to electricity by the photovoltaic effect. This means that the assumption stated above for conventional architectural glazing, “that all of the absorbed solar radiation is converted to heat”, no longer applies. When the PV layer of a BIPV glazing unit is connected to an external electric circuit, some of the absorbed solar radiation is extracted as electricity and removed from the glazing unit; the amount of heat which can be transported indoors is reduced, decreasing the SHGC value of the BIPV glazing unit.

As illustrated in Fig. 1 and Fig. 3, the second, frequently encountered property of semi-transparent BIPV glazing is optical inhomogeneity at a macroscopic level, meaning that different regions of the glazing unit are characterised by different transmittance and reflectance properties. Most commonly, the “photovoltaic glazing layer” consists of a PV glass-glass laminate or a glass-backsheet laminate, where one main area is occupied by crystalline silicon PV cells and a second significant area is transparent, with a transparent encapsulation material such as ethylene vinyl acetate (EVA) or polyvinyl butyral (PVB) embedded between the front and back covers. There may also be significant areas covered by metal interconnectors between the cells or by an electronic junction box that is exposed to solar radiation and thus is visible from outdoors. Photovoltaic glazing based on inorganic thin-film technology may also consist of different macroscopic areas alternating between coated and laser-ablated areas to provide areas for clear vision. (The fine laser-

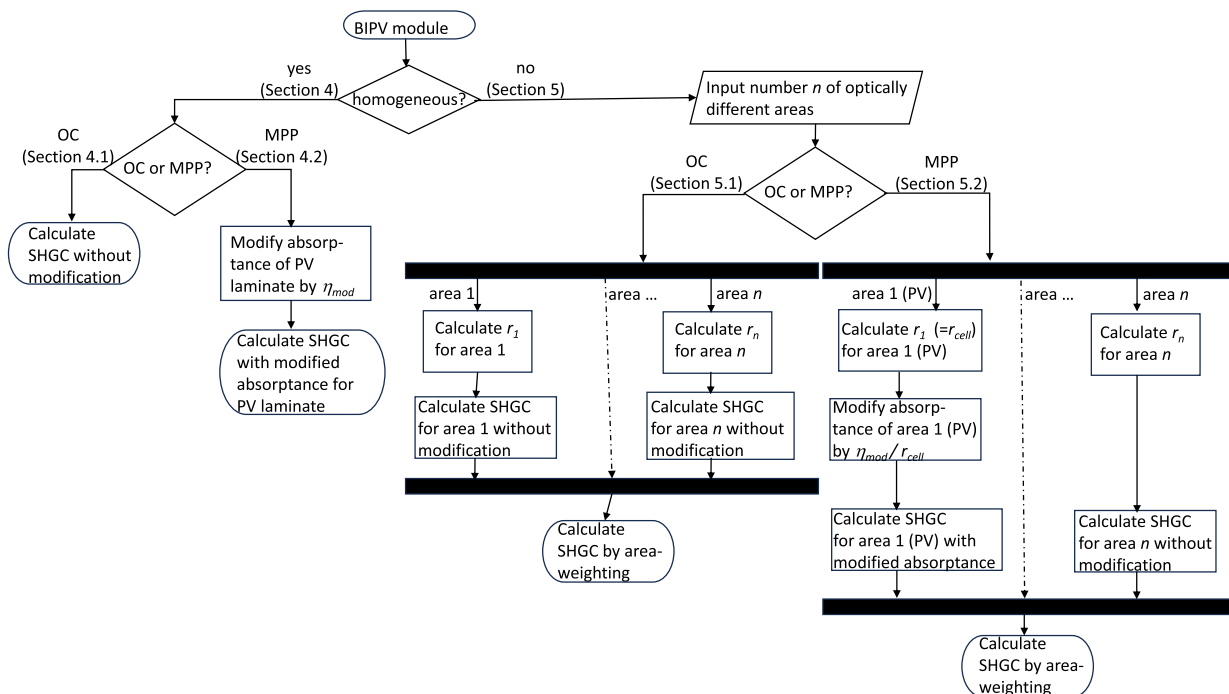


**Fig. 1.** PV semi-transparent glazing manufactured by Onyx Solar and installed in the Kubik experimental building at Tecnalia facilities in Derio, Spain, within the BIPVBoost project.  
Source: Eneko Setien, Tecnalia

ablated lines that are intrinsic to the construction of inorganic thin-film PV modules are not usually treated as “optically different” areas because of their small dimensions compared to the beam cross-sections used to determine optical properties spectrophotometrically. In this case, the PV laminate can be treated as optically homogeneous.) In principle, organic PV glazing with differently coloured PV regions may also be characterised by the proposed approach, providing that not only the optical

properties but also the power conversion efficiency is available for each different PV region, and the different PV regions are not connected electrically in series.

An approach to take these features of BIPV modules into account is described in detail in the following two Sections 4 and 5. An overview of the procedure and references to the relevant Subsections is provided by Fig. 2.



**Fig. 2.** Flow chart outlining the modifications needed to take optical inhomogeneity (if relevant) and extraction of electricity into account when calculating the SHGC of BIPV modules. Details are provided in the indicated Sections of this paper.

#### 4. Proposed modification to SHGC determination to account for photovoltaic conversion of incident solar radiation on an optically homogeneous BIPV glazing unit

##### 4.1. Open-circuit case

If the cells of a BIPV glazing unit are exposed to solar radiation but are not connected to an external circuit, i.e. are in the open circuit (OC) state, all of the absorbed solar radiation is converted to heat. If the whole area of the glazing unit can be considered to be homogeneous, as is often the case for organic and inorganic thin-film photovoltaics, the method for determining the SHGC of the BIPV glazing in the OC state is identical to that for non-photovoltaic glazing, based on measurements of the transmittance and reflectance spectra for the PV laminate and any other further panes of the glazing unit, i.e. no modification to the SHGC determination procedure is necessary.

##### 4.2. Maximum-power-point case

Still considering the optically homogeneous case, but with the PV laminate connected to an external electric circuit, some of the absorbed solar radiation is converted photovoltaically into electricity and is extracted from the BIPV glazing. For a PV module in the form of a single PV laminate (i.e. not within a BIPV glazing unit), the photovoltaic conversion efficiency is defined in IEC TS 61836:2016 [20] as the “ratio of electric power generated by a PV device per unit area to its incident irradiance”. Introducing the symbol  $\eta_{mod}$  for this quantity, the extraction of electricity from an optically homogeneous BIPV glazing unit can thus be taken into account by modifying Eq. (2). For the isolated  $i$ th layer that consists of the optically homogeneous PV laminate, the absorptance spectrum  $\alpha_i(\lambda)$  for the outdoor-facing surface is given by Eq. (9):

$$\alpha_i(\lambda) = 1 - \tau_i(\lambda) - \rho_i(\lambda) - \eta_{mod,i} \quad (9)$$

where  $\tau_i(\lambda)$  is now specifically the transmittance spectrum of the PV laminate,  $\rho_i(\lambda)$  is the reflectance spectrum for radiation incident on the outdoor-facing surface of the PV laminate and  $\eta_{mod,i}$  is the power conversion efficiency of the homogeneous PV module (i.e., the PV laminate).

Most commonly, the PV module will be the external layer of the BIPV glazing unit, in which case  $i = 1$  in Eq. (9). However, Eq. (9) is also valid if the PV module is included in a different position and the glazing layers located between the solar radiation and the PV module feature spectrally constant optical properties, such that the use of a constant value for  $\eta_{mod,i}$  is justifiable. This condition of spectral constancy is fulfilled sufficiently by panes of low-iron glass, which would be an advisable choice for panes positioned between the solar radiation and the PV module to minimize the loss in generated electricity due to absorption in the intervening panes. The condition of spectral constancy is not met e.g. by low-e coated glass. In this case, the spectrum of the radiation incident on the PV module differs significantly from that specified in [21] for determination of  $\eta_{mod,i}$ . In that case, the relevant value for  $\eta_{mod,i}$  would have to be redetermined, taking the spectral response of the PV module into account. Considering firstly, that the spectral response is not usually supplied by PV module manufacturers, and secondly, that the PV module will be the outer pane in the great majority of BIPV multiple-pane glazing units, the authors have decided to retain Eq. (9) in the presented simple form. As a corollary, its use will lead to errors if it is applied to multiple-pane BIPV glazing with the PV module “behind” glazing layers with strong spectral variation of the transmittance. The magnitude of the error depends on the combination of the PV spectral response and the spectral variation of the glazing transmittance.

To obtain the SHGC value of the complete BIPV glazing unit, Eq. (2) is replaced by Eq. (9) for the  $i$ th layer that consists of the PV laminate in the multi-layer calculations documented in EN 410:2011 [16] or ISO 9050:2003 [15]. For monofacial PV laminates, Eq. (3) remains

unchanged. For bifacial PV laminates, it would be necessary to differentiate between the values of  $\eta_{mod,i}$  for irradiation of the outdoor-facing and indoor-facing surfaces. Equation (3) would need to be modified by subtracting the value of  $\eta'_{mod,i}$  for irradiation of the indoor-facing surface. In addition, the use of a single value for  $\eta'_{mod,i}$  is permissible only if the relative spectral distribution of the radiation incident on this indoor-facing surface agrees sufficiently with that of the solar spectrum used for spectral weighting. This would not be the case e.g. for solar radiation after reflection by a glass pane with a low-e coating.

The module photovoltaic conversion efficiency  $\eta_{mod,i}$  is usually based on the maximum power point (MPP) value, meaning the point on the current-voltage characteristic for the module at which maximum power can be extracted. As noted in IEC TS 61836 [20], the photovoltaic conversion efficiency is “typically measured under standard test conditions (STC)”, which are defined in the same document as “in-plane irradiance ... = 1 000 Wm<sup>-2</sup>, PV cell junction temperature (25 °C) and air mass (AM) = 1.5”. Among these conditions, the PV cell temperature is the most influential parameter on PV efficiency in the solar-shading context and mainly depends on ambient temperature and solar irradiance (PV efficiency typically decreases between 0.4% and 0.2% for every degree increase in cell temperature) [22]. In BIPV applications, the PV cell junction temperature usually reaches values above 25 °C. In addition, the radiation is normally incident on the module during the test measurement, whereas the solar radiation is often obliquely incident on BIPV arrays, resulting in higher reflection losses. Standard test conditions are thus more favourable for photovoltaic electricity generation than those that are usually experienced in building-integrated applications, so for practical purposes concerning SHGC determination for product characterisation, the value of  $\eta_{mod,i}$  can be considered to represent an upper limit for the electricity extracted from a BIPV glazing unit. In other words, the SHGC value determined according to the proposed method under MPP conditions will be lower than is frequently encountered in reality. Again, it is emphasized that this method is intended to enable product comparison under well-defined conditions; it is not intended for use in building energy simulations.

Although the photovoltaic conversion of radiation to electricity has a spectral dependence which is characterized by the spectral response of the photovoltaic device, the integral value of  $\eta_{mod,i}$  is considered to be adequate for the purpose of product characterization addressed in this paper. (Exceptions have been noted in the discussion above on Eq. (9) and the special case of a bifacial PV laminate within a multi-layer BIPV glazing unit. In such cases,  $\eta_{mod,i}$  or  $\eta'_{mod,i}$  should be replaced by the suitably normalized spectral response function. This approach was described by Zhou et al. [12]. The conditions specified in IEC 60904-9:2020 [21] for the solar simulators that are used in measuring  $\eta_{mod,i}$  include requirements on the spectral mismatch. According to those definitions, the solar spectra documented in EN 410:2011 [16] and ISO 9050:2003 [15] both satisfy the spectral mismatch requirements for a “category A” solar simulator. In other words, the value reported for  $\eta_{mod,i}$  in the data sheet of a PV module would be very similar, within the category A tolerance values, to that obtained on the basis of the spectral response and the solar spectra documented in EN 410:2011 [16] and ISO 9050:2003 [15]. A further argument supporting the use of  $\eta_{mod,i}$  in Eq. (9) is its widespread availability in PV module data sheets, whereas the spectral response of a PV module (as distinct from a “naked” solar cell) is not generally available.

Finally, once the modified absorptance  $\alpha_i(\lambda)$  of the PV module in isolation has been obtained according to Eq. (9), the solar direct absorptance  $\alpha_{ei}$  of the  $i$ th pane within a multi-pane BIPV glazing unit is determined by applying the multilayer optical calculations and spectral integration according to EN 410:2011 [16] or ISO 9050:2003 [15]. It is noted that computer programs to perform the multilayer optical calculations commonly use input files containing the spectra for  $\tau(\lambda)$ ,  $\rho(\lambda)$  and  $\rho'(\lambda)$  of the individual glazing layers. A convenient method to ensure use of the modified value of  $\alpha(\lambda)$  according to Eq. (9) is to add the  $\eta_{mod}$  value to the input  $\rho(\lambda)$  values for the PV laminate. However, it must be



remembered that this modified input file should be used only for calculation of the modified value of  $\alpha_{ei}$  for use in the SHGC calculation; it should not be used for calculation of the purely optical properties such as solar direct transmittance or solar direct reflectance of the BIPV glazing unit.

The modified value of  $\alpha_{ei}$  is then inserted into the relevant expression for the secondary heat transfer factor towards the inside  $q_i$  of the BIPV glazing unit, which varies according to the number of glazing layers in the unit. For the boundary conditions prescribed by the underlying standards [18] or [19] for the  $U$  value, the temperature change due to the extraction of electricity has a negligible effect on the  $U$  value and can be ignored [23]. Application of Eq. (1) with the modified value of  $q_i$  results in the SHGC value that applies for the MPP state, i.e. when electricity is extracted.

## 5. Proposed modifications to SHGC determination to account for inhomogeneous optical properties

Although conventional architectural glazing is usually optically homogeneous over its entire surface area, non-photovoltaic exceptions exist in the form of printed glazing. Ceramic prints are applied by screen-printing or digital methods, often as a means to reduce the SHGC value by reducing the solar direct transmittance, or to create translucent areas for daylighting functions, or for decorative purposes. As is documented by Appendix C to EN 410:2011 [16], a recognised method to calculate the optical characteristics and the SHGC of optically inhomogeneous glazing units is to determine the transmittance and reflectance spectra separately for each of the different regions, carry out the multi-pane calculations and then weight the contributions of the different regions to obtain the final, integrated results according to the relative area of each region. In accordance with the remainder of [16], this applies for normally incident radiation. This approach ignores the fact that regions with different solar direct absorptance values will heat to different temperatures when irradiated, which would cause lateral heat flow within the optically inhomogeneous layer, changing the transmission of heat through the glazing unit. This effect was considered to be small enough to be neglected in the existing Annex C of EN 410 for optically inhomogeneous, non-photovoltaic glazing, and the same assumption is made here for optically inhomogeneous BIPV glazing.

An optically inhomogeneous PV module – e.g. a laminate consisting of individual crystalline silicon solar cells separated by translucent or transparent regions – of total surface area  $A_{mod}$  typically contains different regions with the following surface areas:

$A_{cell}$  the surface area covered by PV cells within the total module area.

$A_{jb}$  the surface area covered by the junction box within the total PV module area.

(If the junction box is not exposed to solar radiation,  $A_{jb} = 0$ .)

$A_{intercon}$  the surface area covered by interconnectors between PV cells within the total PV module area.

$A_{inact}$  the surface area covered by electrically inactive material (e.g. transparent encapsulant) between PV cells within the total PV module area.

It then follows that

$$A_{mod} = A_{cell} + A_{jb} + A_{intercon} + A_{inact} \quad (10)$$

The corresponding ratios of the component surface areas to the total surface area are:

$$r_{cell} = A_{cell}/A_{mod} \quad (11)$$

(also known as the cell coverage ratio  $CR$ )

$$r_{jb} = A_{jb}/A_{mod} \quad (12)$$

$$r_{intercon} = A_{intercon}/A_{mod} \quad (13)$$

$$r_{inact} = A_{inact}/A_{mod} \quad (14)$$

It then follows that

$$1 = r_{cell} + r_{jb} + r_{intercon} + r_{inact} \quad (15)$$

Separate transmittance and reflectance spectra are to be available for each of the component areas defined above. The thermal resistance from front to back of the PV laminate is considered to be constant over all of its optically different regions, as the insertion of highly conductive semiconductor cells or metal interconnectors will have a negligible effect on the thermal resistance caused by the dielectric glass, encapsulant or backsheet components. Depending on the required accuracy of the final optical and SHGC results, it may be possible to ignore the contribution of small areas such as interconnectors. Taking the case of interconnectors as a possible example,  $A_{intercon}$  and  $r_{intercon}$  would then be set equal to zero in Equations (10) and (15), respectively, and the “missing” area should be added to the  $A_{inact}$  and  $r_{inact}$  components. Ignoring the contribution of opaque interconnectors would mean that the solar direct transmittance corresponding to the “inactive” region is too high. As it will not be completely compensated by the resulting increase in secondary heat transfer towards the inside, the resulting SHGC value would be slightly higher than taking a non-zero value of  $r_{intercon}$  into account, i.e. the error is on the conservative side, assuming that a lower SHGC is usually desired for solar-shading purposes. In [7], the effect of a region with a relative area less than 0.05 was found to be negligible on the SHGC value.

### 5.1. Open-circuit case

For the open-circuit case (OC), the optical properties and the SHGC value should be calculated according to the multi-layer calculation procedures of EN 410 [3,16] or ISO 9050 [2,15] separately for each PV laminate region combined with the remaining panes of the glazing configuration. The area weighting to obtain each optical property and SHGC value should be done using the final calculated properties for the different areas of the complete glazing configuration that correspond to the different regions of the PV laminate.

Thus, taking the solar direct reflectance of a BIPV triple glazed unit as an example,

$$\begin{aligned} \rho_{e, mod, triple\ glazing} = & r_{cell} \times \rho_{e, cell, triple\ glazing} + r_{jb} \times \rho_{e, jb, triple\ glazing} + r_{intercon} \\ & \times \rho_{e, intercon, triple\ glazing} + r_{inact} \times \rho_{e, inact, triple\ glazing} \end{aligned} \quad (16)$$

where

$\rho_{e, cell, triple\ glazing}$  is the solar direct reflectance of a hypothetical triple glazed unit in which the PV module area is covered completely by PV cells.

$\rho_{e, jb, triple\ glazing}$  is the solar direct reflectance of a hypothetical triple glazed unit in which the PV module area is covered completely by the junction box.

$\rho_{e, intercon, triple\ glazing}$  is the solar direct reflectance of a hypothetical triple glazed unit in which the PV module area is covered completely by interconnectors.

$\rho_{e, inact, triple\ glazing}$  is the solar direct reflectance of a hypothetical triple glazed unit in which the PV module area is covered completely by electrically inactive material (e.g. transparent encapsulant).

and the multi-layer calculation procedures for triple glazing are applied to calculate the solar direct reflectance,

$\rho_{e, xx, triple\ glazing}$ , with “xx” referring to each PV component area separately.

NOTE: In the case of multiple-pane glazing, it is not correct to initially calculate area-weighted spectra for the optically inhomogeneous PV laminate and then use these spectra for subsequent calculations.

## 5.2. Maximum-power-point case

For the maximum-power-point case (MPP), the spectral optical properties (transmittance, reflectance and absorptance) remain unchanged and thus are equal to the optical properties for the OC case. However, to calculate the SHGC value for the MPP case, the effect of extracting electricity on the solar direct absorptance of the PV layer must be taken into account. The value of  $\eta_{mod}$ , as introduced in Section 4.2, is again the basis, as for the optically homogeneous case. However, when this value is reported in the data sheet for an optically inhomogeneous PV module, it refers to the whole module with its combination of PV cells and non-PV regions. To quantify the power conversion efficiency specifically for the area covered by PV cells in the module, the quantity  $\eta_{cell,mod}$  is introduced and is defined by Eq. (17) as follows:

$$\eta_{cell,mod} = \eta_{mod} / r_{cell} \quad (17)$$

where  $\eta_{mod}$  is again the module (power) conversion efficiency as defined in IEC TS 61836 [20] and  $r_{cell}$  (equal to the cell coverage ratio  $CR$ ) is as defined in Eq. (11). Both quantities in Eq. (17),  $\eta_{mod}$  and  $r_{cell}$ , must refer to the same PV module and will usually be documented in the electrical data sheet for the PV module in question.  $\eta_{cell,mod}$  can also be understood as the photovoltaic conversion efficiency of a hypothetical PV module which is completely covered by solar cells, i.e. where  $r_{cell} (= CR) = 1$ .

For the solar cell region of the isolated, optically inhomogeneous PV laminate that is used as the  $i$ th glazing layer of the BIPV glazing unit, the absorptance spectrum  $\alpha_{i,cell,MPP}(\lambda)$  for the outdoor-facing surface is given by Eq. (18):

$$\alpha_{i,cell,MPP}(\lambda) = 1 - \tau_{i,cell}(\lambda) - \rho_{i,cell}(\lambda) - \eta_{i,cell,mod} \quad (18)$$

where  $\tau_{i,cell}(\lambda)$  is now specifically the transmittance spectrum of the cell region of the PV module,  $\rho_{i,cell}(\lambda)$  is the reflectance spectrum for radiation incident on the outdoor-facing surface of the cell region of the PV laminate and  $\eta_{i,cell,mod}$  is defined by Eq. (17). As above, the absorptance spectrum  $\alpha'_{i,cell,MPP}(\lambda)$  for irradiance incident on the indoor-facing surface can be calculated analogously if that surface is photovoltaically active. The same restrictions on the validity of Eq. (9) and its equivalent for irradiation of an indoor-facing surface apply equally to Eq. (18) and its equivalent for irradiation of an indoor-facing surface.

The modified absorptance spectrum  $\alpha_{i,cell,MPP}(\lambda)$  according to Eq. (18) is then used to determine the solar direct absorptance  $\alpha_{ei,cell,MPP}$  of the solar cell region of the PV laminate as the  $i$ th pane within a multi-pane BIPV glazing unit by applying the multilayer optical calculations and spectral integration according to EN 410 [16] or ISO 9050 [15]. The modified value of  $\alpha_{ei,cell,MPP}$  is then inserted into the relevant expression for the secondary heat transfer factor towards the inside  $q_{i,cell,MPP}$  of the cell region of the BIPV glazing unit. Application of Eq. (1) with  $q_i$  replaced by  $q_{i,cell,MPP}$  results in  $g_{cell,MPP}$  as the SHGC value that applies for the cell region of the BIPV glazing unit in the MPP state, i.e. when electricity is extracted.

The SHGC values for all other regions of the BIPV glazing unit remain unchanged by the extraction of electricity from the cell region. The SHGC value for the complete BIPV glazing unit in the MPP state is then calculated by area weighting, using  $g_{cell,MPP}$  as the component for the cell region. Taking the SHGC value  $g_{mod,MPP, double glazing}$  of a BIPV double glazing unit as an example,

$$\begin{aligned} g_{mod,MPP, double glazing} = & r_{cell} \times g_{cell,MPP, double glazing} + r_{jb} \times g_{jb, double glazing} \\ & + r_{intercon} \times g_{intercon, double glazing} + r_{inact} \\ & \times g_{inact, double glazing} \end{aligned} \quad (19)$$

where

$g_{cell,MPP, double glazing}$  is the SHGC value of a hypothetical double glazed unit in which the PV module area is covered completely by PV cells in

the MPP state.

$g_{jb, double glazing}$  is the SHGC value of a hypothetical double glazed unit in which the PV module area is covered completely by the junction box. (This value is zero if the junction box is not exposed to solar radiation.)

$g_{intercon, double glazing}$  is the SHGC value of a hypothetical double glazed unit in which the PV module area is covered completely by interconnectors.

$g_{inact, double glazing}$  is the SHGC value of a hypothetical double glazed unit in which the PV module area is covered completely by electrically inactive material (e.g. transparent encapsulant).

As BIPV glazing units are commonly manufactured with a wide range of heights, widths and cell coverage ratios, it is recommended that the SHGC values for 100% coverage of each of the optically different regions should be reported separately. Both the OC and MPP values should be reported for the PV cell regions. The overall SHGC value for any specific BIPV glazing unit can then be easily calculated, using the relevant area ratios for the optically different regions.

## 6. Application of modified SHGC determination procedure to realistic cases of BIPV glazing

The authors of this paper collaborated within the framework of IEA-PVPS Task 15, "Enabling framework for the development of BIPV" to develop and then apply the methodology described in the previous Sections to realistic cases of semi-transparent BIPV glazing units. Each participant calculated the SHGC values of specified BIPV glazing samples in the OC and MPP states under well-defined boundary conditions, most participants using the standard that is applicable to their global region for SHGC calculations as the individual starting point. Duplication in the choice of standards among the participants allowed cross-checking and verification of the individual results.

The exercise had three main goals:

- to determine the magnitude of the effect of electricity extraction on the SHGC value for different BIPV glazing configurations and solar cell coverage values.
- to compare the magnitude of the electricity extraction effect with that of other influences on the calculated SHGC value, such as the solar spectrum used for weighting or the heat transfer coefficients used to calculate thermal transmittance.
- to determine whether the effect of electricity extraction on the SHGC was large enough to warrant efforts to include it within international SHGC standards.

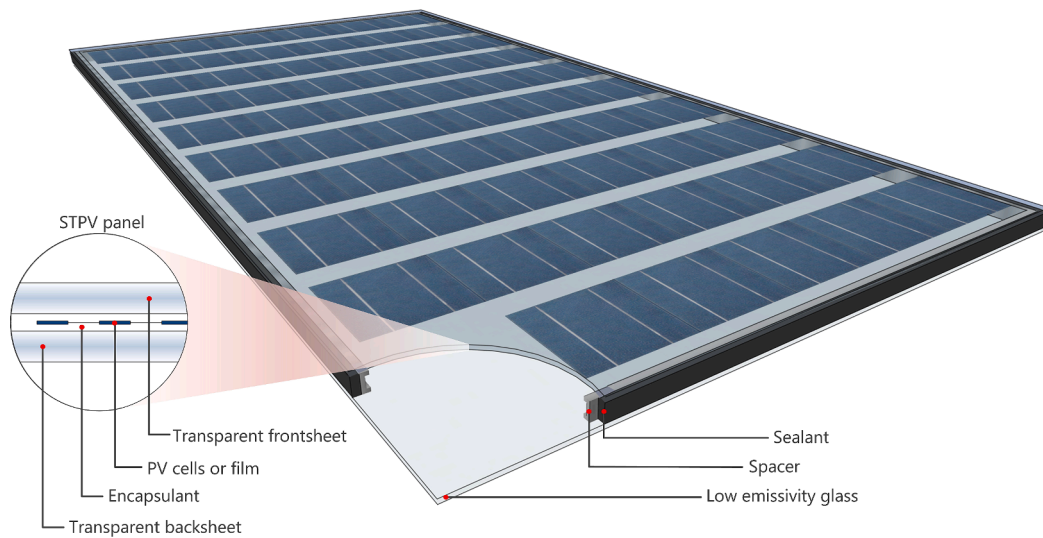
### 6.1. Specification of samples

A partly transparent, glass-glass PV laminate with monofacial crystalline silicon solar cells was taken as the starting point. To illustrate the effect of different cell coverage ratios, variants with a total of 36 cells or 72 cells were considered. Three different glazing configurations were considered to investigate the effect of different  $U$  values:

- the glass-glass PV laminate alone
- a BIPV double glazing unit (DGU 1) with the PV laminate as the outer layer, a 25.4 mm air-filled cavity and a glass pane with a pyrolytic low-e coating as the inner pane. (This corresponds to the BIPV double glazing unit that was investigated experimentally by Kapsis [7].)
- a BIPV double glazing unit (DGU 2) with the PV laminate as the outer layer, a 12 mm argon-filled cavity and a glass pane with a silver-based low-e coating as the inner pane

Fig. 3 illustrates the schematic configuration of the BIPV double glazing units.

It is noted here that in many European countries, energy-saving regulations effectively require the use of triple glazing units in many



**Fig. 3.** Schematic diagram of a semi-transparent BIPV double glazing unit integrating a partly transparent, crystalline silicon, glass-glass PV laminate as the outer layer [7].

buildings. Although triple glazing units were not included in the calculation exercise, the results allow conclusions about BIPV triple glazing units to be drawn and are presented later.

Parameters specifying the geometric configuration of the BIPV glazing units and the thermal properties of their components were fixed and are documented in Table 1. Transmittance and reflectance spectra for each of the glazing layers were provided to the participants; separate sets were provided for the solar cell region of the PV glass-glass laminate and the transparent region. The small areas corresponding to the interconnectors were not taken into account and the junction box was not exposed to solar radiation, so  $r_{intercon}$  and  $r_{jb}$  were set equal to zero.

6.2. Variable parameters

For historical reasons, several different solar spectra are specified in standards for SHGC calculation, resulting in different values of the solar direct transmittance value  $\tau_e$  of Eq. (1), which was thus one of the variable parameters in the joint exercise. These solar spectra are widely used in standards to characterise products for solar energy application, and are intended to represent “typical” spectra for use in product comparison. (A much wider range of spectral distributions is encountered at any given location in reality, depending on the solar altitude and atmospheric conditions.) A second variable is the approach taken by different standards to calculating the  $U$  value and its components, which

**Table 1**  
Geometrical and thermal parameters of the layers of the investigated BIPV glazing.

Parameter	Unit	Value
$\eta_{mod}$ of 72-cell PV laminate (92.2% coverage)	[-]	0.15
efficiency $\eta_{cell,mod}$ of all-cell PV laminate (100% coverage)	[-]	0.1627
effective conductivity of PV laminate	$Wm^{-1}K^{-1}$	0.6
thickness of PV laminate	mm	5
$\epsilon_{out}$ of PV laminate	[-]	0.84
$\epsilon_{in}$ of PV laminate	[-]	0.84
effective conductivity of low-e-coated glass pane (1) NFRC ID 9924	$Wm^{-1}K^{-1}$	1
thickness of low-e-coated glass pane (1)	mm	5.64
$\epsilon_{out}$ of low-e-coated glass pane (1)	[-]	0.157
$\epsilon_{in}$ of low-e-coated glass pane (1)	[-]	0.84
effective conductivity of low-e-coated glass pane (2)	$Wm^{-1}K^{-1}$	1
thickness of low-e-coated glass pane (2)	mm	5.85
$\epsilon_{out}$ of low-e-coated glass pane (2)	[-]	0.028
$\epsilon_{in}$ of low-e-coated glass pane (2)	[-]	0.84

are needed to determine the the secondary heat transfer factor of the glazing towards the inside,  $q_b$ , the second term of Eq. (1). The standards [19] and [18] apply the same static method, fixing the average temperature and the temperature difference between the outermost and innermost glazing layers. These two standards differ only in the specified values for the external and internal heat transfer coefficients, and are referenced by ISO 9050:2003 [15] and EN 410:2011 [16] respectively, the standards addressed by the proposed modification. By contrast, the ISO 15099:2003 standard [11] applies a dynamic heat-transfer calculation method, where the outdoor and indoor air temperatures are the specified boundary conditions and the heat transfer coefficients vary with the temperature of the glazing layers once thermal equilibrium has been achieved. To minimize differences caused by the different U-value calculation methods, all participants agreed to use the same sets of values for the external and internal heat transfer coefficients and to use the same value for the air and adjacent glazing surface temperature. Table 2 documents the participating institutions and the standards which they applied.

In total, the solar direct transmittance, U value, secondary heat transfer factor towards the inside and SHGC value were calculated by each participant for 48 variants. This resulted from two values each for the external and internal heat transfer coefficients, two electrical states (OC and MPP), three glazing configurations as specified in Section 6.1 and two different coverage ratios (corresponding to PV laminates with 36 and 72 solar cells). The values for these parameters, together with the fixed values of the outdoor and indoor temperatures, are listed in Table 3. The two values for the external heat transfer coefficient  $h_{out}$ ,  $25 Wm^{-2}K^{-1}$  and  $12 Wm^{-2}K^{-1}$ , are typical of values specified by standards to represent “winter” and “summer” conditions, respectively. The two

**Table 2**  
Institutions participating in the comparative calculation exercise, the standards which they applied and the underlying solar spectra. AM = air mass, g = global, d = direct. See list of authors for the full names of the institutions.

	LIXIL, RMIT	CIEMAT, Tecnalia	Hunan U	ConcU, ISE, LBNL
Solar spectrum	AM 1.5g	AM 1.0g	AM1.5g	AM1.5d
U value	ISO 10292	EN 673	ISO 15099	ISO 15099
SHGC	ISO 9050	EN 410	JGJ / T 151–2008	ISO 15099 with NFRC 300

**Table 3**  
Thermal boundary conditions applied and values of varied parameters.

$T_{out}$	$T_{in}$	$h_{out}$	$h_{in}$	Electrical state	Cell coverage ratio	Glazing configuration
°C	°C	$Wm^{-2}K^{-1}$	$Wm^{-2}K^{-1}$			
25.1	25.0	25	8.1	OC	0.922	PV laminate alone (glass-glass)
		12	6.6	MPP	0.461	PV laminate; 25.4 mm air; low-e pane 1
						PV laminate; 12 mm Ar; low-e pane 2

values for the internal heat transfer coefficient  $h_{in}$ , 8.1  $Wm^{-2}K^{-1}$  and 6.6  $Wm^{-2}K^{-1}$ , span a range of values that could be typically encountered indoors.

### 6.3. Results

The first sets of results are for the solar direct transmittance of the BIPV glazing units, which varies with the cell coverage ratio and glazing configuration, but is independent of the electrical state (OC or MPP). As expected and presented in Table 4 for the investigated PV laminates with opaque crystalline silicon solar cells, the cell coverage ratio dominates in determining the solar direct transmittance value, followed by the transmittance-reducing effect of the low-e-coated panes in the two BIPV double glazing units. By comparison, the variation resulting from applying different solar spectra to determine the  $\tau_e$  value for a given glazing configuration and CR value is relatively small. For the more densely covered samples, the maximum variation is 0.003. A maximum difference of 0.016 is observed for the lower CR value and the glass-glass PV laminate alone.

The calculated thermal transmittance  $U$  values depend only on the input values for the outdoor and indoor heat transfer coefficients, temperatures and thermal properties of the three different glazing configurations. They are considered to be independent of the electrical state (OC or MPP) and the cell coverage ratio CR as discussed in Section 4. Table 5 documents the results calculated according to the different  $U$ -value standards listed in Table 2. The  $U$  values from the different standards agree to two significant figures for a given set of input parameters and the boundary conditions specified for the exercise. The last three columns of Table 5 present values for the ratio  $U/h_{out}$ , which indicates the distribution between outward and inward flow of heat originating from the outermost glazing layer, i.e. the PV laminate for the discussed examples. The dominating influence on its value is the thermal resistance provided by the glazing itself; the relatively low thermal resistance of the glass-glass PV laminate leads to the highest values of  $U/h_{out}$ , indicating that the inward-flowing share of heat is greatest for this glazing configuration, in accordance with the discussion presented in Section 2. The  $U/h_{out}$  ratio is lowest for the second BIPV double glazing unit (DGU 2) with an argon-filled cavity and a soft low-e coating on the

**Table 4**

Solar direct transmittance values obtained for the different BIPV glazing units, calculated using the different solar spectra specified by the applied international SHGC standards. AM = air mass,  $\tau_e$  = solar direct transmittance, CR = (cell) coverage ratio, DGU = double glazing unit.

Glazing configuration, CR	$\tau_e$ ISO 9050 (AM1.5g)	$\tau_e$ EN 410 (AM1.0g)	$\tau_e$ NFRC 300 (AM1.5d)
PV laminate, CR = 0.922	0.066	0.063	0.064
DGU 1, CR = 0.922	0.046	0.045	0.044
DGU 2, CR = 0.922	0.021	0.021	0.019
PV laminate, CR = 0.461	0.451	0.435	0.441
DGU 1, CR = 0.461	0.316	0.308	0.304
DGU 2, CR = 0.461	0.144	0.146	0.134

indoor pane, where the high thermal resistance of the glazing unit ensures that the inward heat flow is low. For each glazing configuration, the  $U/h_{out}$  ratio is lowest when the external heat transfer is high and the internal heat transfer is low, i.e. when relatively little heat flows inward through the glazing and into the indoor space. Conversely, the ratio is highest when the external heat transfer is low and the internal heat transfer is high. For the double glazing units, the ratio is effectively independent of the internal heat transfer coefficient due to the high thermal resistance of the glazing unit itself.

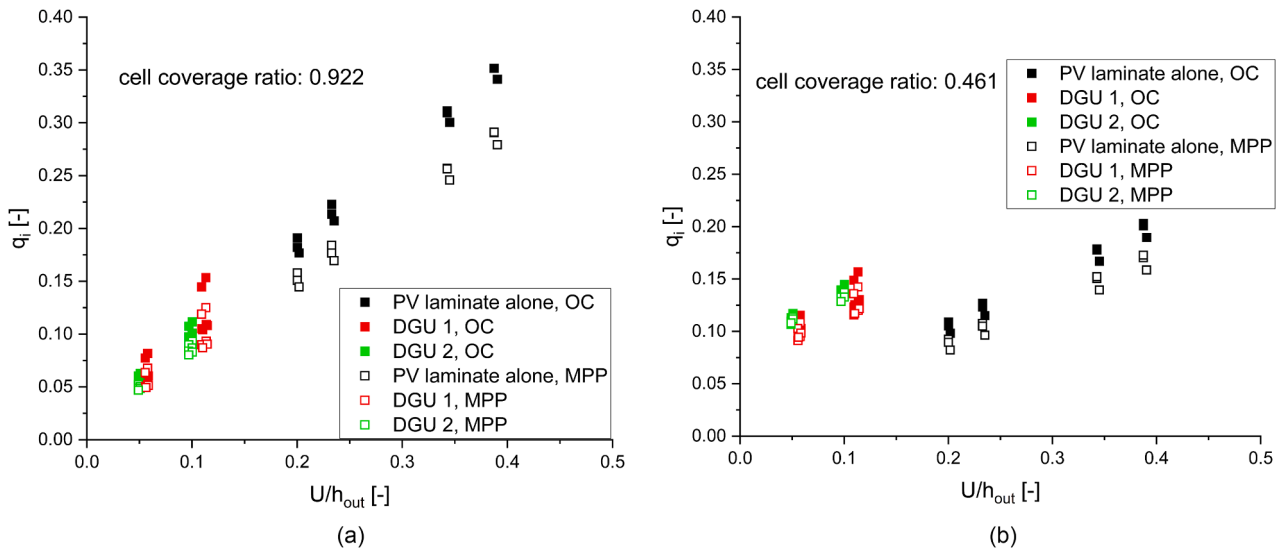
As expected from the discussion at the end of Section 2 and illustrated in Fig. 4(a) and (b), the  $U/h_{out}$  ratio is useful as an independent variable when analysing the variation of the secondary heat transfer factor towards the inside  $q_i$  among the different BIPV glazing variants. Considering first the case of BIPV glazing with the higher cell coverage ratio of  $CR = 0.922$  shown in Fig. 4(a), a general trend of  $q_i$  increasing with the  $U/h_{out}$  ratio is observed for both the OC and the MPP cases. With this high cell coverage ratio, the heat absorbed in the solar cells of the PV laminate dominates the total amount of heat absorbed in the BIPV glazing units, and the share which flows inward is significantly higher for the poorly insulating PV laminate alone than for the BIPV double glazing units. The  $q_i$  value for the PV laminate alone also varies strongly with the choice of both outside and inside heat transfer coefficients, for the same reasons as discussed in the previous paragraph with respect to the  $U/h_{out}$  ratio. By contrast, the high thermal resistance of the double glazing units decouples the effect of heat transfer to the outdoors and the indoors: for a given value of the  $U/h_{out}$  ratio, which is predominantly determined by the  $h_{out}$  value, the  $q_i$  values increase significantly with the  $h_{in}$  value. As expected, the  $q_i$  value for a given glazing configuration and  $U/h_{out}$  ratio is higher for the OC state than for MPP, with the magnitude of the difference correlating with the magnitude of  $q_i$  in the OC state. For heat transfer coefficients similar to those specified by EN 410 [3,16] and ISO 9050 [2,15] to represent winter conditions,  $h_{out} = 25 Wm^{-2}K^{-1}$  and  $h_{in} = 8.1 Wm^{-2}K^{-1}$ , the calculated difference in  $q_i$  caused by the extraction of electricity is  $0.038 \pm 0.001$  for the PV laminate alone, whereas it is only  $0.003 \pm 0.001$  for DGU 2. (Please note that the tolerance values indicate the range of values calculated by the participants using the methods of the different standards documented in Table 2; they should not be interpreted as uncertainty values.) For values that are more typical for summer conditions,  $h_{out} = 12 Wm^{-2}K^{-1}$  and  $h_{in} = 8.1 Wm^{-2}K^{-1}$ , the calculated differences in  $q_i$  due to extraction of electricity for the densely covered PV laminate alone and the DGU 2 increase to  $0.061 \pm 0.001$  and  $0.016 \pm 0.002$ , respectively.

Turning to the case of a lower cell coverage ratio of  $CR = 0.461$ , as may be more typical for applications requiring significant daylighting through a partly transparent BIPV glazing unit, the dependence of  $q_i$  on the  $U/h_{out}$  ratio is more complex, as illustrated by Fig. 4(b). The effect of reducing the cell coverage is easily explained for the PV laminate alone; halving the cell-covered area essentially halves the solar direct absorptance and thus the amount of heat flow to the inside for any given value of the  $U/h_{out}$  ratio. The difference in the  $q_i$  value caused by electricity extraction is also halved. For the BIPV double glazing units, however, the solar radiation that is absorbed in the low-e-coated indoor pane

**Table 5**

Input values for outdoor and indoor heat transfer coefficients ( $h_{out}$  and  $h_{in}$ , respectively) and the resulting thermal transmittance values  $U$  and  $U/h_{out}$  ratios for the three different glazing configurations (PV laminate alone, DGU 1 and DGU 2). DGU = double glazing unit. As discussed in the text, these values are assumed to be independent of the cell coverage ratio CR and the electrical state (OC or MPP).

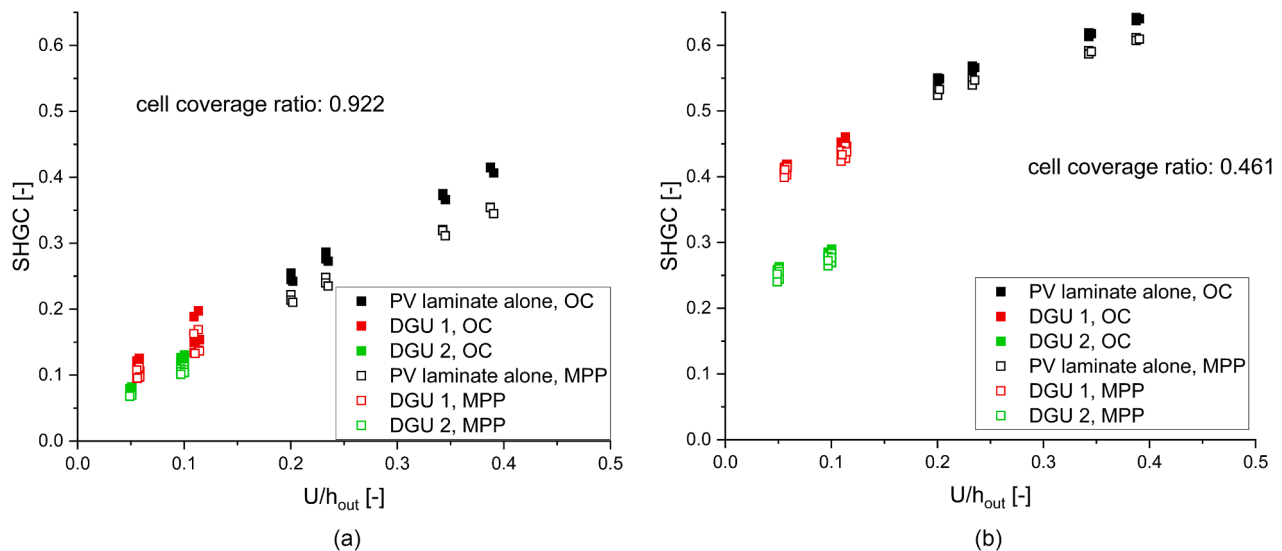
$h_{out}$ Wm <sup>-2</sup> K <sup>-1</sup>	$h_{in}$ Wm <sup>-2</sup> K <sup>-1</sup>	$U$			$U/h_{out}$		
		Wm <sup>-2</sup> K <sup>-1</sup>			[-]		
		PV laminate	DGU 1	DGU 2	PV laminate	DGU 1	DGU 2
25	6.6	5.0	1.4	1.2	0.20	0.06	0.05
25	8.1	5.8	1.4	1.3	0.23-0.24	0.06	0.05
12	6.6	4.1	1.3	1.2	0.34-0.35	0.11	0.10
12	8.1	4.6	1.4	1.2	0.39	0.11	0.10



**Fig. 4.** Dependence of the secondary heat transfer factors toward the inside  $q_i$  on the  $U/h_{out}$  ratio for different BIPV glazing configurations in the OC and MPP electrical states and cell coverage ratios (a) of  $CR = 0.922$  and (b)  $CR = 0.461$ . OC = open circuit, MPP = maximum power point, DGU = double glazing unit (as specified in Section 6.1 and Table 1).

contributes significantly to the heat flowing inward when more than half of the outdoor pane, the PV laminate, is transparent. For the OC state, the combined contribution of heat generated in the PV cells and heat generated in the irradiated sections of the indoor pane results in  $q_i$  values

that are higher for  $CR = 0.461$  than for  $CR = 0.922$ . Again, the difference in  $q_i$  between the OC and MPP states, caused by extraction of electricity for a given glazing configuration and  $U/h_{out}$  ratio, is halved when the cell coverage ratio is halved.



**Fig. 5.** Dependence of the solar heat gain coefficient SHGC on the  $U/h_{out}$  ratio for different BIPV glazing configurations in the OC and MPP electrical states and cell coverage ratios (a) of  $CR = 0.922$  and (b)  $CR = 0.461$ . OC = open circuit, MPP = maximum power point, DGU = double glazing unit (as specified in Section 6.1 and Table 1).

The slight scatter of points in Fig. 4 for a given value of the  $U/h_{out}$  ratio, glazing configuration and electrical state is due to the fact that the participants used three different standards, NFRC 300 [17], EN 410 [16] and ISO 9050 [15], as the basis of the calculations. The previously mentioned differences in the solar spectrum cause slight variations in the determined value of the solar direct absorptance  $\alpha_e$  and slightly different approaches are specified to calculate the U value; both effects contribute to the visible variation in  $q_i$ .

The range of SHGC values calculated for the 48 parameter combinations explored in this sensitivity exercise are documented in Fig. 5(a) and (b), again plotted versus the  $U/h_{out}$  ratio. In accordance with Eq. (1), they were obtained as the sum of the solar direct transmittance values  $\tau_e$  of Table 4 and the secondary heat transfer factors  $q_i$  toward the inside, from Fig. 4. In addition to the slight variations in  $q_i$  and  $U/h_{out}$  caused by the different underlying standards that were visible in Fig. 4, the different solar spectra also cause slight variations in the solar direct transmittance  $\tau_e$  component of the SHGC plotted in Fig. 5.

For the low solar direct transmittance values of the configurations with  $CR=0.922$ , the SHGC behaviour is dominated by the  $q_i$  component and the same arguments apply as in the discussion of influences on  $q_i$ . However, for the investigated configurations with  $CR = 0.461$ , the solar direct transmittance contribution can represent up to two-thirds of the SHGC value. Clearly, the solar direct transmittance does not affect the magnitude of the difference in SHGC due to electricity extraction for a given glazing configuration and  $U/h_{out}$ ; the difference in SHGC between the OC and MPP states is identically equal to the corresponding difference in  $q_i$ .

The results illustrated in Fig. 5 for “DGU 1” agree well, within experimental error, with the experimental results reported for the double glazing unit investigated by Kapsis [7], providing evidence of the validity of the component-based approach proposed here.

For the summer conditions characterized by  $h_{out} = 12 \text{ Wm}^{-2}\text{K}^{-1}$  and  $h_{in} = 8.1 \text{ Wm}^{-2}\text{K}^{-1}$ , Fig. 6 illustrates the dependence of the calculated SHGC of the different glazing configurations and electrical states on the cell coverage ratio  $CR$ . The SHGC values illustrated in Fig. 5 for  $CR = 0.922$  and  $0.461$  were used as inputs to define these linear functions. For clarity, only the results calculated according to ISO 9050 [15] are shown as an example. As expected, in the absence of solar cells ( $CR = 0$ ), the SHGC values are identical for the “OC” and “MPP” electrical states, and the difference in SHGC for a given glazing configuration increases with

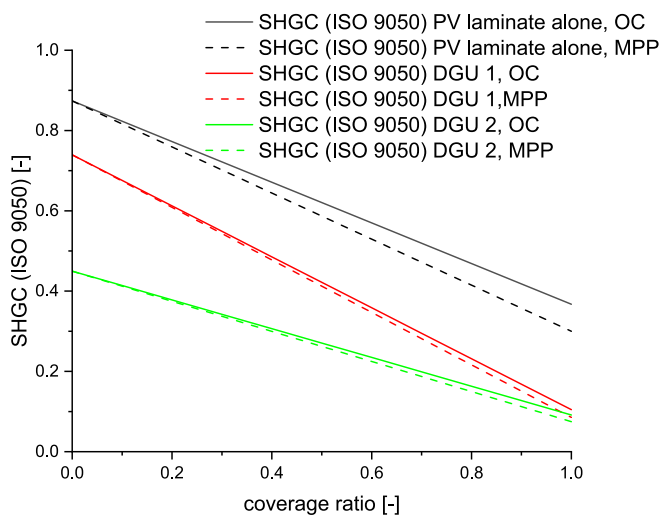


Fig. 6. Solar heat gain coefficient SHGC versus the cell coverage ratio  $CR$  for different BIPV glazing configurations in the OC and MPP electrical states, illustrating the linear dependence. OC = open circuit, MPP = maximum power point, DGU = double glazing unit (as specified in Section 6.1 and Table 1). For clarity, only the SHGC values calculated according to ISO 9050, with  $h_{out} = 12 \text{ Wm}^{-2}\text{K}^{-1}$  and  $h_{in} = 8.1 \text{ Wm}^{-2}\text{K}^{-1}$  (summer conditions) are shown as an example.

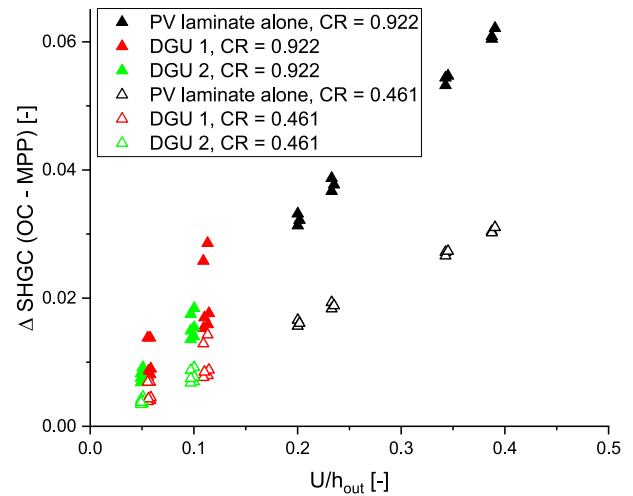


Fig. 7. Dependence of the difference between solar heat gain coefficient SHGCs in the OC and MPP electrical states on the  $U/h_{out}$  ratio for different BIPV glazing configurations and cell coverage ratios,  $CR = 0.922$  (solid symbols) and  $CR = 0.461$  (hollow symbols). OC = open circuit, MPP = maximum power point, DGU = double glazing unit (as specified in Section 6.1 and Table 1).

the coverage ratio. This linear dependence of the SHGC on the coverage ratio for both electrical states has also been confirmed experimentally, e.g. by Kapsis [7].

For ease of consultation, the differences in SHGC due to electricity extraction are illustrated in Fig. 7 for the 24 investigated combinations of cell coverage ratio, glazing configuration and outside and inside heat transfer coefficients. Values between 0.062 and 0.003 were determined for the investigated variants. The largest difference of 0.062 was determined for the single glazing variant with  $CR = 0.922$  under summer conditions. Values greater than 0.03 were determined only for the poorly insulating, single glazing variants consisting of the PV laminate alone.

## 7. Discussion

Returning to the stated goals of the calculation exercise using the proposed calculation methodology, the results presented here for realistic cases of BIPV single and double glazing document that

- the magnitude of the effect of electricity extraction on the SHGC value for the investigated BIPV glazing configurations reached a value of up to about 0.06 for a PV laminate alone with a high cell coverage ratio. The value became typically less than 0.02 when BIPV double glazing units with one low-e coating and a high cell coverage ratio were considered. Comparable results have been obtained in experimental investigations, such as those reported by Kapsis [7]. However, it should also be remembered that the examples were calculated using a module power conversion efficiency of 15%. With current module power conversion efficiencies already exceeding 20%, the magnitude of the electricity extraction effect on the SHGC value shown in Fig. 7 can be expected to increase proportionately to the power conversion efficiency. However, it should also be remembered that the electricity extraction effect based on a given  $\eta_{mod}$  value for standard test conditions and the MPP represents an upper limit that will often not be reached in practice.
- the size of the electricity extraction effect on the calculated SHGC value for a given BIPV glazing unit, particularly for the double glazing units, is observed to be of the same order or magnitude as that caused by evaluation applying different solar spectra specified in different standards or the values used for the outdoor and indoor heat transfer coefficients when calculating the thermal transmittance. This underscores the importance of clearly stating the

input parameters used when presenting calculated SHGC values – not only for BIPV glazing!

- the size of the determined effect of electricity extraction on the SHGC was considered to be large enough to warrant inclusion within international SHGC standards and is currently being addressed by the appropriate technical committees for architectural glazing within CEN and ISO.

The presented results also document the general trend of the effect of the reduction in SHGC value due to electricity extraction decreasing as the thermal insulation provided by a glazing unit improves. Considering that triple glazing units with two low-e-coated panes typically have a  $U$  value of  $0.8 \text{ Wm}^{-2}\text{K}^{-1}$  or less, the trend shown in Fig. 7 indicates that the difference in SHGC value due to electricity extraction will be typically less than 0.01 for a BIPV triple glazing unit, which would usually be regarded as negligible.

Although the derivation of the proposed SHGC calculation approach has concentrated on semi-transparent BIPV glazing, where at least one region of the PV laminate layer has a non-zero solar direct transmittance, it is equally valid for a completely opaque BIPV glazing unit. In this case, the solar direct transmittance for the entire PV laminate layer would be set to zero. However, the  $q_i$  component will still ensure that the SHGC is greater than zero, and, in the case of a PV laminate alone, can reach a value of 0.30 or more.

## 8. Conclusion

A simple modification to existing methods to calculate the SHGC of conventional architectural glazing has been presented, which allows the effect on the SHGC value of extracting electricity from a BIPV glazing unit to be calculated. The only additional information needed to take electricity extraction from the PV component into account is the power conversion efficiency of the PV laminate and the coverage ratio of solar cells within it. As BIPV glazing units are commonly manufactured with a wide range of heights, widths and cell coverage ratios, it is recommended that the SHGC values for 100% coverage of each of the optically different regions should be reported separately. Both the OC and MPP values should be reported for the PV cell regions. The overall SHGC value for any specific BIPV glazing unit can then be easily calculated, using the relevant area ratios for the optically different regions.

Like the underlying calculation methods, the presented approach is intended for the comparison of BIPV glazing at the product level, not for dynamic calculation of the SHGC under variable boundary conditions within the building energy simulation context. As in the underlying calculations, the assumptions of normally incident solar radiation, essentially non-scattering, parallel and planar glazing layers, and simplified calculation of one-dimensional thermal transmission apply. Within these constraints, the authors are convinced that the presented approach is useful, allowing the SHGC of many widespread and diverse BIPV glazing products to be declared in both the OC and the MPP electrical states. They hope that this will support the dissemination of BIPV glazing and thus its contribution to increasing the share of electricity generated from renewable sources.

## CRedit authorship contribution statement

**Helen Rose Wilson:** Writing – review & editing, Writing – original draft, Validation, Methodology, Investigation, Conceptualization. **Tilmann E. Kuhn:** Writing – review & editing. **Hisashi Ishii:** Validation. **Daniel Valencia-Caballero:** Validation, Methodology, Investigation. **Nuria Martin Chivelet:** Writing – review & editing, Validation, Investigation. **Jinqing Peng:** Validation. **Rebecca Jing Yang:** Writing – review & editing, Supervision. **Yukun Zang:** Writing – review & editing, Validation. **Hua Ge:** Writing – review & editing, Supervision. **Kai Ye:** Validation. **Jacob C. Jonsson:** Validation. **Konstantinos Kapsis:** Methodology.

## Declaration of competing interest

The authors declare that they have no known competing financial interests or personal relationships that could have appeared to influence the work reported in this paper.

## Data availability

Data will be made available on request.

## Acknowledgements

This article is based on work carried out by the authors within the framework of the IEA-PVPS Task 15, ‘Enabling framework for the development of BIPV’. The authors gratefully acknowledge the input of colleagues who conducted the calculations and the feedback from members of standardisation committees. Sincere thanks are extended to the following sources of funding for the reported research:

- the German Federal Ministry for Economic Affairs and Climate Action (BMWK), within the Standard BIPV-System project, grant number 03EE1061A.
- the Japanese New Energy and Industrial Technology Development Organization (NEDO), within the Wall-Installed Solar PV System Technology Development project.
- the European Union’s Horizon 2020 research and innovation programme, within the BIPVBOOST project, under grant agreement No. 817991.
- the Spanish Ministry of Science and Innovation and the European Regional Development Fund, within the RINGS-BIPV project, grant number PID2021-124910OB-C31.
- the Assistant Secretary for Energy Efficiency and Renewable Energy, Building Technologies Program, of the U.S. Department of Energy, United States under Contract No. DE-AC02-05CH11231.

## References

- [1] J.L.J. Rosenfeld, W.J. Platzer, H. van Dijk, A. Maccari, Modelling the optical and thermal properties of advanced glazing – Overview of recent developments, *Solar Energy* (2001), [https://doi.org/10.1016/S0038-092X\(01\)00028-7](https://doi.org/10.1016/S0038-092X(01)00028-7).
- [2] ISO 9050, Glass in building — Determination of light transmittance, solar direct transmittance, total solar energy transmittance, ultraviolet transmittance and related glazing factors, 1990.
- [3] EN 410, Glass in building – Determination of luminous and solar characteristics of glazing, 1998.
- [4] T. Kuhn, Calorimetric determination of the solar heat gain coefficient  $g$  with steady-state laboratory measurements, *Energy and Buildings* 84 (2014) 388–402, <https://doi.org/10.1016/j.enbuild.2014.08.021>.
- [5] H. Ishii, Thermal Performance (G-value and U-value) Evaluation of BIPV Applied to Glass Façade, *Conf. Proc. EU-PVSEC*, 2017.
- [6] H. Ishii, Evaluation of Thermal Properties for BIPV in Façade Part 2 Experimental Results of G value for Crystal Silicon BIPV Module according to ISO 19467, *Conf. Proc. EU PVSEC*, 2018.
- [7] K. Kapsis, A. Athienitis, S. Harrison, Determination of solar heat gain coefficients for semitransparent photovoltaic windows: An experimental study, *ASHRAE Conf 123* (2017) 82–94.
- [8] L. Olivieri, E. Caamaño-Martin, F. Olivieri, J. Neila, Integral energy performance characterization of semi-transparent photovoltaic elements for building integration under real operation conditions, *Energy and Buildings* 68 (2014) 280–291, <https://doi.org/10.1016/j.enbuild.2013.09.035>.
- [9] F. Chen, S.K. Wittkopf, P.K. Ng, H. Du, Solar heat gain coefficient measurement of semi-transparent photovoltaic modules with indoor calorimetric hot box and solar simulator, *Energy and Buildings* 53 (2012) 74–84, <https://doi.org/10.1016/j.enbuild.2012.06.005>.
- [10] M. Mittag, I. Haedrich, T. Neff, S. Hoffmann, U. Eitner, H. Wirth, Harry, TPedge: Qualification of a gas-filled, encapsulation-free glass-glass photovoltaic module, *Conf. Proc. EU-PVSEC 2015* (2015), <https://doi.org/10.4229/EUPVSEC20152015-1CO.11.4>.
- [11] ISO 15099:2003, Thermal performance of windows, doors and shading devices - Detailed calculations, 2003.
- [12] H. Zhou, J. Peng, H.R. Wilson, M. Wang, J. Jonsson, T. Ma, B. Wu, B. Wu, G. Fu, Investigation of decoupling of thermal and electrical performance of semi-transparent photovoltaic windows based on the external quantum efficiency,

- Energy and Buildings 277 (2022) 112539, <https://doi.org/10.1016/j.enbuild.2022.112539>.
- [13] ISO 19467-1:2017, Thermal performance of windows and doors – Determination of solar heat gain coefficient using solar simulator, 2017.
- [14] ISO 19467-2:2021, Thermal performance of windows and doors - Determination of solar heat gain coefficient using solar simulator – Part 2: Centre of glazing, 2021.
- [15] ISO 9050:2003, Glass in building - Determination of light transmittance, solar direct transmittance, total solar energy transmittance, ultraviolet transmittance and related glazing factors, 2003.
- [16] EN 410:2011, Glass in building – Determination of luminous and solar characteristics of glazing, 2011.
- [17] NFRC 300-2023 [E0A1], Test method for determining the solar optical properties of glazing materials and systems, 2023.
- [18] EN 673:2011, Glass in building – Determination of thermal transmittance (U value) – Calculation method, 2011.
- [19] ISO 10292:1994, Glass in building – Calculation of steady-state U values (thermal transmittance) of multiple glazing, 1994.
- [20] IEC TS 61836:2016, Solar photovoltaic energy systems – Terms, definitions and symbols.
- [21] IEC 60904-9:2020, Photovoltaic devices – Part 9: Solar simulator performance requirements, 2020.
- [22] N. Martin-Chivelet, K. Kapsis, H.R. Wilson, V. Delisle, R. Yang, L. Olivieri, J. Polo, J. Eisenlohr, B. Roy, L. Maturi, G. Otnes, M. Dallapiccola, W.M.P.U. Wijeratne, Building-Integrated Photovoltaic (BIPV) products and systems: a review of energy-related behavior, Energy and Buildings 262 (2022) 111998, <https://doi.org/10.1016/j.enbuild.2022.111998>.
- [23] D. Valencia Caballero. Thermal transmittance and solar factor in BIPV operating conditions. Conf. Proc. 7th Advanced Building Skins Conference & Expo, 20.-21.10.2022 Berne Switzerland, 2022.



